

2005

## Carbon nanofiber purification and functionalization for improved polymeric nanocomposites

William Gewand Fox  
*University of Dayton*

Follow this and additional works at: [https://ecommons.udayton.edu/graduate\\_theses](https://ecommons.udayton.edu/graduate_theses)

---

### Recommended Citation

Fox, William Gewand, "Carbon nanofiber purification and functionalization for improved polymeric nanocomposites" (2005). *Graduate Theses and Dissertations*. 2723.  
[https://ecommons.udayton.edu/graduate\\_theses/2723](https://ecommons.udayton.edu/graduate_theses/2723)

This Thesis is brought to you for free and open access by the Theses and Dissertations at eCommons. It has been accepted for inclusion in Graduate Theses and Dissertations by an authorized administrator of eCommons. For more information, please contact [mschlangen1@udayton.edu](mailto:mschlangen1@udayton.edu), [ecommons@udayton.edu](mailto:ecommons@udayton.edu).

**CARBON NANOFIBER PURIFICATION AND FUNCTIONALIZATION  
FOR IMPROVED POLYMERIC NANOCOMPOSITES**

THESIS

Submitted In Partial Fulfillment of the Requirements for the Degree  
Master of Science in Materials Engineering

By

William Gewand Fox

The School of Engineering

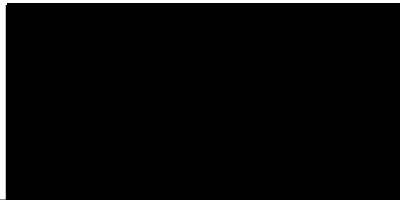
UNIVERSITY OF DAYTON

Dayton, Ohio

May 2005

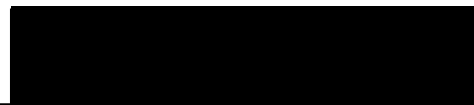
## **CARBON NANOFIBER PURIFICATION AND FUNCTIONALIZATION FOR IMPROVED POLYMERIC NANOCOMPOSITES**

APPROVED BY:



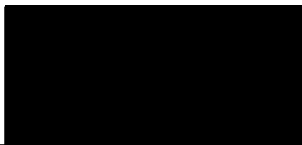
---

Khalid Lafdi, D.Sc., Ph.D.  
Research Advisor  
Advisory Committee Chairman  
Professor, Chemical and Materials  
Engineering



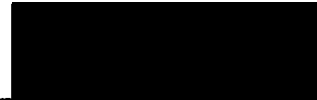
---

Donald Klosterman, Ph.D.  
Committee Member  
Professor, Chemical and Materials  
Engineering



---

C. William Lee, Ph.D.  
Committee Member  
Professor, Chemical and Materials  
Engineering



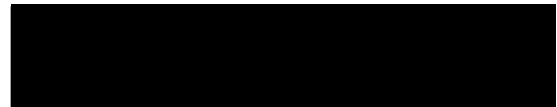
---

Daniel Eylon, D.Sc.  
Academic Advisor  
Director, Materials Engineering  
Professor, Chemical and Materials  
Engineering



---

Donald L. Moon, Ph.D.  
Associate Dean  
Graduate Engineering Programs &  
Research, School of Engineering



---

Joseph Saliba, Ph.D., P.E.  
Dean, School of Engineering

## ABSTRACT

### **CARBON NANOFIBER PURIFICATION AND FUNCTIONALIZATION FOR IMPROVED POLYMERIC NANOCOMPOSITES**

Name: Fox, William Gewand  
University of Dayton

Research Advisor: Dr. Khalid Lafdi

The definition of a nanocomposite material has broadened significantly to encompass a large variety of systems such as one-dimensional, two-dimensional, three-dimensional and amorphous materials, made of dissimilar components and mixed at the nanometer scale. This rapidly expanding field is generating many exciting new materials with novel properties. The latter can be derived by combining properties from the parent constituents into a single material. The properties of nanocomposite materials also depend on the morphology and interfacial characteristics of the individual constituents. The current work focused on nanocomposites of carbon nanofibers in a polymer matrix with an emphasis on purification, surface functionalization, and heat treatment temperature of nanofibers.

Two methods (heat treatment and Soxhlet extraction) were used for purification and cleaning of the as-received nanofibers. These methods resulted in chemical and physical property improvements due to the removal of the

surface dielectric layer. In addition, Soxhlet extraction of the nanofibers progressively with acetone, THF, toluene, and pyridine resulted in an elimination of an unwanted early reaction with epoxy during subsequent nanocomposite curing.

Heat treatment of carbon nanofibers lead to alignment of graphene layers within the nanofibers which allowed for a more efficient transfer of phonons and electrons. This in turn resulted in significant decreases in electrical resistivity and increases in thermal conductivity nanocomposite compared to the neat epoxy resin. However, heat treatment beyond 1800°C lead to increased conversion to graphene layers and resulted in lower mechanical properties due to poor adhesion to the epoxy matrix.

Functionalization of nanofibers showed that measurement of the oxygen content of a nanofiber did not correlate with improved adhesion to an epoxy matrix. Instead, the type of functional group was a factor in determining mechanical properties and curing rates of the nanocomposite. For example, the alcohol group improved adhesion with the epoxy matrix to a greater degree than carboxylic acid groups. Oxygen functional groups caused a negative impact on electrical properties of the nanocomposite, but did not affect thermal properties.

Based on the results of the testing of heat treated and surface functionalized nanofiber based polymer composites, the possibility exists for tailoring of nanocomposite physical properties.

## ACKNOWLEDGEMENTS

I would like to extend my sincere gratitude to Dr. Khalid Lafdi for his time and dedication to my research work over the past two years. While it has been difficult at times, I still maintain that I have learned and developed more as an engineer during this period than I did during my previous time in industry, and for that, I will forever be appreciative. I would also like to acknowledge Dr. Daniel Eylon who gave me the opportunity to study and grow at the University of Dayton, and was always available when I had questions and concerns. In addition, I would like to thank Dr. Bill Lee and Dr. Don Klosterman for the time and effort they provided in being a part of my thesis review committee.

I would also like to thank Dr. Emel Yildiz and Dr. Weiming Lu for their help in different areas of my research. Emel has been an unbelievable asset to our research group, and she has always taken the extra time to explain her experiments and discuss test results with me. Weiming was an excellent resource for providing suggestions on electrochemical treatment methods and brought with him his expertise in carbon functionalization techniques. I know that I have improved as a researcher because of the time and knowledge that both Emel and Weiming have afforded me.

Within MLBC at the Air Force Research Labs I would like to thank Bill Ragland, Bill Price, Ken Lindsey, and Thao Gibson for all of their support in lab training and scheduling. Similarly at the University of Dayton, I would like to thank Mary Galaska who has been a tremendous asset in my lab training. I would also like to thank Mindy Call, Matt Grogg, and Dr. Panagiotis Tsonis who graciously assisted in the biological work. And of course I would like to thank my fellow students within our research group, Greg Rosebrock, Tom Beechem, Matt Matzek, Paul Bowman, and Osama Mesalhy for being available to share problems and accomplishments.

I would like to thank DAGSI (Dayton Area Graduate Studies Institute) for their tuition financial support, and the many research and development organizations that have provided the financial support for our nanocomposite research.

Finally, to my wife Tracey – thank you for your support and faith in me. I cannot think of too many people in this world who would have not only allowed me to pursue this experience, but would have done it knowing, before even I did, that it would make me a better person. You are truly my inspiration, and I will always love you.

## TABLE OF CONTENTS

ABSTRACT.....	iii
ACKNOWLEDGEMENTS.....	v
TABLE OF CONTENTS.....	vii
LIST OF FIGURES.....	xi
LIST OF TABLES.....	xv
LIST OF SYMBOLS.....	xvi
CHAPTER 1: INTRODUCTION.....	1
CHAPTER 2: BACKGROUND AND LITERATURE REVIEW.....	6
2.1    CARBON FIBERS AND NANOFIBERS.....	6
2.2    EPOXY RESIN.....	16
2.3    CARBON NANOFIBER REINFORCED POLYMERIC NANOCOMPOSITES.....	19
2.4    CARBON SURFACE FUNCTIONALIZATION AND ITS EFFECT ON COMPOSITE PROPERTIES.....	23
2.4.1    Heat Treatment of Carbon Nanoparticulates.....	23
2.4.2    Chemical Treatment of Nanometric and Micrometric Carbon.....	28
2.5    METHODS FOR CARBON SURFACE FUNCTIONALIZATION....	32
2.5.1    The Diazonium Formation Reaction.....	34
2.5.2    Oxidation Methods.....	38



2.5.3	Plasma Treatment Methods.....	41
2.5.4	Fluorination Methods.....	44
CHAPTER III: EXPERIMENTAL METHODS.....		46
3.1	NANOCOMPOSITE MATERIAL DESCRIPTION.....	46
3.2	NANOCOMPOSITE PANEL FABRICATION.....	47
3.3	THERMAL ANALYSIS.....	47
3.3.1	Differential Scanning Calorimetry.....	47
3.3.2	Thermal Diffusivity.....	50
3.3.3	Thermogravimetric Analysis.....	52
3.4	ELECTRICAL ANALYSIS.....	53
3.4.1	Four-Point Probe Electrical Resistivity.....	53
3.4.2	Volume Resistivity.....	53
3.5	MECHANICAL ANALYSIS.....	55
3.6	INVERSE GAS CHROMATOGRAPHY.....	56
3.7	BRUNAUER EMMETT TELLER (BET) SURFACE AREA.....	57
3.8	ELECTRON MICROSCOPY.....	58
3.9	X-RAY PHOTOELECTRON SPECTROSCOPY.....	58
3.10	RHEOLOGICAL ANALYSIS.....	61
3.11	SOXHLET EXTRACTION.....	63
CHAPTER IV: EFFECT OF CARBON NANOFIBER CLEANING AND PURIFICATION ON NANOFIBER AND POLYMERIC NANOCOMPOSITE PROPERTIES.....		65
4.1	CARBON NANOFIBER STRUCTURE.....	65

4.2	CARBON NANOFIBER CLEANING AND PURIFICATION AND ITS EFFECT ON NANOFIBER PROPERTIES.....	71
4.3	EFFECT OF CARBON NANOFIBER CLEANING AND PURIFICATION ON POLYMERIC NANOCOMPOSITE CURING REACTION.....	79
4.4	CONCLUSIONS.....	84
CHAPTER V: EFFECT OF CARBON NANOFIBER HEAT TREATMENT ON PHYSICAL PROPERTIES OF POLYMERIC NANOCOMPOSITES.....		86
5.1	INTRODUCTION.....	86
5.2	EXPERIMENTAL SETUP.....	86
5.3	RESULTS AND DISCUSSION.....	87
5.4	CONCLUSIONS.....	92
CHAPTER VI: ELECTROCHEMICAL OXIDATION OF CARBON NANOFIBERS: SURFACE CHEMISTRY AND POLYMER ADHESION.....		94
6.1	INTRODUCTION.....	94
6.2	EXPERIMENTAL SETUP.....	94
6.2.1	Electrochemical Treatment.....	95
6.2.2	Nanofiber Characterization by X-Ray Photoelectron Spectroscopy.....	96
6.2.3	Nanocomposite Characterization.....	101
6.3	RESULTS AND DISCUSSION.....	102
6.4	CONCLUSIONS.....	108
CHAPTER VII: ATTACHMENT OF CARBOXYLIC ACID AND ALCOHOL FUNCTIONAL GROUPS TO CARBON NANOFIBERS: THE CHEMISTRY, ANALYSIS, AND EFFECT ON POLYMER ADHESION.....		110

7.1	INTRODUCTION.....	110
7.2	EXPERIMENTAL SETUP.....	111
7.2.1	Chemical Modifications of Carbon Nanofibers.....	111
7.2.2	Nanofiber Characterization.....	116
7.2.3	Nanocomposite Sample Procedure.....	116
7.2.4	Nanocomposite Characterization.....	117
7.3	RESULTS AND DISCUSSION.....	117
7.4	CONCLUSIONS.....	127
CHAPTER VIII: SUMMARY OF CARBON NANOFIBER PURIFICATION AND SURFACE TREATMENT METHODS.....		130
CHAPTER IX: BIOLOGICAL APPLICATION OF CARBON FOAM.....		135
9.1	INTRODUCTION.....	135
9.2	EXPERIMENTAL SETUP.....	142
9.3	RESULTS AND DISCUSSION.....	143
9.4	CONCLUSIONS.....	145
REFERENCES.....		147

## LIST OF FIGURES

2.1	Carbon nanofiber tensile strength.....	10
2.2	Chemical structure of (a) EPON 862 epoxy and (b) EPI-CURE Curing Agent W.....	17
2.3	Chemical structure of diazonium ion.....	34
3.1	Specific heat analysis of nanocomposite by DSC.....	48
3.2	Heat of reaction analysis of nanocomposite by DSC.....	49
3.3	Glass transition temperature analysis of nanocomposite by DSC.....	49
3.4	Thermal diffusivity analysis of nanocomposite by flash diffusivity.....	51
3.5	Degradation analysis of nanofiber by TGA.....	52
3.6	Fixture for testing carbon nanofiber volume resistivity.....	54
3.7	Mechanical analysis of nanocomposite by three-point flexural strength...	55
3.8	Viscosity as a function of temperature for neat resin.....	62
3.9	Determination of gelation time by rheological analysis.....	63
3.10	Experimental setup for Soxhlet extraction.....	64
4.1	Bright field image of as-received PS carbon nanofibers.....	65
4.2	Models of nanofiber configurations.....	67
4.3	SEM micrograph of as-received carbon nanofibers indicating thick, dark edges.....	67

4.4	SEM micrograph indicating no adhesion between the nanofiber and the resin matrix.....	68
4.5	Carbon plane structure as a function of heat treatment temperature.....	69
4.6	Bright field image of nested cone type carbon nanofiber following heat treatment to 3000°C.....	70
4.7	High-resolution image of localized area of nested cone type carbon nanofiber following heat treatment to 3000°C.....	71
4.8	Volume resistivity of as-received carbon nanofibers.....	73
4.9	Residue on sample tube following BET surface area testing.....	74
4.10	TGA results for carbon nanofibers.....	75
4.11	Filtrate following PS nanofiber Soxhlet extraction in acetone.....	77
4.12	Volume resistivity of AG nanofibers as a function of extraction solvent and coinciding filtrate colors.....	78
4.13	DSC curve for neat epoxy resin.....	79
4.14	DSC curve for 5 wt. % as-received PS nanofibers in EPON 862 / W.....	80
4.15	DSC curves for as-received PS and LHT nanofibers in EPON 862 without curing agent.....	81
4.16	DSC curve for as-received HHT nanofibers in EPON 862 without curing agent.....	82
4.17	DSC curves for (a) EPON 862 / W with 5 wt. %PS nanofibers extracted in toluene, (b) EPON 862 / W with 5 wt. % PS nanofibers extracted in pyridine, (c) EPON 862 / W with 5 wt. % HHT nanofibers.....	83-84
5.1	Nanocomposite flexural modulus percent improvement over neat resin as a function of nanofiber heat treatment temperature.....	89
5.2	Nanocomposite flexural strength percent improvement over neat resin as a function of nanofiber heat treatment temperature.....	89
5.3	Nanocomposite electrical resistivity as a function of nanofiber heat treatment temperature.....	91

5.4	Nanocomposite thermal conductivity as a function of nanofiber heat treatment temperature.....	92
6.1	Procedure for electrochemical treatment of carbon nanofibers.....	96
6.2	Esterification of C-OH groups by TFAA.....	99
6.3	XPS plots of chemically derivatized carbon nanofibers.....	99
6.4	Esterification of C-OOH groups by TFE.....	100
6.5	Esterification of C=O groups by PFPH.....	101
6.6	Oxygen content weight percent as a function of nanofiber electrochemical treatment time.....	102
6.7	Nanocomposite flexural modulus and strength as a function of nanofiber electrochemical treatment time.....	104
6.8	Alcohol group content weight percent as a function of nanofiber electrochemical treatment time.....	106
6.9	Nanocomposite electrical resistivity as a function of nanofiber electrochemical treatment time.....	107
6.10	Nanocomposite thermal conductivity as a function of nanofiber electrochemical treatment time.....	108
7.1	Diazonium salt of aminobenzoic acid formation reaction.....	113
7.2	Reaction resulting in covalent attachment of aminobenzoic acid diazonium salt to the carbon surface.....	113
7.3	Diazonium salt of amino phenol formation reaction.....	114
7.4	Reaction resulting in covalent attachment of amino phenol diazonium salt to the carbon surface.....	114
7.5	Mechanisms for the covalent attachment to an epoxy polymer of (a) alcohol group functionalized carbon nanofibers and (b) carboxylic acid functionalized carbon nanofibers.....	115
7.6	DSC curve as-received C-OOH functionalized nanofibers in EPON 862 without curing agent.....	118

7.7	DSC curve for Soxhlet extracted C-OOH functionalized nanofibers in EPON 862 / W.....	118
7.8	DSC curves for as-received C-OOH functionalized nanofibers in EPON 862 / W.....	119
7.9	DSC curves for (a) cleaned PS grade nanofibers functionalized with carboxylic acid groups reacted with EPON 862 / W, (b) cleaned PS grade nanofibers functionalized with alcohol groups reacted with EPON862 / W, (c) cleaned LHT grade nanofibers functionalized with carboxylic acid groups reacted with EPON 862 / W, (d) cleaned LHT grade nanofibers functionalized with alcohol groups reacted with EPON 862 / W.....	121-123
9.1	Compressive strength of PCL-infiltrated carbon foam aged in SPF.....	143
9.2	Compressive modulus of PCL-infiltrated carbon foam aged in SPF.....	144
9.3	Adherence of osteoblast cells adhering to the carbon foam surface at 20x objective through UV filter.....	145

## LIST OF TABLES

2.1	Carbon nanofiber mechanical properties and density.....	9
2.2	Carbon nanofiber electrical and thermal properties.....	15
2.3	Cured neat resin properties of EPON 862 / W resin system as a function of cure schedule.....	17
4.1	Description of tested carbon nanofibers.....	72
4.2	Surface area and surface energy of carbon nanofibers.....	74
4.3	TGA weight loss of PS nanofibers following sequential Soxhlet extraction.....	77
6.1	Deconvolution of XPS C 1s spectra indicating weight percent of five specific carbon bonds as a function of electrochemical treatment time.....	103
7.1	Degradation onset temperatures for neat resin and nanocomposites....	120
7.2	TGA results for PS, heat treated PS, and heat treated and functionalized PS nanofibers.....	124
7.3	Nanofiber properties following functionalization.....	125
7.4	DSC and rheology results for carboxylic acid modified carbon nanofiber polymeric nanocomposites.....	126
7.5	DSC and rheology results for carboxylic acid modified carbon nanofiber polymeric nanocomposites.....	127



## LIST OF SYMBOLS

$\alpha$	thermal diffusivity
$\varepsilon$	applied strain
$\rho$	density, electrical resistivity
$\sigma$	electrical conductivity, applied stress
$A$	cross-sectional area, effective area of measuring electrode
$BE$	photoelectron binding energy
$C_p$	specific heat
$E$	elastic modulus
$f_s$	work function
$h_n$	X-ray photon energy
$I$	current
$K$	thermal conductivity
$K_s$	partition coefficient
$KE$	kinetic energy
$L$	thickness, distance between leads
$P_v$	volume resistivity
$R, R_v$	resistance
$T_g$	glass transition temperature
$t$	thickness
$t_{1/2}$	time at half maximum voltage
$V$	voltage, volume
$V_N$	net retention volume
$W_s$	sample mass

## CHAPTER I

### INTRODUCTION

The definition of a nanocomposite material is a system of distinctly dissimilar components mixed at the nanometer scale to generate a new material with novel properties. These properties are derived by combining properties from the parent constituents into a single material. Pure materials are limited in applications by their inherent properties. For example, polymeric materials are limited in applications by their inherent low thermal conductivity, low thermal stability, high electrical resistivity, and ductile mechanical properties. Similarly, ceramic materials are limited in their inherent low thermal conductivity, high electrical resistivity, low toughness, and brittle mechanical properties. All pure materials have limited applications, and the addition of a filler material can lead to enhanced properties.

Several approaches have been taken to modify the properties of a pure material. Present day fiber-reinforced composites constitute the incorporation of a micrometric filler material to a host matrix. This type of filler material improves mechanical properties, but does not improve the chemical properties of the material. A nanometric filler should act as a modifier to change both chemical and physical properties. An ideal nanometric additive should have inherent

chemical and physical properties that are beneficial to the host matrix. Periodic Table Group IV elements including carbon, silicon, etc. represent materials that have the ability to form strong  $sp^2$  bonds, thereby forming the basis for materials with strong mechanical properties, and high electrical and thermal conductivity.

The properties of nanocomposite materials depend not only on the properties of their individual parents but also on their morphology and interfacial characteristics. Three basic shapes are predominant among carbon nanofiller materials – spherical, lamellar, and cylindrical. The spherical shape hinders the ability to adhere to the host matrix. Lamellar structures will shear under certain stress applications. A cylinder represents a mix of these two shapes that will provide increased sites for adhesion to a host matrix, and a single cylinder will not shear under stress. Carbon nanofibers consist of a cylindrical shape and possess significantly high mechanical, thermal and electrical properties.

Research on vapor grown carbon fibers has increased in recent years partly due to the discovery of carbon nanotubes. Such fibers are characterized by an extraordinarily high tensile modulus and tensile strength and high electrical and thermal conductivity. A decrease in the diameter of a vapor grown carbon fiber causes gradual improvement in mechanical properties. As the fiber diameter reaches the threshold value of  $0.1\mu m$ , characterizing the transition from a fiber to a nanofiber, the improvement in mechanical properties becomes more significant. Vapor grown carbon nanofibers can be prepared with diameters ranging from 15nm to 100nm. Their morphology resembles that of carbon

nanotubes. Nanofibers can have a number of different internal structures, wherein graphene layers are arranged as concentric cylinders, nested truncated cones, segmented structures, or stacked coins. External morphologies include kinked and branched structures with diameter variation. The percolation threshold for carbon nanofibers is low indicating that only a small amount of nanofiber additive is required for conducting filler applications. The intrinsic stiffness and strength of carbon nanofibers, combined with superior transport properties, present the opportunity to develop multifunctional nanofiber composites with tailored physical and mechanical properties.

Experimental results from previously published research efforts indicate that carbon nanofibers are suitable reinforcing agents for polymers. Lozano and Barrera demonstrated a 100% increase in the dynamic mechanical properties with only two weight percent carbon nanofibers in a polypropylene matrix [1]. Other work by Kuriger et al. indicated a 50% increase in tensile strength with a higher loading of carbon nanofibers in polypropylene [2]. Patton et al. combined carbon nanofibers with an epoxy and poly(phenylene sulfide) to improve the flexural properties of the matrix materials, obtaining 68 and 91% increases in the flexural strength in epoxy and poly(phenylene sulfide), respectively, with a nominal nanofiber loading of twenty percent by volume [3].

The limitations of nanometric additives can be broken into two categories. The first is related to material production – the currently high cost of mass production, the lack of production control over the range of resulting material

configurations, and residual impurities formed during production. The second is the ability to incorporate the nanometric additive into a host matrix seamlessly. Nanofillers tend to agglomerate – incomplete dispersion of the material will form inclusions in the host matrix and reduce the benefit of the filler. The nanofiller must adhere to the host matrix – poor adhesion will cause the nanofiller to act as a defect in the continuous phase.

Fiber functionalization is considered necessary to improve mechanical properties in nanofiber-reinforced composites by increasing the stress transfer between the nanofiber and the matrix of a nanocomposite structure. Fiber-matrix adhesion is governed by the chemical and physical interactions at the interface. Poor fiber-matrix adhesion will result in composite failure at the interface, resulting in decreased longitudinal and transverse mechanical properties of the composite. While a number of methods to functionalize micrometric additives for improved adhesion have been established, these processes cannot simply be transferred to the nanometric scale due to the increased surface area and surface energy of the nanofiller materials. In addition, while a micrometric material can be “held” in place during a functionalization process, the same cannot be easily achieved for a nanometric material.

As a part of this thesis, there were three major modifications to carbon nanofibers to improve nanocomposite properties. The first was to identify and test purification and cleaning processes to remove organic volatiles and inorganic impurities from the nanofiber surface. The second was to examine the effect of

heat treatment temperature on nanocomposite properties. The third was to functionalize the surface of the carbon nanofiber to improve nanofiber adhesion to the matrix. A combination of all three of these techniques will allow for a modification in the nanofiber structure and bonding characteristics to improve nanocomposite properties.

## CHAPTER II

### BACKGROUND AND LITERATURE REVIEW

#### 2.1 *CARBON FIBERS AND NANOFIBERS*

In recent years, ultrahigh-strength carbon nanofibers have made their way from scientific laboratories into industry. Nanofibers are comprised of ultra thin carbon fibers, each less than  $0.1\mu\text{m}$  in diameter. Such fibers are characterized by an extraordinarily high tensile modulus and tensile strength. Other important properties of carbon nanofibers are their high electrical conductivity, extremely high corrosion resistance, invariability of properties over a very wide temperature range (from cryogenic temperatures to more than  $1000^{\circ}\text{C}$ ), and excellent compatibility with living tissues.

Carbon nanofibers are closely related to micron-sized carbon fibers, which are widely used in industry and are produced at an annual rate above ten thousand tons. Micrometric carbon fibers are also a relatively new material, whose properties, in particular, tensile strength, have been greatly improved over the last decade. However, carbon nanofibers are superior to micrometric carbon fibers in many aspects while still having room for improvement.

The most straight-forward method for micrometric carbon fiber production is the charring of natural or synthetic textile fibers in the absence of air. In this

manner, practical use is made of fibers based on viscose or polyacrylonitrile. The production of polyacrylonitrile-based fibers (PAN fibers) now constitutes up to 80% of the global production of carbon fibers. The thickness of polyacrylonitrile-based fibers is on the same order as the thickness of the initial textile fibers – no smaller than 3-5 $\mu\text{m}$ . The properties of polyacrylonitrile-based fibers depend on the parameters of charring, which is performed in several steps and involves stabilization in air at 200-300°C, carbonization in an inert-gas atmosphere at 1200-1400°C, and high-temperature annealing in vacuum or an inert-gas atmosphere at 2000-3000°C [4, 5].

Another important type of fibers is pitch-based fibers, which are produced from coal-tar or petroleum pitches. Fibers are extruded from a dense pitch through spinnerets and are then subjected to heat treatment according to a procedure similar to the heat treatment of polyacrylonitrile-based fibers. Like the polyacrylonitrile-based fiber, the typical diameter of a pitch-based fiber is several micrometers. The properties of these fibers are determined by the properties of the raw material – depending on the type of the pitch used, either isotropic or mesophase fibers are produced.

The third important type of carbon fibers is vapor grown carbon fibers (VGCF). Vapor grown carbon fibers are produced through the pyrolysis of carbon-containing gases (methane, ethylene, acetylene, carbon monoxide, etc.) on a metal (most often iron) catalyst at 500-1500°C [4, 6–8]. Fibers grown by pyrolysis can also be subjected to additional high-temperature annealing in



vacuum or an inert-gas atmosphere at 2000-3000°C [4]. The properties of vapor grown carbon fibers are determined by the growth and annealing conditions. Vapor grown carbon fibers cannot be produced as threads of infinite length. The length of a vapor grown carbon fiber is limited by the growth conditions and can be anywhere from several micrometers to several tens of centimeters. This fact has limited the range of application of vapor grown carbon fibers. The advantage of vapor grown carbon fibers is that their diameter can be arbitrarily small and is limited by the minimum theoretical diameter of a monomolecular carbon nanotube (0.7nm) [7–9]. Nanofibers are vapor grown carbon fibers less than 0.1 $\mu$ m in diameter. At this smaller diameter, the properties of a fiber, particularly its strength, change qualitatively.

The most important mechanical property of fibrous materials is the tensile strength. This value is the maximum tensile stress at which the fiber remains unbroken. Other important mechanical characteristics are Young's modulus (which determines the stiffness of a fiber during stretching) and the ultimate strain (which is the maximum elongation at which a fiber still remains unbroken).

Conventionally, carbon fibers have been classified according to their strength into high-strength ( $\sigma > 3\text{GPa}$ ) and ultrahigh-strength ( $\sigma > 4.5\text{GPa}$ ) fibers; and according to Young's modulus into low-modulus ( $E < 100\text{GPa}$ ), medium-modulus ( $E = 200\text{--}320\text{GPa}$ ), high-modulus ( $E > 350\text{GPa}$ ), and ultrahigh-modulus ( $E > 450\text{GPa}$ ) fibers [5]. This classification is conditional and gradually becoming obsolescent. As these fibers found use in the aerospace industry, account was

also taken of other parameters, such as the ultimate strain of fibers. In addition, polyacrylonitrile-based fibers and vapor grown carbon fibers were created, which combine an ultrahigh strength with an ultrahigh modulus. Therefore, at the present time, a more general classification of fibers into general-purpose (GP) fibers and high-performance (HP-grade) fibers is applied. Nanofibers are simultaneously ultrahigh-strength and ultrahigh-modulus. The strength of nanofibers can reach 20GPa. Table 2.1 shows a comparison of carbon nanofiber mechanical properties to that of steel and silicon. Carbon nanofibers are fifty times stronger than steel and over four times less dense. In addition, carbon nanofibers can sustain up to ten percent tensile strain, and behave as a brittle material at low temperatures and a ductile material at high temperatures. Figure 2.1 shows the significant improvement in tensile strength for carbon nanofibers over that of common present-day carbon and aramid micrometric fibers.

Table 2.1 – Carbon nanofiber mechanical properties and density

<b>Material</b>	<b>Young's Modulus (GPa)</b>	<b>Tensile Strength (GPa)</b>	<b>Density (g/cm<sup>3</sup>)</b>
Silicon	47	1 (brittle)	2.3
Steel	208	0.4 (ductile)	7.8
Carbon Nanofibers	1000	20*	1.8

\*brittle at low temperatures, ductile at high temperatures

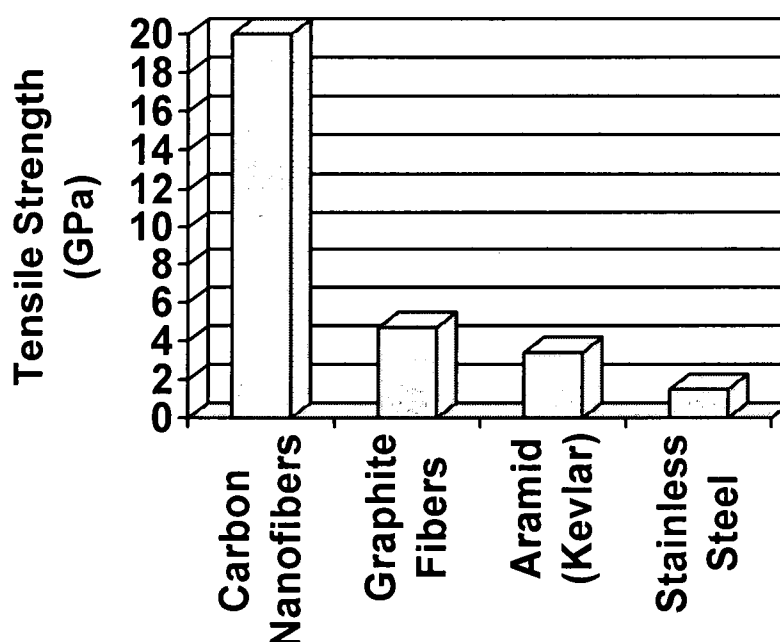


Figure 2.1 – Carbon nanofiber tensile strength

The mechanical properties of carbon fibers, even those of identical origin and equal thickness, can differ considerably from one another. This difference is determined by variations in the fiber structure.

Mesophase pitch-based fibers consist of straight graphite strips or flakes aligned with the fiber axis. At a cross section, these flakes can form various packings – stellar, stratified, or random. Such a structure provides for high fiber stiffness, since, along a fiber, there are practically no elements that can be stretched. However, the strength depends entirely on the length of flakes, making a high strength difficult to ensure. These observations are fully consistent with data showing that pitch-based fiber can be high-modulus but not high-strength.

Polyacrylonitrile-based fibers have a more complex structure and consist of many tubular elements combined into a three-dimensional structure. Such a structure provides high strength due to the overlap of tubular elements, but its high stiffness is difficult to preserve solely by increasing the structure density and decreasing the total pore volume.

Vapor grown carbon fibers consist of many tubes inserted into one another and have a hollow core. High-temperature annealing causes the slightly ordered carbon layers of tubes to crystallize into graphite flakes several micrometers in size and transforms the round tubular elements into polyhedral ones. Such a structure could ensure a high stiffness in combination with a high strength, provided that there is strong adhesion between concentric tubes. However, this adhesion is actually weak and the most typical failure of a vapor-grown carbon fiber can be likened to a sword being pulled from a sheath. As a result, vapor-grown carbon fibers are characterized by a very wide scatter in their properties and low reliability.

Nanofibers, like micron sized vapor-grown carbon fibers, have a tubular structure. However, the difference between them is not only in their respective scales but also in the fact that tubes constituting a nanofiber are monomolecular objects.

In forming a carbon tube from a graphite sheet, the graphite sheet is rolled up so that the upper and lower edges coincide to form a cylinder. This is accompanied by a shift due to a band of carbon hexagons inserted into the tube

around which to form a coil. If the sheet is rolled up in other directions, tubes of different diameter and pattern will be produced. Due to a high strength and the conjugation of bonds in a graphite sheet, this sheet is a single planar molecule with an extraordinarily high tensile modulus (1000GPa) and high tensile strength (20GPa) [8, 9]. However, in graphite crystals, individual sheets are bonded to one another by very weak van der Waals forces. As a result, the graphite is extremely brittle and breaks down at a shear stress of only 0.48MPa [8, 9]. A carbon nanotube rolled up from a graphite sheet inherits the high mechanical properties of the sheet and all the advantages of any tubular structure. A defect free carbon nanotube has a tensile modulus of 1800GPa and minimum strength of 30GPa, which exceeds the parameters of single-crystal diamond whiskers. The closer a nanofiber structure is to the described ideal model and the longer an individual fiber, the closer the fiber strength is to theoretical values.

A decrease in the diameter of a vapor grown carbon fiber causes gradual improvement in mechanical properties. As the fiber diameter approaches the threshold value 0.1 $\mu$ m, which characterizes the transition from a fiber to a nanofiber, this becomes more significant. Nanofibers can consist of nanotubes with one to one hundred tubular monomolecular layers.

Methods for producing nanofibers are the same as methods for manufacturing ordinary vapor grown carbon fibers. A carbon-containing gas (methane, ethylene, acetylene, carbon monoxide, benzene or ethanol vapor) is decomposed on a metal (iron-based) catalyst at 500-1500°C [4, 6–8]. The

carbon containing component is usually mixed with hydrogen. Manufacturers usually do not divulge details of the process; however, the main principles of the process are described in sufficient detail, as they have been worked out over the last twenty years at several competing scientific centers [7, 8, 10-17].

The largest contribution to the process development of carbon nanofiber production has been made by the Endo Laboratory, Shinshu University, Japan [7, 8, 11, 12]. This process is performed by one of two methods whereby fibers are grown either on a substrate or in a gas flow. In the method for growing nanofibers on a substrate, a catalyst must be applied on a graphite or ceramic substrate. For this purpose, the substrate is painted with an iron paint, which is a suspension of fine iron powder in an organic solvent, where the solvent is removed by evaporation. Another method of catalyst application is the spraying of a solution of iron compounds (nitrates, ferrocene, etc.) onto a substrate with the subsequent decomposition of these compounds by heating in hydrogen to form metallic iron. In addition, iron containing organometallic compounds can be introduced directly into the reactor – their decomposition results in the deposition of iron particles onto a substrate placed into the reactor beforehand. With the method for growing nanofibers in a gas flow, a carbon-containing gas must be supplemented with a volatile iron compound (iron carbonyl or ferrocene). Another method for introducing a catalyst into the reaction zone during nanofiber growth in a gas flow involves the injection of a suspension of a fine iron powder in an organic solvent directly into the reactor. In all of the cases, a catalyst

particle is trapped by a growing fiber and each fiber ends with a metal microcrystal cap. An advantage of the method of growing nanofibers on a substrate is that the length of nanofibers grown by this method (up to several tens of centimeters) is much larger than the nanofiber length (several millimeters) achieved by the method of growing nanofibers in a gas flow. However, a large drawback of the process is that it is not continuous.

The purity of the gas affects catalyst activity. The presence of water vapor at a concentration of several tens of parts per million decreases the reaction yield and the fiber length. Purification is particularly important if the carrier gas is not hydrogen, but rather the products of the steam-air reforming of methane [14, 15]. The gas composition can affect the nanofiber thickness and structure. In particular, nanofibers with a nontubular structure can form. The effect of gas composition on the structure of the product is best illustrated by the effect of a small amount of phosphorus impurity [17]. It was shown that the pyrolysis of acetylene containing phosphorus impurity gives rise to coiled nanofibers, which are a kind of microscopic spring. Such nanofibers are not high-strength, but their elasticity is close to that of ordinary rubber.

The particle size of the catalyst has a substantial effect on both the yield and rate of the reaction, as well as nanofiber thickness. For nanofiber growth to be efficient, the diameter of a catalyst particle must be no larger than 20nm. The average rate of nanofiber growth on a catalyst with particles of 10-20nm is 1mm/min, whereas the rate of increase in thickness is 1-2nm/min [4]. The

lengthening and thickening of nanofibers do not take place simultaneously. Lengthening requires a lower temperature. An increase in the temperature of the process and a decrease in the catalyst activity cause the nanofibers to thicken, thereby transforming them from nanofibers into ordinary micron-sized vapor grown carbon fibers [12]. The practically important problem of growing nanofibers of the maximum possible length is solved by controlling the temperature conditions of the reaction and by ensuring higher catalyst stability. This prevents thickening of nanofibers (their transformation into micron-sized fibers) and prolongs the growth stage –consequently, increasing the fiber length.

The percolation threshold for carbon nanofibers is low indicating superior transport properties. Table 2.2 compares the electrical and thermal properties of carbon nanofibers to graphite and copper. The theoretical electrical resistivity and thermal conductivity of carbon nanofibers are on the same magnitude as that of graphite, but show a significant improvement over copper which is used in many present-day thermal and electrical applications.

Table 2.2 – Carbon nanofiber electrical and thermal properties

<b>Property</b>	<b>Carbon Nanofibers</b>	<b>Graphite</b>	<b>Copper</b>
Electrical Resistivity ( $\Omega$ -cm)	$10^{-5}$	$2.5 \times 10^{-6}$ to $3.0 \times 10^{-3}$	$1.7 \times 10^{-4}$
Thermal Conductivity (W/m-K)	~1900	1180	400

Carbon nanoparticulates are often contaminated with metal catalyst, sulfur and nitrogen containing substances following processing. These impurities negatively influence the properties of the carbon nanoparticulates thereby limiting

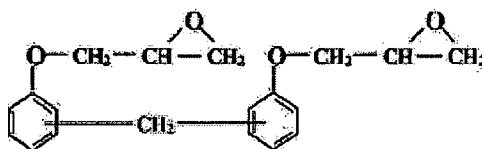


their applications. There are several purification techniques in literature and a commonly followed purification method involves thermal and/or acid oxidation treatment [18]. To reduce the damage caused by direct oxidation, non-conventional methods have been studied such as filtration [19], chromatography [20], microwave irradiation [21], and polymer-assisted purification [22, 23].

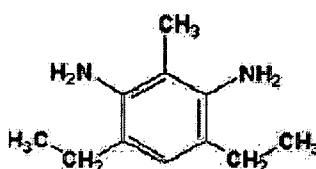
## 2.2 EPOXY RESIN

EPON 862/EPI-CURE Curing Agent W resin system consists of a diglycidyl ether of bisphenol-F (DGEBF) monomet and an aromatic amine; it has been used extensively in aerospace composite research and resin-infusion and filament winding applications. EPON 862 is a relatively low molecular weight difunctional epoxide formulated from the reaction of epichlorohydrin and bisphenol-F. The main ingredient of EPI-CURE Curing Agent W is diethyltoluenediamine (DETDA) – an aromatic amine curing agent. The chemical structures of both materials are shown in Figure 2.2.

This epoxy system has a high glass transition temperature and involves non-MDA aromatic amines. The cured neat resin properties as a function of cure schedule are presented in Table 2.3. The low viscosity feature of the resin system permits low injection pressures, less fiber washout, high fiber loading, and lower mold costs for resin transfer molding (RTM) composite fabrication. The long working life and low viscosity of the materials make it suitable for filament winding composite fabrication processes. The resulting epoxy yields high mechanical, adhesive, electrical and chemical resistance properties.



(a)



(b)

Figure 2.2 – Chemical structure of (a) EPON 862 epoxy and  
(b) EPI-CURE Curing Agent W

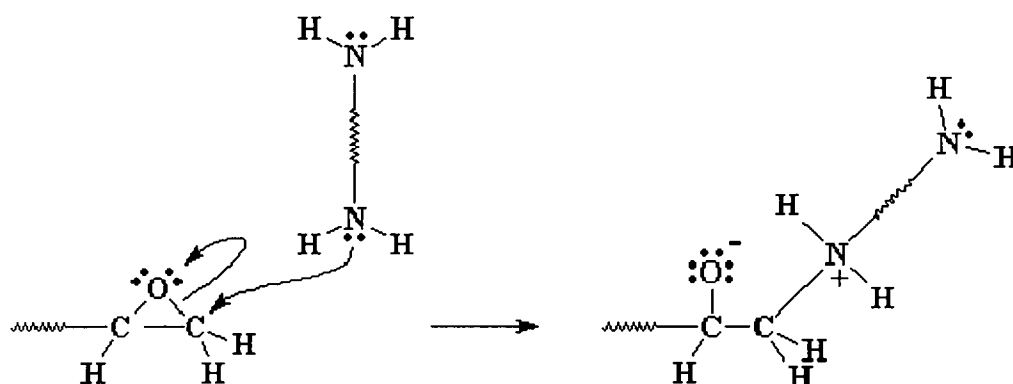
Table 2.3 – Cured neat resin properties of the EPON 862 / W as a function of  
cure schedule [24]

Cure schedule, hrs at 350°F	0.5	1.5	2.5
Density, g/cc	-	1.2003	-
Glass transition temperature, °F	266	302	322
Fracture toughness, psi-in <sup>1/2</sup>	528	657	820
Flexure strength, ksi	No failure	12.5	18.6
Flexure modulus, ksi	458	433	424
Flexure elongation, %	No failure	7.9	8.3
Water absorption, wt%	2.2	2.1	2.1

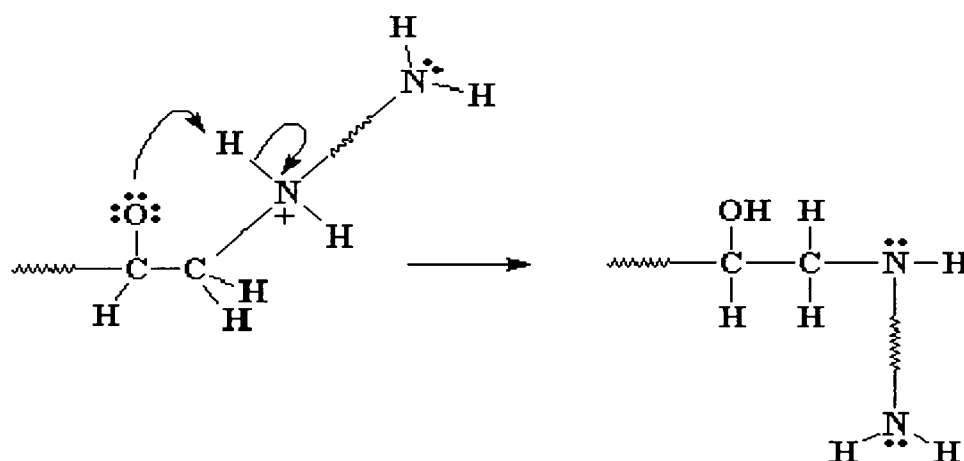
Cure schedule, hrs at 250°F	4	8
Glass transition temperature, °F	235	273
Fracture toughness, psi-in <sup>1/2</sup>	541	583
Flexure strength, ksi	18.4	18.0
Flexure modulus, ksi	496	455
Flexure elongation, %	7.5	8.5
Water absorption, wt%	8.2	8.5

The reaction of the diamine curing agent and the epoxy can be outlined in four main steps:

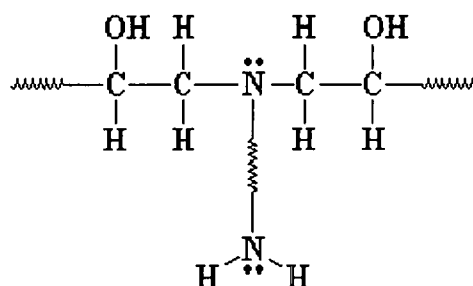
- 1- The diamine's electrons attack the carbon atom next to the epoxide oxygen, giving a negative charge on the oxygen, and a positive charge on the nitrogen.



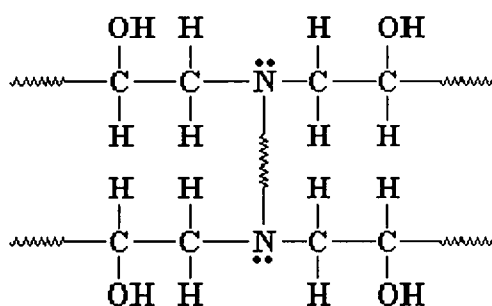
- 2- The oxygen's extra pair of electrons swipes a hydrogen from the ammonium nitrogen, making an alcohol group and an amine group.



3- Another epoxide end group adds to the same amine group.



4- Then two more epoxide groups add to the amine at the other end of the diamine, eventually tying all the diepoxy oligomers into one big molecular network.



## 2.3 CARBON NANOFIBER REINFORCED POLYMERIC NANOCOMPOSITES

In advanced composites, there has been considerable effort to improve the physical properties of reinforcing fibers and the adhesive properties between the matrix and fiber [25, 26, 27]. A novel approach has been proposed to dramatically enhance the mechanical, thermal, and electrical properties of the neat resin matrix with the inclusion of carbon nanofibers. Transferring these

improved characteristics of the polymeric resin into advanced composites will serve as the beginning of the next generation of advanced composites.

The percolation threshold for carbon nanofibers is low indicating that only a small amount of nanofiber additive is required for conducting filler applications. The intrinsic stiffness and strength of carbon nanofibers, combined with these superior transport properties, present the opportunity to develop multifunctional nanofiber based polymeric composites with tailored physical and mechanical properties. The walls of nanofibers are comprised of exposed graphitic planes increasing the surface area available for bonding thereby allowing a greater degree of interaction between the nanofiber and the resin matrix. Orientation and effective dispersion of the filler improves the physical properties of the resulting nanocomposite.

Through the use of a twin-screw extruder Ma et al. achieved good dispersion of carbon nanofibers in poly(ethylene terephthalate) (PET) resin resulting in a limited improvement of mechanical properties [28]. The as-grown (AG), pyrolytically-stripped (PS), and two AG surface functionalized Pyrograf III nanofibers were used in this study. The PS nanofibers had their outer layer of deposited amorphous carbon – the result of carbon vapor deposition – removed. The carbon nanofibers were added to PET powder and dry-mixed by ball-milling or hand mixing. All of the nanocomposite samples contained five weight percent nanofibers. The mixture was then vacuum dried and melt mixed through a twin extruder and spun into fibers. The two surface functionalized nanofibers were

oxidized resulting in a surface chemistry consisting of oxygen and sulfur groups along with the carbon. Even with the addition of functional groups to the surface of the nanofibers, the tensile moduli were only slightly higher than that of the neat PET resin, and the tensile strengths of the nanocomposites were the same or slightly less than the neat resin. The authors claimed that the poor results with the nanofiber addition to the PET were due to the off-axis orientation of the graphitic planes within the individual nanofibers.

Kuriger et al. used the combination of twin-screw extrusion along with an annular die to disperse and orient the nanofibers within polypropylene to improve the mechanical, thermal and electrical properties of the thermoplastic [2]. Two different Pyrograf III nanofibers were used in this study – PS and heat treated PS (HHT). Using X-ray diffraction the orientation of the nanofibers within the final nanocomposite was measured showing that as the amount of carbon nanofiber was increased from 2.5 volume percent to 23 volume percent, the degree of orientation decreased. This was attributed to an increase of the nanofiber-nanofiber and nanofiber-wall interactions that hinder the ability of the nanofiber to orient in the direction of flow. At 11 volume percent the tensile strength was 20% greater when the nanofibers were oriented. This represented a 100% improvement over the neat polypropylene resin.

Applied Sciences Incorporated, producers of Pyrograf III carbon nanofibers, conducted a study involving the inclusion of two different diameter Pyrograf III nanofibers into powdered polypropylene and polyamide 66 to

enhance the electrical and mechanical properties of the resin [29]. Three different grades of each nanofiber were used in this study – AG, PS and HHT. Improved mechanical properties due to graphitization of the nanofibers did not translate into an increased tensile strength for the nanocomposites; however, the heat treatment caused the exposed graphitic planes to become ordered reducing the surface area available for wetting by the resin. A reduction in interfacial area between the two phases adversely affected the ability of the resin to transfer load to the filler decreasing the mechanical properties of the nanocomposite.

Patton et al. investigated using a carbon nanofiber and phenolic resin composite as a replacement material in solid rocket motor nozzles [30]. In order for the nanocomposite to be a successful replacement, the material must be able to maintain its physical integrity under extreme temperatures and pressures. These properties were measured via ablation testing. Using a processing technique used in creating epoxy nanocomposites [3] there was a decrease in the mechanical properties of the nanocomposites. This difference can be attributed to the change in resin matrix and the phenolic resin's inability to form an effective interface with the carbon nanofiber. Weight percentage or processing technique of the nanofiber had little influence upon the thermal conductivity of the nanocomposite. The thermal conductivity was consistently double that of the phenolic resin at all loading rates. The ablation tests revealed that the phenolic nanocomposites do provide possibilities as a replacement material as they had lower weight losses and lower load changes when

compared to the currently used baseline. One measure in which the nanocomposite did fail to exceed the baseline was that of erosion rate.

## **2.4 CARBON SURFACE FUNCTIONALIZATION AND ITS EFFECT ON COMPOSITE PROPERTIES**

Nanofiber functionalization is considered necessary to improve mechanical properties in nanofiber-reinforced composites by increasing the stress transfer between the nanofiber and the matrix of a nanocomposite structure. Nanofiber-matrix adhesion is governed by the chemical and physical interactions at the interface. An extensive literature exists on surface treatment of conventional carbon fibers by methods such as oxidation in gas and liquid phases and anodic etching. Poor fiber-matrix adhesion may result in composite failure at the interface, resulting in decreased longitudinal and transverse mechanical properties of the composite.

### **2.4.1 HEAT TREATMENT OF CARBON NANOPARTICULATES**

Graphitization is an effective method of removing defects from carbon nanofibers that diminish their electrical and mechanical properties. The structure of the initial carbon generally determines the physical properties of graphitized carbon materials due to the thermally activated kinetic process of graphitization. It is important to understand graphitization behavior for carbon nanofibers because structural changes, purification, and enhanced structural perfection by heat treatment may improve a specific application of the nanofibers.

Endo et al. [31] heat treated stacked cup type carbon nanofibers from 1800 to 3000°C to examine structural changes. The truncated cones cause a



high chemical reactivity in the outer surface and the inner hollow core because these end planes of graphene layers are active edge sites. Heat treatment to 3000°C resulted in transformation to a rugged surface and the formation of energetically stable loops between adjacent graphene layers from the unstable edge planes in both the outer surface and the inner hollow cores. Examination of the fibers by X-ray diffraction and Raman spectroscopy identified that the interlayer spacing of the graphitized samples increased possibly due to the large number of loop formations between adjacent graphene layers. The absence of separation of (101) and (100) lines and low intensity of (004) lines indicated that the nanofibers achieved relatively low graphitizability following heat treatment to 3000°C. The formation of loops began below 2100°C and was followed by few changes up to 3000°C on the outer surface of the carbon nanofibers. With increasing heat treatment temperature, there was a progressive decrease in the electrical resistivity in the bulk state for carbon nanofibers due to the amount of loops, especially on the outer surface of the carbon nanofibers. There was a significant decrease in the electrical resistivity from the as-grown nanofiber to the nanofiber heat treated to 1800°C due to the evolution of volatile material.

Katayama et al. examined the effect of heat treatment on multiwall carbon nanotubes with bamboo-like structures [32]. Heat treatment at 2800°C reduced the interlayer spacing to that of graphite. In addition, encapsulates in the bamboo-structure with a small diameter were opened, and metal impurities were entirely removed from the nanotube. The decrease in interlayer spacing lies in

contrast to the observance reported by Endo et al. for stacked cup type carbon nanofibers heat treated to 3000°C.

Kiselev et al. examined by high resolution electron microscopy the structural changes to multiwall carbon nanotubes following heat treatment [33]. Links formed between the neighboring open edges by loops along the tube sides on both the insides and outsides of the nanotubes. The radii of curvature of the loops were noted at 1.05-1.40nm which is close to the diameter of single wall nanotubes. The degree of carbon layer linking was dependent on the temperature of the heat treatment. After treatment at 1200°C, only a small amount of linked layers were observed along the external sides. At treatment above 2000°C, the number of loops per unit volume increased and loops were observed on both the external and internal surfaces.

A number of results have been reported on the effect of heat treatment of carbon nanofibers on nanocomposite properties. Xu et al. included nanofibers heat treated to 3000°C in an examination of electrical properties of vinyl ester nanocomposites [34]. The percolation threshold was found to be between two and three weight percent nanofiber loading. The heat treated nanofibers were better electrical conductors than pyrolytically stripped nanofibers. The higher surface activity of the heat treated nanofibers should lead to thicker resin coating and more complete resin infusion into the nanofibers during mixing. However, the measured flexural modulus of the nanocomposite was equal to that of the pure resin. This may have been due to poor nanofiber dispersion or adhesion to

the matrix. In addition, the measured glass transition temperature of the nanocomposite with heat treated nanofibers was nearly 20°C higher than that of the nanocomposite with pyrolytically stripped nanofibers.

Finegan et al. [35] noted that nanofibers of higher graphitization index tend to make composites having both lower strength and modulus. Graphitized nanofibers projected much further from the fracture surface of a polypropylene nanocomposite than air-etched nanofibers implying that the interfacial shear strength of the graphitized nanofibers was significantly lower. The polymer did not appear to wet the nanofiber surface in both cases, indicating that low interfacial strength is not singularly dependent on surface wetting. The results from this study may have been impacted by ball milling of all nanofiber samples resulting in lower nanofiber aspect ratios.

Kuriger et al. examined the thermal and electrical properties of heat treated nanofiber reinforced polypropylene nanocomposites [2]. The electrical resistivity decreased with nanofiber volume fraction. This is governed by percolation and quantum mechanical tunneling between the nanofibers. The electrical resistivity was significantly lower than glass fiber reinforced polymers. The thermal conductivity increased with nanofiber loading, and reached a maximum in the longitudinal direction with 23% nanofiber volume fraction.

Ma et al. included heat treated nanofiber reinforced polyester nanocomposites in their study of nanocomposite properties [28]. Bulk analysis of the nanofibers showed that heat-treatment removed nearly all of the oxygen

groups located on the surface of the nanofiber. Thermogravimetric analysis showed that the onset of degradation for nanofibers heat treated at 3000°C was nearly 700°C compared to approximately 300°C for as-grown nanofibers. The tensile modulus of the nanocomposite was slightly higher than that of the neat resin, and the tensile strength was comparable to the neat resin and significantly higher than its pyrolytically stripped nanofiber based nanocomposite counterpart. The inability of the heat treated nanofibers to improve the tensile properties of the neat resin may be due to the encapsulation of the ends of graphitic planes removing potential bonding sites. In addition, the heat treated nanofibers were ball milled leading to attrition of the nanofiber aspect ratio which is detrimental to the tensile properties. The compressive strength and torsional modulus of the heat treated nanofiber based nanocomposite was significantly higher than that of the neat resin. The nanofibers may have acted as a barrier to kink propagation, thereby improving compressive properties.

Lim et al. studied "stacked coin" type nanofibers and the impact of mechanical and chemical treatments on the morphology of the nanofibers [36]. Heat treatment at 2800°C induced closed loop ends on the surface of the nanofibers formed by folding of some planar hexagons at their edges. The heat treatment removed C-H bonds and densely stacked hexagonal layers of graphene, forming chemically active sites on the edges. The edges were stabilized by bonding to each other, even though the bonding caused high tension through the formation of a sharp curvature. Acidic oxidation of the

nanofibers cut off the closed looped ends, resulting in improved overall alignment of graphene layers. Both treatments generated many free edges and a high graphitization extent, indicating the possibility of improved interfacial bonding with a polymer matrix.

#### **2.4.2 CHEMICAL TREATMENT OF NANOMETRIC AND MICROMETRIC CARBON**

Toebe et al. [37] examined the effect of liquid phase oxidation of carbon nanofibers in nitric acid and mixtures of nitric and sulfuric acid for times up to two hours. The graphitic structure of the nanofibers was not altered by the treatments, but the texture of the nanofibers was significantly changed through an increase in the specific surface area and pore volume due to opening of the nanofiber inner tubes. The total oxygen content and surface oxygen functional groups was affected by the treatment time and acid type. Oxygen groups formed in the first 2-3nm of the sub-surface of the nanofibers.

Bubert et al. [38] investigated the influence of plasma treatment on the surface properties of carbon nanofibers by X-ray photoelectron spectroscopy (XPS) in combination with ion sputtering, acid-base titration, derivatization of carbonyl groups, pyrolysis and CH analysis. The results indicated that the nanofiber surface was covered by a monomolecular oxygen-containing layer and that plasma treatment allowed complete oxygen functionalization of the uppermost surface layer. XPS provided an average value for the content of functional groups of the first ten to fifteen molecular layers.

A number of results have been reported on the effect of chemical modification of carbon nanoparticulates on nanocomposite properties. Xu et al. included a nitric acid-oxidized nanofiber reinforced vinyl ester in an examination of electrical properties of nanocomposites [34]. The resistivity of the oxidized nanofiber based nanocomposites was much higher than those produced with untreated nanofibers. The oxidation was reported to have increased oxygen percentage by approximately 20% with the addition of anhydride, quinine, ether, and ester functional groups. The oxidized layer could reduce electrical conductivity through percolation pathways. The functional groups also should improve wetting by the polymer matrix. A strong bond between the matrix and the nanofiber could encase the nanofiber and serve as an insulating covering.

Finegan et al. [35] examined the mechanical properties of carbon nanofiber reinforced polypropylene nanocomposites in an attempt to optimize carbon nanofiber surface treatment. The fiber-matrix adhesion was qualitatively studied by scanning electron microscopy (SEM), and the strength and stiffness of the nanocomposites were evaluated from tensile tests. One sample of nanofibers was oxidized in air at 450°C and a second sample was oxidized with carbon dioxide in a tube furnace. Nanofiber adhesion to the matrix was improved by moderately oxidizing the nanofibers in either air or carbon dioxide. The carbon dioxide oxidation was more effective as it increased the external surface area and the surface energy of the nanofibers. However in the preparation of the nanocomposites, the nanofibers were either ball milled or force-sieved, thereby

possibly altering the nanofiber aspect ratios resulting in decreased mechanical testing results.

Cortes et al. [39] exposed carbon nanofibers to a series of chemical treatments in nitric acid prior to mixing with polypropylene. The oxidized nanofiber based nanocomposites did not improve electrical properties of the polymer, and did not produce significant changes in the mechanical properties of the nanocomposites, actually showing a decrease in tensile strength. The nanocomposites produced only had five weight percent nanofiber compositions. Higher nanofiber content may have lead to increases in the mechanical properties of the composites.

In conventional carbon fiber-reinforced composites, there have been a number of studies completed to generate strong adhesion between the fiber surface and matrix to improve stress transfer from the matrix to the reinforcing fibers. Continuous surface electrochemical oxidation has been the preferred method of fiber surface treatment to enhance interfacial bonding. Electrochemical treatments have been carried out in acid and alkaline aqueous solutions of ammonium sulfate, ammonium bicarbonate, sodium hydroxide, diammonium hydrogen phosphate, and nitric acid.

Anodic oxidation of fibers in electrolytes can produce a variety of chemical and physical changes in the fiber surface. Harvey et al. [40] examined surfaces of conventional carbon fibers by XPS after electrochemical treatment by galvanostatic and potentiostatic cell control under varying potential, reaction time,

and electrolytes. The authors noted that the rise in interlaminar shear strength (ILSS) with surface treatment was not dependent on O 1s : C 1s ratios or the amount of carboxyl functionality on the surface, thereby supporting the view that mechanical keying of the resin to the fiber surface plays an important role in forming the resin-fiber bond.

Gulyas et al. [41] subjected PAN based carbon fibers to electrochemical oxidation under a wide variety of conditions – varying electrolyte, electrolyte concentration, and applied voltage. The functional groups formed on the surface of the fibers was dependent on the type of electrolyte used, and the number of functional groups found on the fiber surface was dependent on electrolyte concentration and voltage. A close correlation was found between surface chemistry and adhesion between the fiber and matrix. The concentration of certain functional groups could be quantitatively related to ILSS.

Yue et al. [42] continuously electrochemically oxidized high strength PAN based carbon fibers in one percent by weight potassium nitrate. Fiber weight loss increased with electrochemical oxidation. A large internal microporous surface area was generated due to the formation of acidic functions. XPS indicated that the concentration of oxygen within the outer 50 Angstroms of the fibers increased on oxidation. XPS C 1s and O 1s spectra showed an increase in primarily carboxyl or lactone groups. The oxygen-rich surfaces in the microporous regions chemisorbed oxygen and water. The O 2s – C 2s peak



separation increased in the valence band spectra as the extent of oxidation increased due to carbonyl group contribution.

## 2.5 *METHODS FOR CARBON SURFACE FUNCTIONALIZATION*

Carbon surface modification plays a fundamental role in the application of organic and inorganic supports in industrial and environmental processes, such as selective purification processes, gas separation, solvent recovery, drinking water purification, adsorption of taste, odor and other micro-pollutants, ion exchange properties for metal adsorption, catalyst preparation, adhesion phenomena, electrode modification and polymer technologies. Much effort has been expended over the last several decades to modify the surface chemistry of carbon materials. While it is possible to deposit physically absorbed material onto the surface of a carbon material, permanently changing its surface chemistry is substantially more difficult. Modification of carbon surfaces is an important objective in electrochemistry and material science. Most important from the industrial point of view is the surface modification of carbon fibers aiming to improve the mechanical properties of carbon composite materials, particularly carbon-epoxy composites. These mechanical properties depend not only on the intrinsic characteristics of each of the components but also on those of the interface between them. It is thus anticipated that chemical modification of the carbon surface may improve the properties of the composite. In this connection, chemical binding of the carbon surface with the epoxy resins commonly used in the manufacturing of composites is of particular interest.

The carbon black industry has attempted to improve carbon black dispersibility by oxidative after-treatments. All carbon blacks contain some chemisorbed oxygen complexes on their surface. However, further oxidation of the carbon black surface increases the volatile content of the carbon black. The term volatile is used because under high temperature baking (at about 900°C) these groups are almost completely removed. The volatiles are believed to consist of a mixture of carboxylic acids, alcohols, epoxides, ketones and other groups.

Presumably, one or more surface groups contribute to enhanced interactions between the additive surface and the dispersants or resins in industrial formulations. The chemical modification of the carbon black surface has shown that certain treatments significantly increase the speed and stability of carbon black dispersion in a variety of coating media. It is important to note that the base carbon black is not changed but that its surface properties are modified. The treatment process allows control of the amount and type of chemical groups placed on the surface of the carbon black.

Since covalent bonds attach the groups to the carbon black surface, they cannot be desorbed into the formulation. This ensures that the treatment will not interfere with the function of other additives or the performance of the composite materials [43].

### 2.5.1 THE DIAZONIUM FORMATION REACTION

One of the processes for preparing a product having an organic group covalently attached to a carbon material is the diazonium formation reaction [19, 20, 22, 44–48]. This chemical reaction applies to products such as graphite powders, graphite fibers, carbon fibers, carbon mats, carbon blacks, and carbon nanoparticulates. The diazonium salt is a general description of any class of organic compounds that have a diazonium ion as shown in Figure 2.3. This compound is generally unstable above 10°C.

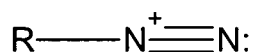
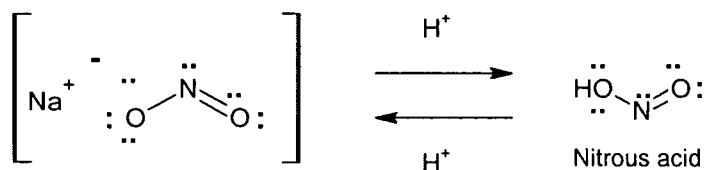


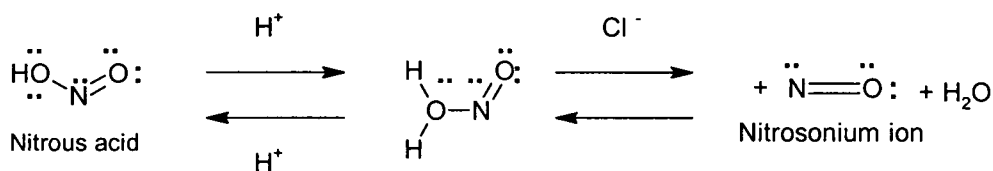
Figure 2.3 – Chemical structure of diazonium ion

The diazonium salt formation reaction mechanism includes three main steps:

- 1- Formation of nitrous acid by the reaction of sodium nitrite ( $\text{NaNO}_2$ ) and a strong acid such as hydrochloric acid ( $\text{HCl}$ ) or sulfuric acid ( $\text{H}_2\text{SO}_4$ ):

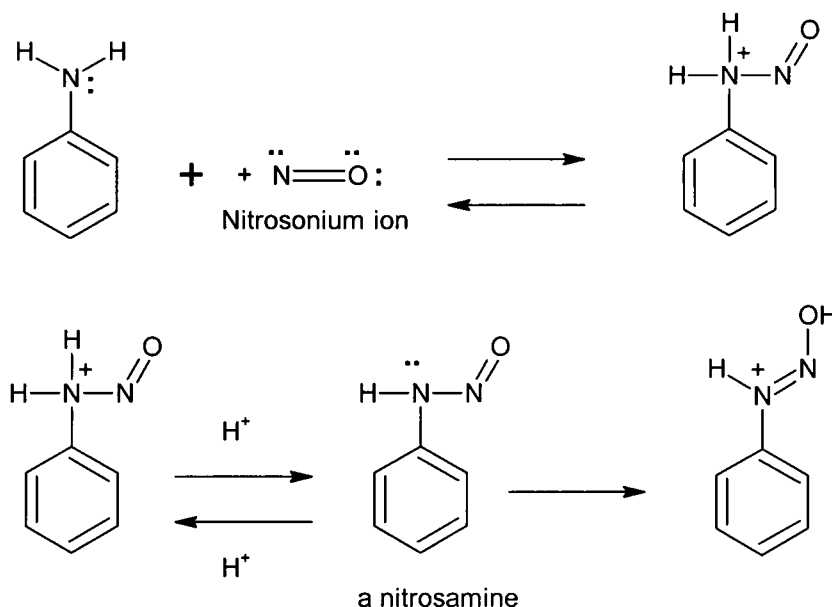


- 2- The formation of a nitrosonium ion:

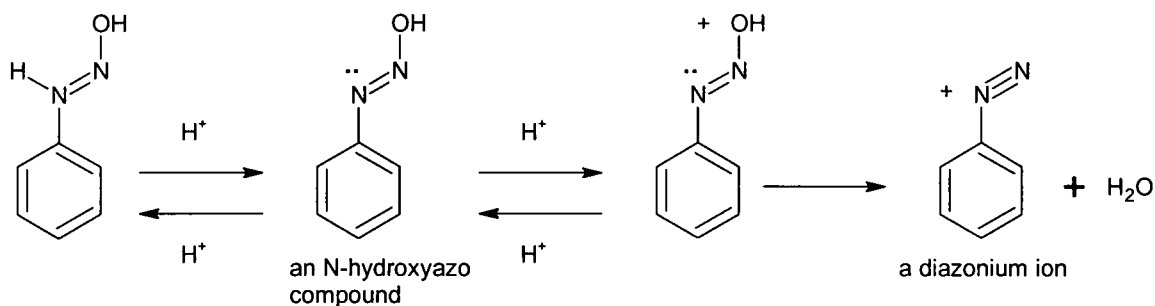


3- The diazonium salt formation by the reaction of a nitrosonium ion and an amino group via the following reactions:

a- Nitrosamine formation



b- Diazonium ion formation



Nitrous acid reactions of primary aryl amines generate more relatively stable diazonium species than aliphatic ones. Diazonium compounds serve as intermediates for a variety of aromatic substitution reactions. Loss of nitrogen is slower than in aliphatic primary amines because the C-N bond is stronger, and

aryl carbocations are comparatively unstable. Aqueous solutions of these diazonium ions have sufficient stability from 0°C to 10°C and generally react with nucleophiles by a loss of nitrogen.

The main approach described in literature regarding attaching organic groups onto the carbon surface via the diazonium formation reaction involves the reaction of at least one diazonium salt with a carbon material in the absence of an externally applied current sufficient to reduce the diazonium salt. This process can be carried out under a variety of reaction conditions and in any type of reaction medium, including both protic and aprotic solvent systems and slurries.

Preferably the diazonium salt is formed in situ. In situ generation allows the use of unstable diazonium salts such as alkyl diazonium salts and avoids unnecessary handling or manipulation of the diazonium salt. If desired, the carbon product can be isolated and dried. Furthermore, the resultant carbon product can be treated to remove impurities by known techniques.

The process can be carried out under a wide variety conditions. The reaction conditions must be such that the particular diazonium salt is sufficiently stable to allow it to react with the carbon material. The reaction between the diazonium salt and the carbon material occurs over a wide range of pH. The processes can be carried out at acidic, neutral, and basic pH – preferably, in the pH range from 1 to 9. Diazonium salts are thermally unstable. They are typically prepared in solution at low temperatures, such as 0 – 5°C, and used without

isolation of the salt. Heating solutions of some diazonium salts may liberate nitrogen and form either the corresponding alcohols in acidic media or the organic free radicals in basic media.

The preferred reaction medium is a solvent-based system. The solvent may be a protic solvent, an aprotic solvent, or a mixture of solvents. Protic solvents are solvents, like water or methanol, containing hydrogen attached to an oxygen or nitrogen and thus are sufficiently acidic to form hydrogen bonds. Aprotic solvents are solvents, which do not contain acidic hydrogen, such as hexanes, tetrahydrofuran, acetonitrile and benzonitrile [20, 22, 43].

Another process for modifying the surface of a carbon-containing material that incorporates the diazonium formation reaction consists of grafting an aromatic group to the surface of this material by electrochemical reduction of a diazonium salt including the aromatic group. The carbon-containing material is placed in contact with a diazonium salt solution in an aprotic solvent and is negatively charged with respect to an anode also in contact with the diazonium salt solution. Use of a protic solvent is reported to prevent the electrochemical process from producing the intended product as a result of reducing the diazonium triple bond to yield hydrazine [19]. Electrochemical reduction of a wide variety of aromatic diazonium salts on carbon electrodes (glassy carbon, highly oriented pyrolytic graphite) leads to the covalent attachment of the corresponding aromatic radicals.

### 2.5.2 OXIDATION METHODS

One of the methods for chemical modification of a carbon surface is oxidation. Various reagents have been used as oxidants: concentrated nitric or sulfuric acid, sodium hypochlorite, permanganate, bichromate, hydrogen peroxide, transition metals and ozone-based gas mixtures. The type of surface structures and the extent of their formation depend on the oxidizing agent and the concentration and acidity of the oxidizing solution. Although the creation of oxygen groups on the carbon surface is relatively well known, the functionalization with sulfur and nitrogen containing molecules has not been fully investigated [21].

Oxidation processes primarily lead to the formation of carboxylic acid, quinone, ketone or alcohol groups on the surface that can then be coupled with the molecule to be attached. The main procedures so far employed in this purpose are as follows: (i) Treatment by boiling oxidizing acid solutions such as sulfuric acid or nitric acid, which also results in an increase of the specific surface area of carbon; (ii) Oxidation by air, oxygen, or ozone at elevated temperature that likewise causes roughening of the carbon surface and may eventually lead to degradation of the fiber; and (iii) Electrochemical oxidation using the carbon fibers as an anode in an aqueous solution at the oxygen gas evolution potential in nitric acid solutions. All of these procedures lead to the formation of oxygenated functional groups on the carbon surface whose nature and number

are difficult to identify and control. It would therefore be desirable to design a more versatile and less drastic way of modifying carbon surfaces.

The controlled oxidation of activated carbon can be carried out with concentrated nitric acid under reflux for different periods of time [49]. After this treatment the obtained material is extensively washed with hot water and dried under vacuum. Weight loss increases with the reflux time, probably due to the oxidation of the activated carbon to gaseous products such as carbon dioxide, and water soluble derivatives such as mellitic acid. Infrared spectroscopic analyses of the nitric acid treated carbons shows strong absorption at approximately  $1720\text{ cm}^{-1}$  ( $\text{-C=O}$ ),  $1550\text{ cm}^{-1}$  ( $\text{-COO}^-$ ),  $1250\text{ cm}^{-1}$  ( $\text{-C-O}$ ) and  $3450\text{ cm}^{-1}$  ( $\text{-OH}$ ) which can be assigned to carboxylic acid groups.

The prolonged exposure of activated carbon to ozone gas transforms the chemical composition of the carbon surface [50]. Basic sites are transformed into acid sites because of oxidation. During the treatment, new acid sites are generated, because of the addition of ozone to the double bond of the carbon structure. The extensive oxidation undergone by the carbon generates acidic groups, such as anhydrides, lactones, and carboxylic acid. The latter group is the main cause of the development of a surface charge. The modification in the oxygenated group distribution on the carbon surface influences the adsorptive properties of the original carbon. The ozone action also impacts the carbon textural characteristics; the surface area decreases because of the ozone attack and the increase in oxygenated groups prevents the diffusion of the nitrogen, by



obstructing the entrances of the micropores. These phenomena also reduce the capacity of the carbon to adsorb methylene blue.

The distribution of chemical groups on the carbon surface is significantly affected by the extent of ozonation. The content of alcohol groups decreases with ozonation time, generating more oxidized groups such as lactones, carbonyl, and carboxylic groups. The latter presents a greater concentration as ozone exposure increases. Moreover, the amount of acid sites on the activated carbon drastically increases with ozonation. The increase in acid sites is accompanied by a decrease in basic sites. Approximately five acid sites are formed for each basic site that disappears. Chromene and Á-pyrone type structures are reported to be responsible for the basic character of activated carbons. On the other hand, the basic nature of activated carbon surface has also been related to the presence of delocalized  $\sigma$  electrons on the basal plane of the surface of activated carbon.

One of the applications of carbon nanotubes is the storage of hydrogen for use in fuel cells. Present efforts to incorporate hydrogen into carbon nanotubes involve cooling the tubes to low temperature and applying an over pressure of hydrogen gas for a number of hours [51, 52].

Ye et al. demonstrated that electrochemical methods can be used to incorporate hydrogen and other functional groups into carbon nanotubes [52]. Self-assembled sheets of carbon nanotube paper can be used as the negative electrode in an electrochemical cell with either an aqueous solution of potassium

hydroxide or sodium nitrite as the electrolyte. Electrolysis carried out for a few hours generates protons, which are then attracted to the nanotube electrode. The incorporation of functional groups into the carbon nanotubes was characterized by thermogravimetric analysis and laser Raman spectroscopic technique, indicating that hydrogen, nitrogen dioxide ( $\text{NO}_2$ ) and diatomic oxygen ( $\text{O}_2$ ) groups could be bonded to carbon nanotubes electrochemically.

### 2.5.3 PLASMA TREATMENT METHODS

Sulfur dioxide ( $\text{SO}_2$ ) and sulfur dioxide in water ( $\text{SO}_2 + \text{H}_2\text{O}$ ) plasma treatments have been performed on highly oriented pyrolytic graphite (HOPG), glassy carbon (GC), and several polymers in order to functionalize their surface with sulfur in different oxidation states. X-ray photoelectron spectroscopy and time of flight secondary ion mass spectroscopy (TOF-SIMS) measurements prove that highly oxidized sulfur species ( $\text{SO}_3$ ,  $\text{SO}_3\text{H}$ ,  $\text{SO}_4$  and  $\text{SO}_4\text{H}$ ) as well as covalently bound sulfur and low oxidized sulfur species ( $\text{SO}$ ,  $\text{SO}_2$ ) are formed and chemisorbed at the surface by plasma treatment. The oxidation state of the adsorbed sulfur species depends on the bias potential applied to the sample. The greater the bias is, the lower the oxidation state. The same behavior as a function of the plasma parameters is found for all substrates. The maximal coverage of the surface with sulfur functionalities has been estimated to be about one monolayer [53].

A low-temperature plasma process was devised for attaching specified molecular groups to carbon nanotubes in order to impart desired chemical and/or

physical properties to the nanotubes for specific applications [54, 55]. Unlike previous carbon nanotube functionalization processes, this process does not involve the use of wet chemicals or exposure to high temperatures, and generates very little chemical residue. In addition, this process can be carried out in a relatively simple apparatus and can readily be scaled up to mass production.

The apparatus used in this process includes two vacuum chambers, denoted the target chamber and the precursor chamber. Plasma of the chemical precursor of the molecular groups to be deposited is generated in the precursor chamber. The plasma flows from the precursor chamber to the target chamber, wherein the carbon nanotubes to be functionalized are mounted on a substrate.

The process is best described by use of an example of functionalizing carbon nanotubes with hydrogen atoms. The precursor chamber is backfilled with high-purity (99.9999 percent or greater) hydrogen gas, optionally mixed with an inert carrier gas (nitrogen, neon, or argon), to a total gas pressure between 13 and 130Pa. The gas is irradiated with microwaves, thereby generating free electrons and a partially ionized gas that includes free radicals (in particular, monatomic hydrogen). Instead of a microwave source, a DC, non-microwave-radio-frequency, inductive-discharge, or electron-cyclotron resonance source can also be used to generate the plasma. The temperature of the free electrons is typically of the order of a few electron volts ( $1\text{eV} = 11604\text{K}$ ). The temperature of

the partially ionized gas typically lies in the approximate range from 350 to 1000K.

The two chambers are connected by a curved tube or plug made of polytetrafluoroethylene or other suitable material. The substrate holding the carbon nanotubes is positioned to face directly into the plasma flowing into the target chamber through the hole in the tube or plug. The tube or plug is curved to eliminate a direct line of sight between the interiors of the chambers in order to prevent ultraviolet light originating in the precursor chamber from reaching the carbon nanotubes. This is necessary for the following reason: some ultraviolet radiation is generated in the undesired but unavoidable recombination of some of the monatomic hydrogen into diatomic hydrogen molecules. This radiation is capable of breaking the C-H bonds in hydrogenated materials, including hydrogenated carbon nanotubes. Other ultraviolet radiation generated in the precursor chamber may be capable of breaking C-C bonds in the nanotubes.

There is no need to maintain the temperature in the target chamber at any particular value in order to achieve functionalization. Experiments have shown that carbon nanotubes can be functionalized with hydrogen to the point of saturation in a process time of about 30 seconds, at or below room temperature. It is also possible to functionalize carbon nanotubes with molecular groups other than hydrogen. For example, by choosing a suitable precursor, one could attach halogen or alkali metal atoms or low-molecular weight hydrocarbons.

#### 2.5.4 FLUORINATION METHODS

Because of the high reactivity of carbon-fluorine bonds on the sidewalls of single-wall carbon nanotubes (SWNTs), fluorinated SWNTs (fluoronanotubes) can be used as precursors for further derivatization. One such reaction is to replace the fluorine with aminoalkyl functionality. Fluoronanotubes were heated with terminal diamines ethylene diamine, propylene diamine, butylene, and hexamethylene diamine in solution phase by stirring the reactants at elevated temperatures (100-200°C). Various methods were used to determine the side wall attachment of the aminoalkyl groups and the carbon-to-functional group ratio. Short time stirring or sonication of fluoronanotubes in alkylidene diamine solvents at room temperature resulted in complete dissolution of fluoronanotubes. Alkylamino-derivatized SWNTs were found to be soluble in dilute acids and water. These amino-functionalized SWNTs can be used in a pseudo-nylon reaction by addition of adipoyl chloride [56].

Mickelson et al. reported that large amounts of fluorine could be covalently attached to the side wall of SWNTs [57]. TEM studies had shown that at fluorination temperatures as high as 325°C, the majority of the fluorination product maintained a tube-like structure. They also reported that at 500°C, the single wall tubular structure does not survive the fluorination process and that some multiwall carbon nanotube-like structures were formed. The reaction temperatures in excess of 150°C were necessary to covalently add significant amounts of fluorine. The fluorine present as a result of the 150°C fluorination

reaction could be attributed to a combination of adsorbed fluorine and fluorination of the end caps of the SWNTs.

Fluorine could be effectively removed from SWNTs using anhydrous hydrazine and the rejuvenated product is in fact a SWNT (via the following reaction:  $\text{CF}_n + 1/4n\text{N}_2\text{H}_4 \rightarrow \text{C} + n\text{HF} + 1/2n\text{N}_2$ ). From the defluorination experiments and characterization results, a majority of the tubes were destroyed at fluorination temperatures of around 400°C, whereas only a slight amount of tube destruction occurred at 250°C.

For reactions in which only the outside of the tube was fluorinated, there was a limited stoichiometry of  $\text{C}_2\text{F}$  for which the fluorinated tube could still maintain its tube-like structure. Further addition of fluorine would then lead to the breaking of carbon-carbon bonds and, hence, destruction of the tube.

Single-walled carbon nanotubes functionalized with the alcohol group terminated moieties were prepared by fluorine displacement reactions of fluoronanotubes with a series of diols and glycerol in the presence of alkali – lithium hydroxide (LiOH), sodium hydroxide (NaOH), or potassium hydroxide (KOH) – or with amino alcohols in the presence of pyritium (Py) as a catalyst. The degree of sidewall functionalization in the prepared SWNT derivatives was estimated to be in the range of one in fifteen to 25 carbons, depending on the derivatization method and alcohol reagent used. The alcohol functionalized nanotubes formed stable suspension solutions in polar solvents, such as water, ethanol, and dimethylformamide.

## CHAPTER III

### EXPERIMENTAL METHODS

In this experiment nanofibers of the Pyrograf III family were surface treated and added to an epoxy resin and curing agent to create polymeric carbon nanocomposites. The mechanical, thermal, and electrical properties of the resulting carbon nanocomposites were analyzed using a variety of tests to determine the effects of incorporating the carbon nanofibers into the neat resin. The goal of the investigation was to maximize the improvement to the physical properties of the EPON 862 resin by determining the effect of various nanofiber surface treatments.

In addition, the use of carbon foam as a bone regeneration material was also investigated. This experimentation involved infiltrating the carbon foam with a biodegradable polymer and testing the material for compressive mechanical properties. Also, the adherence of osteoblast cells to the carbon foam was examined to determine the biocompatibility of the material.

#### 3.1 *NANOCOMPOSITE MATERIAL DESCRIPTION*

To serve as a reference material and continuous matrix support for the nanocomposites, EPON 862 – an epoxy resin – was chosen for its ease in processing. The nanofibers selected for this investigation were supplied by

Applied Sciences Incorporated of Cedarville, Ohio. The as-received nanofibers had diameters in the range of 50-100nm. The lengths of all of the nanofibers were between 30 and 100 $\mu$ m.

### 3.2 *NANOCOMPOSITE PANEL FABRICATION*

The carbon nanofibers were dispersed within the epoxy resin at various loadings. The neat resin panel of EPON 862 served as the baseline against which the properties of the carbon nanocomposites were compared. Following the proper dispersion and blending of the nanocomposite, the mix was cast into a 5" x 10" x 0.25" silicone rubber mold and cured under pressure and temperature using the manufacturer recommended curing and post-cure cycle of two hours at 250°F followed by two hours 350°F.

### 3.3 *THERMAL ANALYSIS*

#### 3.3.1 *DIFFERENTIAL SCANNING CALORIMETRY*

Nanocomposite specific heat was tested using a TA Instruments DSC Q1000 according to ASTM E1269-89. Each cured nanocomposite test specimen (less than 15mg), as well as the sapphire standard, was subjected to a five minute isotherm at room temperature followed by a heating rate of four degrees Celsius per minute concluding with another five minute isotherm at 75°C. An example of the resulting plot of this test is shown in Figure 3.1. The amount of energy required for the apparatus to change the temperature of the sample was then compared against the sapphire standard using TA Specialty Library



Software to determine the specific heat of the given nanocomposite over the range of test temperatures.

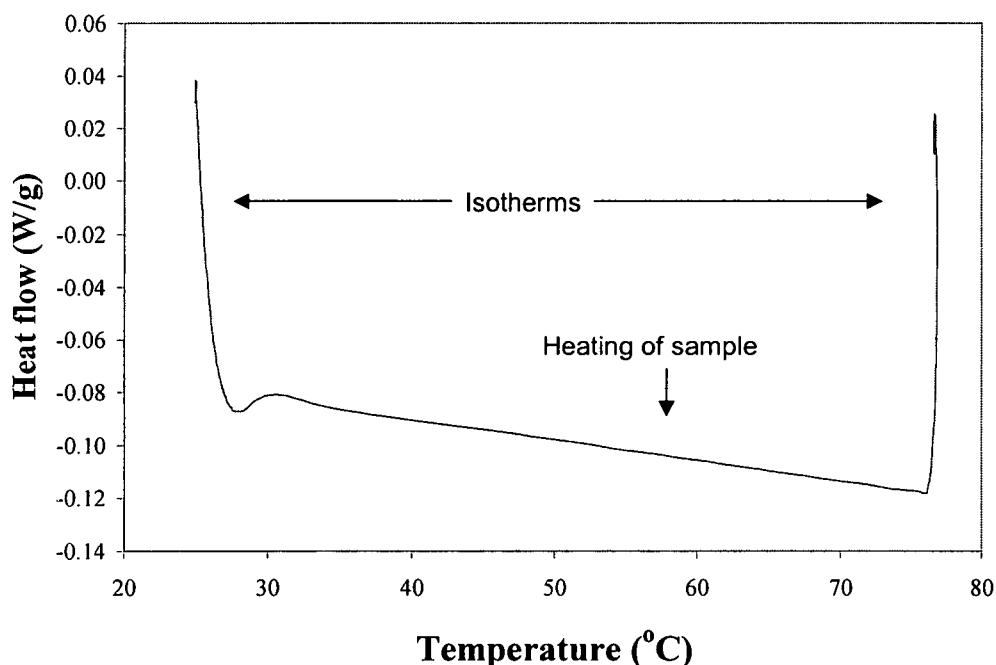


Figure 3.1 – Specific heat analysis of nanocomposite by DSC

Nanocomposite heat of reaction and glass transition temperature were tested using a TA Instruments DSC Q1000 according to ASTM E2160 and ASTM D3417. A small sample (less than 15mg) of uncured resin for heat of reaction analysis and cured resin for glass transition temperature analysis mixed with a given loading of carbon nanofibers was placed in a aluminum DSC pan. The sample was heated along with an empty sample holder at a heating rate of ten degrees Celsius per minute from room temperature to 350°C. The analysis of the resulting curve was performed on TA Universal Analysis 2000 Software. Examples of the resulting curve and analysis for heat of reaction and glass transition temperature are given in Figures 3.2. and 3.3 respectively.

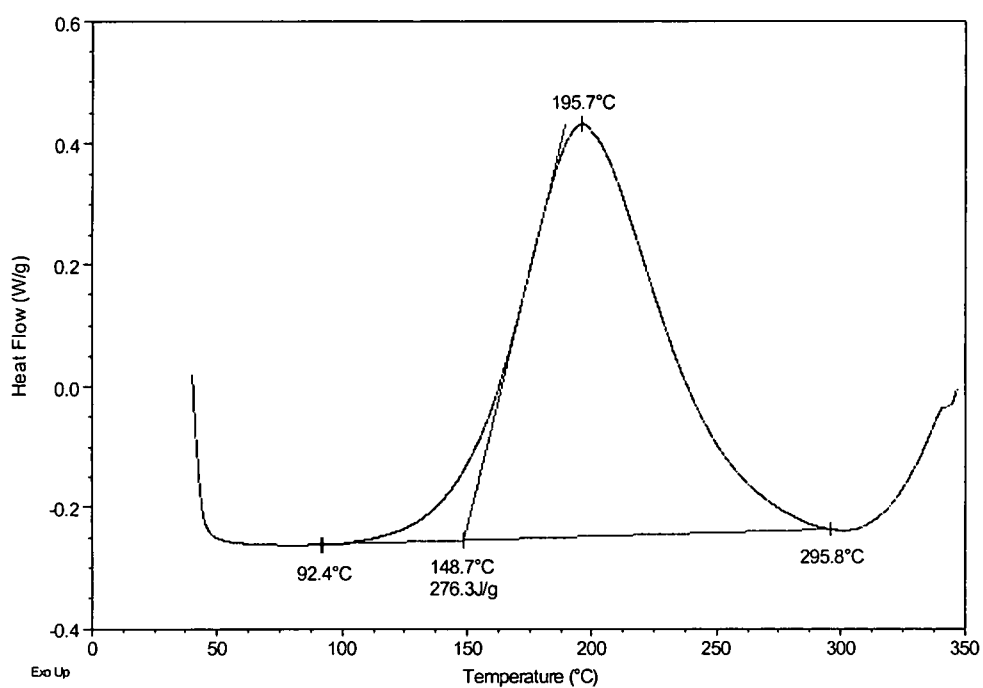


Figure 3.2 – Heat of reaction analysis of nanocomposite by DSC

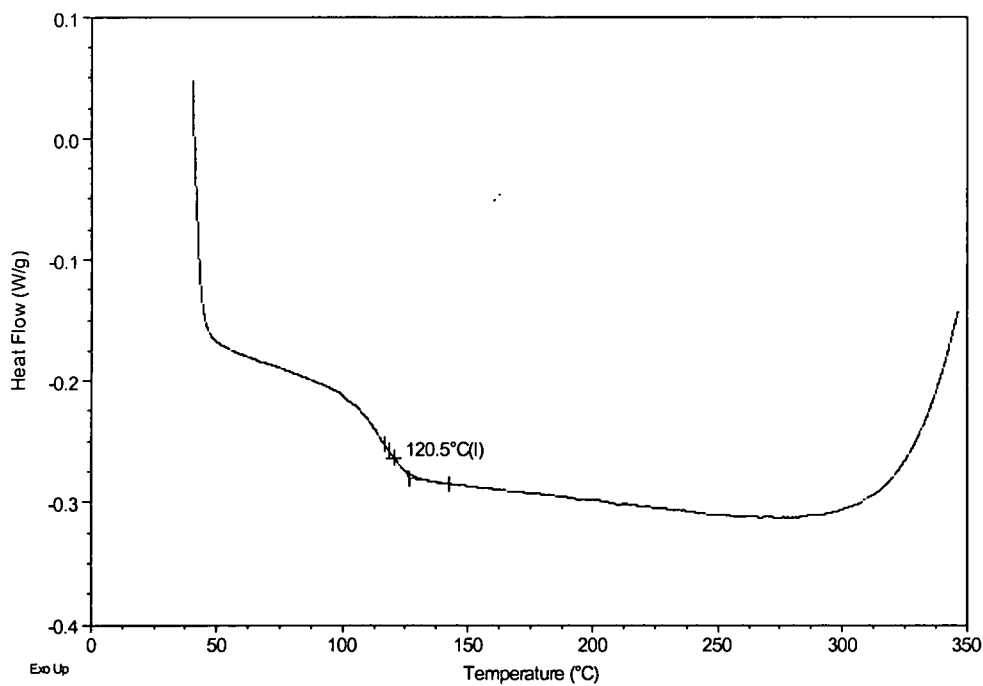


Figure 3.3 – Glass transition temperature analysis of nanocomposite by DSC

### 3.3.2 THERMAL DIFFUSIVITY

The thermal diffusivity of each nanocomposite was tested using a xenon flash diffusivity method. A guarded plate test was utilized as a means to verify the flash diffusivity results. The flash diffusivity analysis was carried out according to testing procedure ASTM C714-72 with a capacitance charge of 3400V and the samples were cut into squares rather than circles. The results of the flash diffusivity were analyzed according to Equation 1 where  $\alpha$  is the diffusivity,  $L$  is the thickness ( $< 0.5$  cm) of the sample and  $t_{1/2}$  is the time (sec) at which one half of the maximum voltage is registered.

$$\alpha = \frac{0.139L^2}{t_{1/2}} \quad (1)$$

As the xenon pulse transmitted through the front face of the nanocomposite sample during the flash diffusivity test, the temperature of the surface facing away from the load was measured via a thermocouple. The typical reading of the type J thermocouple during the flash diffusivity test is shown in Figure 3.4. The upper signal is that of the pulse. The spike occurring just before four seconds signifies time zero – the triggering of the thermal pulse to the nanocomposite sample. The lower signal is registered on the nanocomposite face and has been lowered from its original value of 0.0 mV for easier viewing. The temperature of the nanocomposite increased following the administration of the thermal pulse, demonstrated by the elevated thermocouple reading. After the experimental run was complete the maximum voltage reading

was determined. The time corresponding to one half the maximum voltage value attained was then used in the thermal diffusivity calculation along with the thickness of the nanocomposite sample.

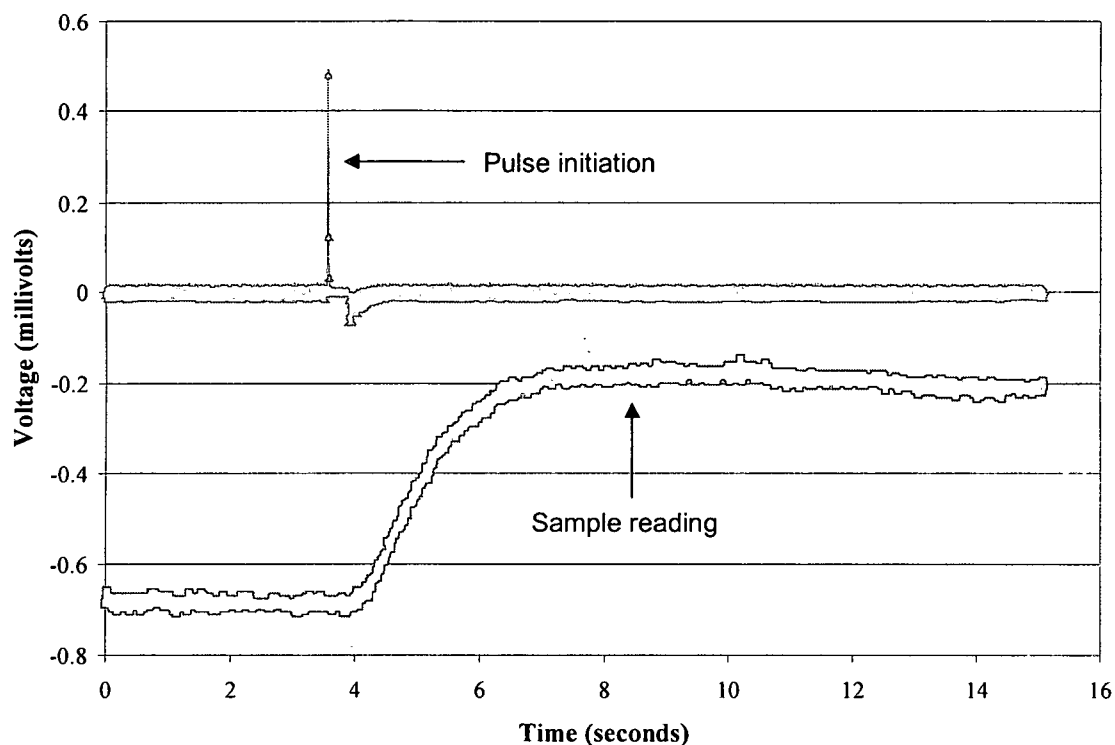


Figure 3.4 – Thermal diffusivity analysis of nanocomposite by flash diffusivity

Thermal diffusivity was combined with the specific heat and density of the nanocomposite to calculate thermal conductivity,  $K$ , according to Equation 2, where  $\rho$  is the density of the nanocomposite (tested according to ASTM C693-74) and  $C_p$  is specific heat or heat capacity of the nanocomposite.

$$K = C_p * \rho * \alpha \quad (2)$$

### 3.3.3 THERMOGRAVIMETRIC ANALYSIS

Thermogravimetric analysis (TGA) measures the weight loss of a sample when heated to a fixed temperature and can be used to detect degradation such as pyrolytic weight loss. TGA of the nanofibers was performed using a DuPont Instruments TGA 2950 according to ASTM D3850. A small sample (less than 15mg) of nanofibers was placed into a ceramic sample holder and loaded into the heating chamber. The heating chamber was kept at room temperature for approximately five minutes to purge the chamber of ambient air. The sample was heated at a rate of five degrees Celsius per minute from ambient temperature to 1000°C in argon. The test equipment measured and recorded the sample weight over the course of the analysis. An example of the resulting curve is given in figure 3.5.

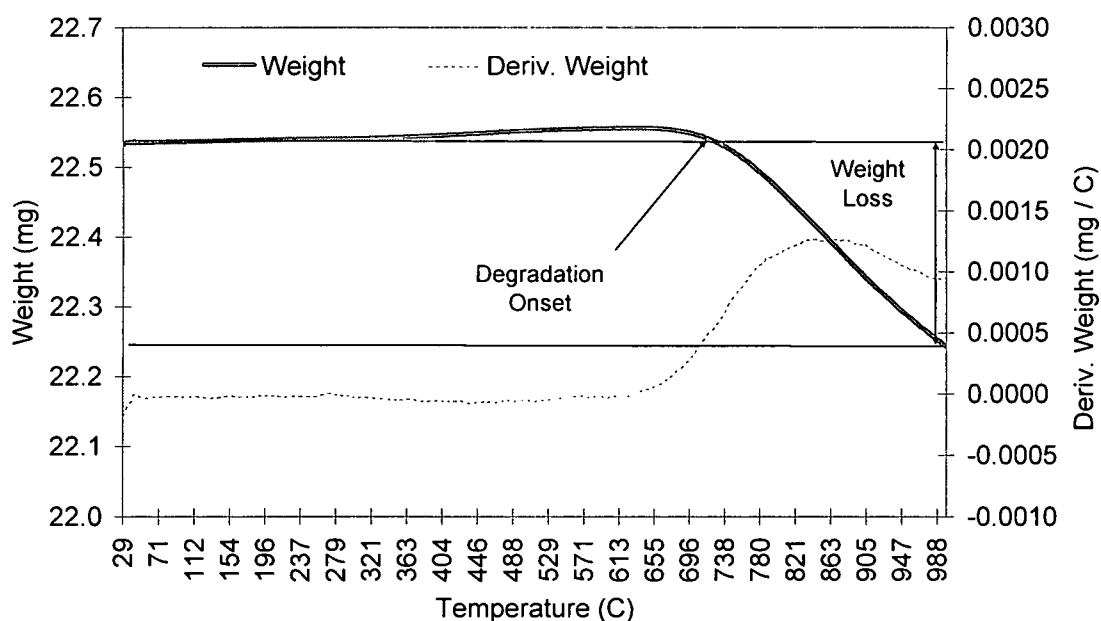


Figure 3.5 – Degradation analysis of nanofiber by TGA

### 3.4 ELECTRICAL ANALYSIS

#### 3.4.1 FOUR-POINT PROBE ELECTRICAL RESISTIVITY

The electrical properties of the nanocomposites were studied utilizing a four-point test according to ASTM B193-87. The two outer leads of the tester were connected to the current source and the two inner leads were used to measure the voltage drop through the nanocomposite. Ohm's law, Equation 3, allows for the resistance of the sample to be determined where  $V$  is equal to voltage,  $I$  is the current and  $R$  is the resulting electrical resistance. By coupling the calculated resistance with the known cross-sectional area ( $A$ ) and distance between leads ( $L$ ), the resistivity ( $\rho$ ) of the sample can be determined according to Equation 4. Electrical conductivity ( $\sigma$ ) is the reciprocal of resistivity and is calculated according to Equation 5.

$$R = \frac{V}{I} \quad (3)$$

$$\rho = \frac{R * A}{L} \quad (4)$$

$$\sigma = \frac{1}{\rho} \quad (5)$$

#### 3.4.2 VOLUME RESISTIVITY

The volume resistivity of the carbon nanofibers was tested according to ASTM D257. The fixture used to complete the testing is shown in Figure 3.6.

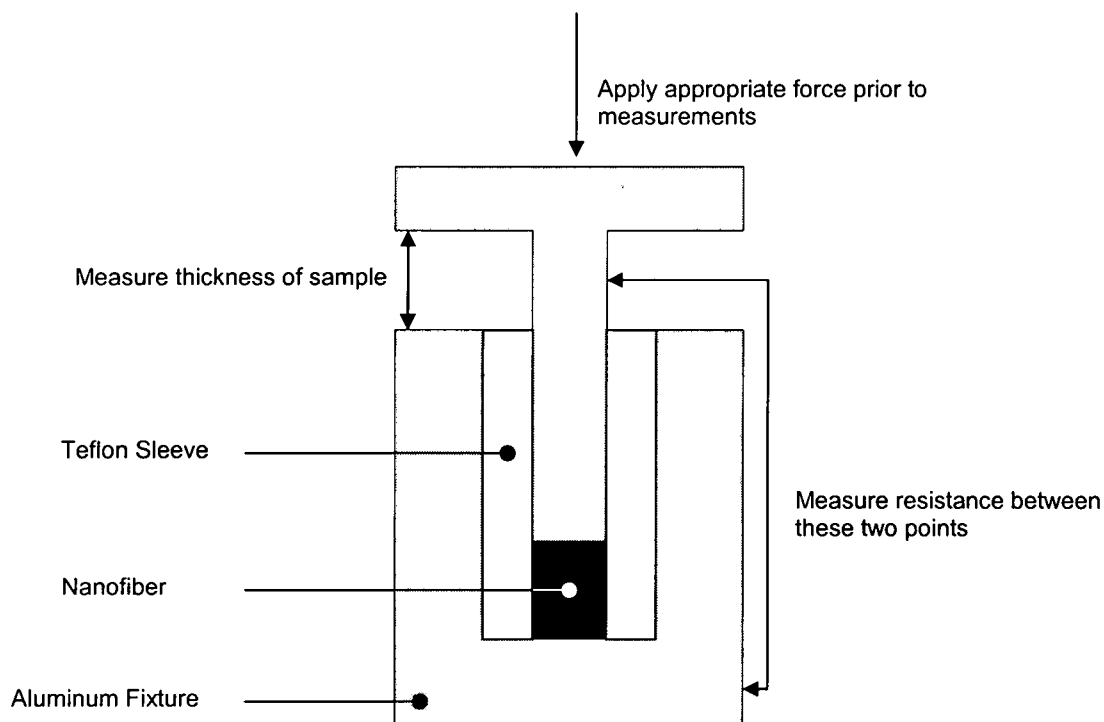


Figure 3.6 – Fixture for testing carbon nanofiber volume resistivity

The fixture was filled with the nanofiber sample, and the weight was recorded. The tamp was inserted into the fixture and an appropriate weight to create a pressure of 16 pounds per square inch was placed on top of the tamp. The distance between the top of the fixture and the tamp was measured and recorded, and the resistance was measured using an ohm-meter. Following the appropriate measurements at 16 pounds per square inch, the procedure was repeated with an appropriate weight to create a pressure of 108 pounds per square inch. The purpose of the two separate load applications is to identify the effect of nanofiber to nanofiber surface contact. A larger load will result in improved contact between the nanofibers yielding a lower resistivity. The volume resistivity is calculated according to equation 6 where  $A$  is the effective area of

the measuring electrode,  $t$  is the sample thickness and  $R_v$  is the measured resistance.

$$P_v = \frac{A * R_v}{t} \quad (6)$$

### 3.5 MECHANICAL ANALYSIS

The mechanical properties of the nanocomposites were studied using the three-point flexural strength test according to ASTM D790-00. The three-point flex test utilizes a sample size measuring 3.0 inches in length and 0.5 inches in width. The depth was sample dependent and a span ratio (span-to-depth) of 12:1 was used. Flexural testing was conducted using an Instron load frame with a crosshead speed of 0.05 inches per minute. This test provided the Young's modulus and ultimate strength for the nanocomposite. The resulting curve from the three-point flexural strength test is shown in Figure 3.7.

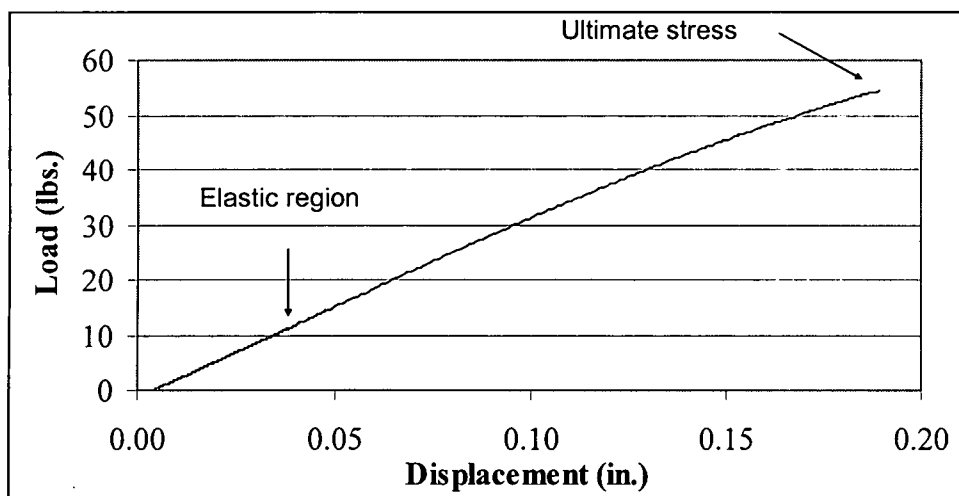


Figure 3.7 – Mechanical analysis of nanocomposite by three-point flexural strength



The elastic modulus and ultimate strength were calculated by the Instron Series IX Automated Materials Testing System. These results were then verified via manual manipulation of the raw data. The ultimate strength is given by the applied load at the point of mechanical failure. The elastic modulus is calculated using the stress/strain slope in the elastic range of deformation, the span of the material being tested, the width of the sample as well as its depth according to Equation 7 where  $\sigma$  is the applied stress and  $\epsilon$  is strain.

$$E = \frac{\frac{\sigma}{\epsilon} * span^3}{4 * width * depth^3} \quad (7)$$

### 3.6 INVERSE GAS CHROMATOGRAPHY

Inverse gas chromatography (IGC) is a gas phase technique for characterizing surface and bulk properties of solid materials. A cylindrical column is uniformly packed with the solid material to be tested. A constant concentration of gas is injected into the column at a fixed carrier gas flow rate, and the time taken for the concentration front to elute through the column is measured by a detector. A series of IGC measurements with different gas phase probe molecules then allows for determination of surface energy of the solid sample.

The injected gas molecules passing over the material absorb on the surface with a partition coefficient,  $K_S$  according to equation 8 where  $V_N$  is the net retention volume – the volume of carrier gas required to elute the injection through the column – and  $W_S$  is the mass of the sample.  $V_N$  is a measure of how

strongly the probe gas interacts with the solid sample and is the fundamental data obtained from an IGC experiment. From this determination, a wide range of surface and bulk properties can be calculated.

$$K_S = V_N / W_S \quad (8)$$

IGC measurements were carried out with a Surface Measurement Systems 6890N (61540N) model IGC. Helium was used as the carrier gas, and the glass columns filled with carbon nanoparticulates were 30cm long with a 3mm inside diameter. A sample size of 5mg was used. The column temperature was 363K. The FID detector was used for all IGC measurements and C7-C10 n-alkanes were selected as non-polar probes, while ethyl acetate, dichloromethane, acetone and water were selected as polar probes.

### 3.7 BRUNAUER EMMETT TELLER (BET) SURFACE AREA

In BET surface area measurements, a sample contained in an evacuated sample tube is cooled typically to cryogenic temperature, and then is exposed to analysis gas at a series of precisely controlled pressures. With each incremental pressure increase, the number of gas molecules adsorbed on the surface increases. The pressure at which adsorption equilibrium occurs is measured and the universal gas law is applied to determine the quantity of gas adsorbed.

As adsorption proceeds, the thickness of the adsorbed film increases. Any micropores in the surface are quickly filled, then the free surface becomes completely covered, and finally larger pores are filled. The process may continue to the point of bulk condensation of the analysis gas. Then the desorption

process may begin in which pressure systematically is reduced resulting in liberation of the adsorbed molecules. As with the adsorption process, the changing quantity of gas on the solid surface is quantified. These two sets of data describe the adsorption and desorption isotherms. Analysis of the isotherms yields information about the surface characteristics of the material.

BET surface areas were measured using a Micromeritics ASAP 2010 automatic single and multi point BET surface area measurement system. The samples (0.125g) were outgassed for five hours at 140°C. The amount of nitrogen gas adsorbed by a sample was measured and used to calculate surface area in  $\text{m}^2/\text{g}$ . The data was analyzed by the standard BET method employed by software from Micromeritics.

### 3.8 *ELECTRON MICROSCOPY*

High-resolution Scanning Electron Microscopy (SEM) and Transmission Electron Microscopy (TEM) provided an analysis of the structural properties of the carbon nanofibers and nanocomposites. These techniques were utilized to analyze the effects of surface treatment on the pristine carbon nanofibers. An emphasis was also placed on the nanocomposite fracture surface. The use of the grey-scale at this location provided a more thorough explanation of the interaction between the nanofiber and the surrounding resin matrix.

Image contrast is obtained in electron microscopy by two phenomena. Mass thickness contrast reflects differences in thickness, density, and the degree of scattering of the specimen. The adsorption of the electron beam into the

specimen is quite small. A bright field image can be obtained when the aperture in the back focal plane of the objective lens is small enough to eliminate undesirable beams, but large enough to allow transmitted electron beams to pass through. Conversely, in the dark field image, the incident beam must be tilted for the  $hkl$  planes to be brought to the Bragg angle. The region emitting the  $hkl$  beam will appear bright on a dark field. The observation of the specific lattice plane extracted from the  $hkl$  planes facing arbitrary directions is possible by changing the tilt angle and the aperture position. However, the dark field electron microscope technique allows a complete exploration of the reciprocal space of distorted materials like turbostratic carbons.

If the aperture is reduced in size, the contrast improves while the resolution deteriorates. This is why the resolution in the dark and bright field images is limited to 3nm. When high resolution is required, the aperture must be opened widely so that both the diffraction electron beams and the transmitted beams are collected to give a lattice fringe image. This describes the phase contrast. High-resolution fringe imaging clearly distinguishes between graphitizable and non-graphitizable isotropic carbons with a random arrangement of constituent lamellae. Difficulties in interpretation owing to the influence of electron optical aberrations on the image-forming process may lead to difficulties in terms of quantitative interpretation.

### 3.9 X-RAY PHOTOELECTRON SPECTROSCOPY

The surface properties of the carbon nanofibers were investigated by X-ray photoelectron spectroscopy (XPS). The XPS was developed in the mid

1960s. The phenomenon is based on the photoelectric effect outlined by Einstein in 1905 where the concept of the photon was used to describe the ejection of electrons from a surface when photons impinge upon it. For XPS, Al K $\alpha$  (1486.6eV) or Mg K $\alpha$  (1253.6eV) are often the photon energies of choice. Other X-ray lines can also be chosen such as Ti K $\alpha$  (2040eV). The XPS technique is highly surface specific due to the short range of the photoelectrons that are excited from the solid. The energy of the photoelectrons leaving the sample is determined using a wavelength that gives a spectrum with a series of photoelectron peaks. The binding energy of the peaks is characteristic of each element. The peak areas can be used (with appropriate sensitivity factors) to determine the composition of the materials surface. The shape of each peak and the binding energy can be slightly altered by the chemical state of the emitting atom. Hence XPS can provide chemical bonding information as well. XPS is not sensitive to hydrogen or helium, but can detect all other elements. XPS must be carried out in ultra-high vacuum conditions.

When the sample is irradiated with X-ray photons, electrons are emitted from the sample if the photon is of sufficient energy. The kinetic energy of these photoelectrons is measured by the analyzer and the binding energy of the photoelectron is calculated from the equation 9 where  $KE$  is the kinetic energy of the emitted photoelectron,  $h\nu$  is the X-Ray photon energy and  $BE$  is the binding energy of the photoelectron which is the energy required to remove the electron from the atom. A work function  $f_s$  is required for photoemission from solids as

extra energy is required to transfer the electron from the surface to the vacuum. This is a predetermined value for each spectrometer.

$$KE = h\nu - BE - \phi_s \quad (9)$$

XPS instrumentation consists of an X-ray source, a series of lenses to focus the photoelectrons and an energy analyzer and detector. Photoelectrons are counted at each kinetic energy value and a spectrum of intensity versus binding energy is generated from the above equation. The binding energy of an electron is characteristic of the element, orbital and chemical environment; therefore XPS can determine the bonding state and/or oxidation states of materials and surface concentrations.

### 3.10 RHEOLOGICAL ANALYSIS

All rheological experiments were carried out using TA Instruments AR 2000 Advanced Rheometer. Initially neat resin was applied between the 25mm diameter parallel plates at a gap of ten millimeters, and the temperature was ramped to 300°C with the angular frequency of oscillation (6.283 rad/s) held constant. The resulting curve is shown in Figure 3.8. Since the minimum viscosity was obtained at approximately 150°C, this temperature was used to determine gelation times for the nanocomposites.

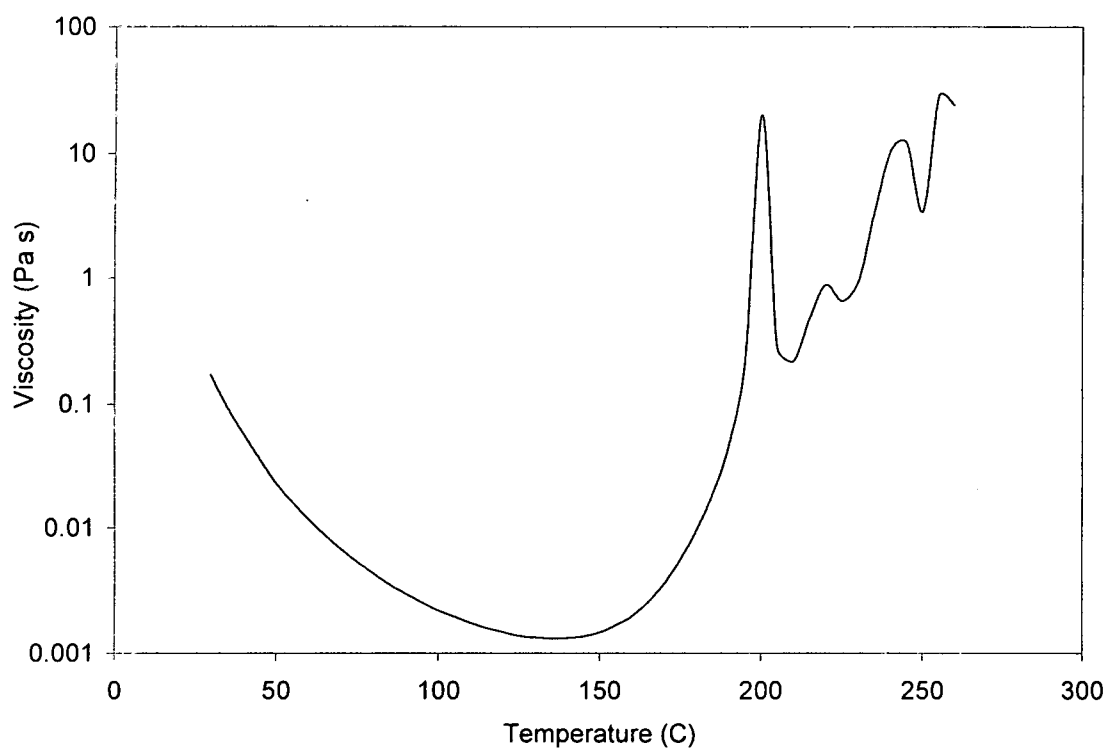


Figure 3.8 – Viscosity as a function of temperature for neat resin

The gelation times of the nanocomposite systems were determined by measuring the development of storage modulus ( $G'$ ) and loss modulus ( $G''$ ) at 150°C and an angular frequency of oscillation of 6.283 rad/s. The rheometer was first preheated to the test temperature and allowed to equilibrate. The nanocomposite sample was then applied between parallel plates at a gap of ten millimeters to initiate the test. The gelation time was calculated as the intersection of  $G'$  and  $G''$  as shown in Figure 3.9.

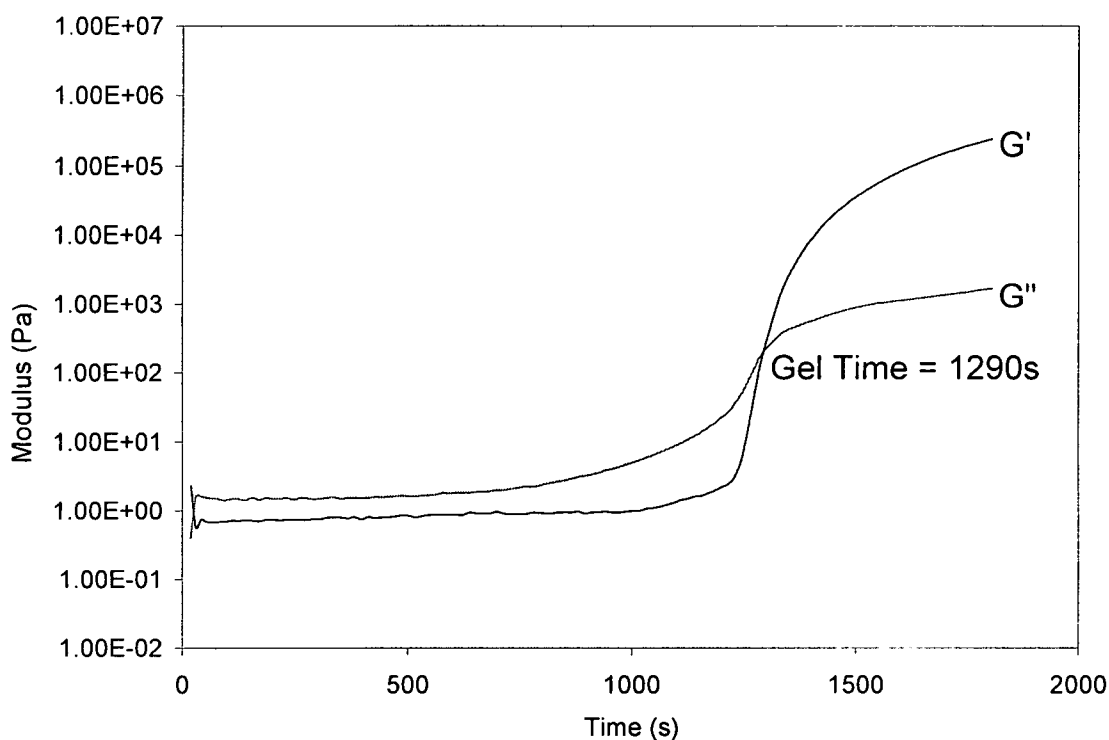


Figure 3.9 – Determination of gelation time by rheological analysis

### 3.11 SOXHLET EXTRACTION

Soxhlet extraction was a method employed to purify and clean the as-received nanofibers. The experimental setup is shown in Figure 3.10. During the process, a solvent of increasing solubility intensity (acetone, THF, toluene, and pyridine) in a round bottom flask is heated to boiling. The vapors rise through the outer chamber and into the condenser. The vapors condense into liquid and fall back into the bottom of the Soxhlet chamber located above the lower round bottom flask. As the distilled liquid solvent rises in the chamber, it seeps through the permeable cellulose extraction thimble that holds the carbon nanofibers. The solvent extracts the compounds of interest and leaves the solid mass behind. The extraction is usually indicated by observing that the solvent



has a different color than it had in its pure form in the flask. As the solvent level rises, the solution is forced through the small inner tube, and the chamber is flushed due to a siphoning effect. The flushed solvent returns to the lower flask taking the extracted compounds with it. The solvent is redistilled from the solution in the flask and condenses in the chamber, repeating the extraction with fresh solvent. The process can be repeated as many times as necessary. Each time the process is repeated, the solution in the flask becomes more concentrated because more impurities are extracted from the solid mass. The Soxhlet extraction is usually completed when the solution in the Soxhlet chamber is the same color as the pure solvent. This means that nothing more is being extracted from the carbon nanofibers by the solvent.

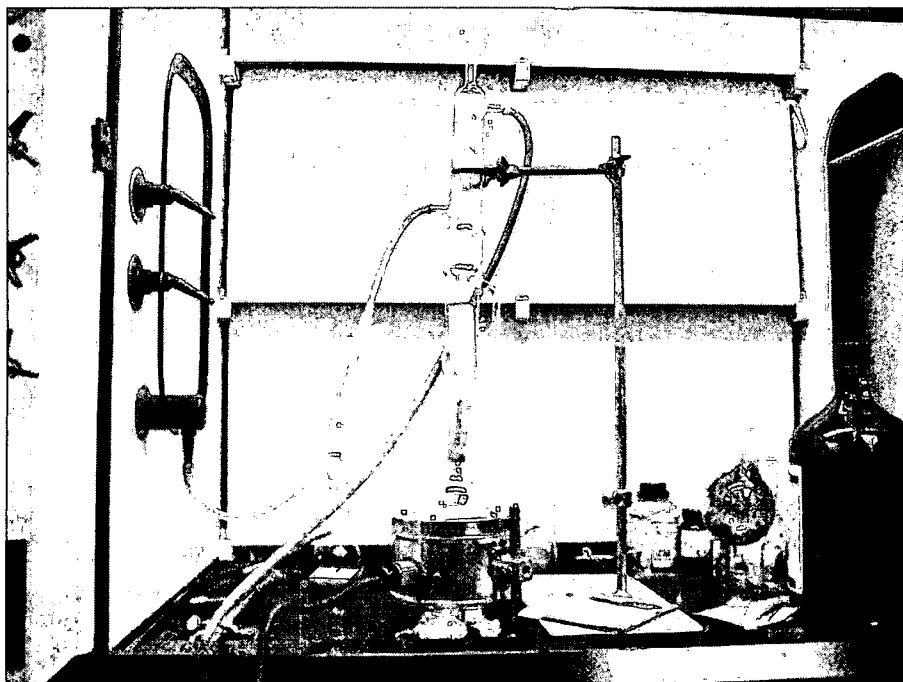


Figure 3.10 – Experimental setup for Soxhlet extraction

## CHAPTER IV

### EFFECT OF CARBON NANOFIBER CLEANING AND PURIFICATION ON NANOFIBER AND POLYMERIC NANOCOMPOSITE PROPERTIES

#### 4.1 CARBON NANOFIBER STRUCTURE

The as-received carbon nanofibers consist of a variety of material morphologies: helical, straight, nested cone, bamboo and carbon blacks with a distribution of diameters and lengths (Figure 4.1).

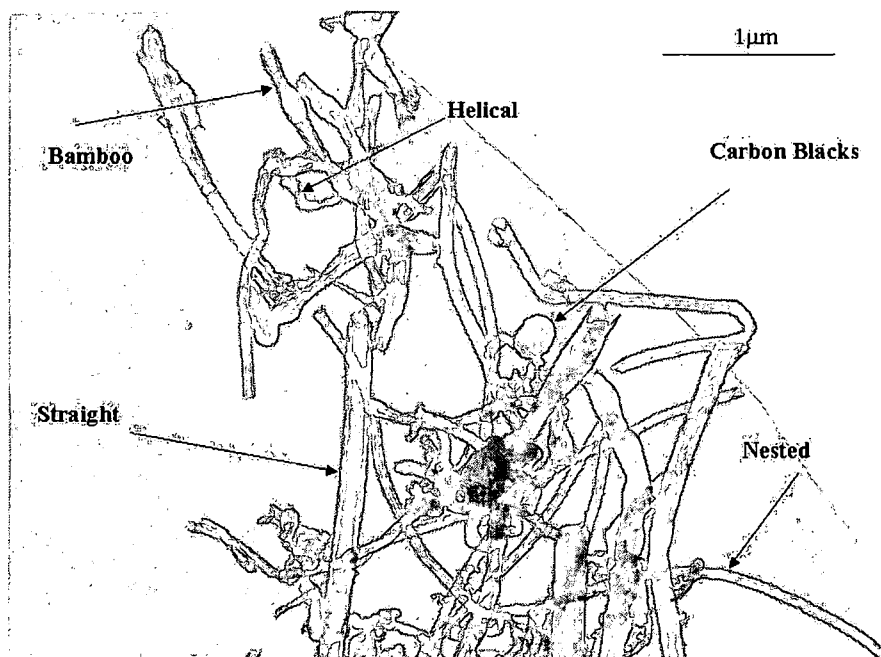


Figure 4.1 – Bright field image of as-received PS carbon nanofibers

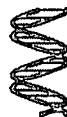
The five major carbon constituents represented as carbon nanofibers are shown in Figure 4.2. The three dominant species include the nested, bamboo-type, and straight carbon nanofibers. The nested, or Dixie® Cup, type structure

and the straight nanofiber represent ideal structures with high surface area and surface energy [58]. The bamboo structure has potential areas of failure as a part of its makeup due to the locations where the individual segments join. Carbon blacks and helical nanofibers make up the remainder of the carbon species within the group. The helical structures are ideal for damping applications, but are not ideal for strengthening applications. Carbon blacks or soot are a by-product of manufacturing that are made up of nanometric spheres of agglomerated carbon. There does not currently exist a process to manufacture individual structures of carbon nanofibers or a process to separate these structures following manufacturing, thereby leading to difficulty in predicting resulting nanocomposite properties. Another drawback of the manufacturing process is that residual materials are present on the surfaces of the nanofibers following production. The SEM micrograph in Figure 4.3 shows the thick edges of the carbon nanofibers appearing darker, indicating the presence of a "skin" of residual material from production.

1. Carbon Blacks : Minor



2. Helical : Minor



3. Straight: Major



4. Nested (D.C.): Dominant



5. Bamboo: Dominant

Figure 4.2 – Models of nanofiber configurations

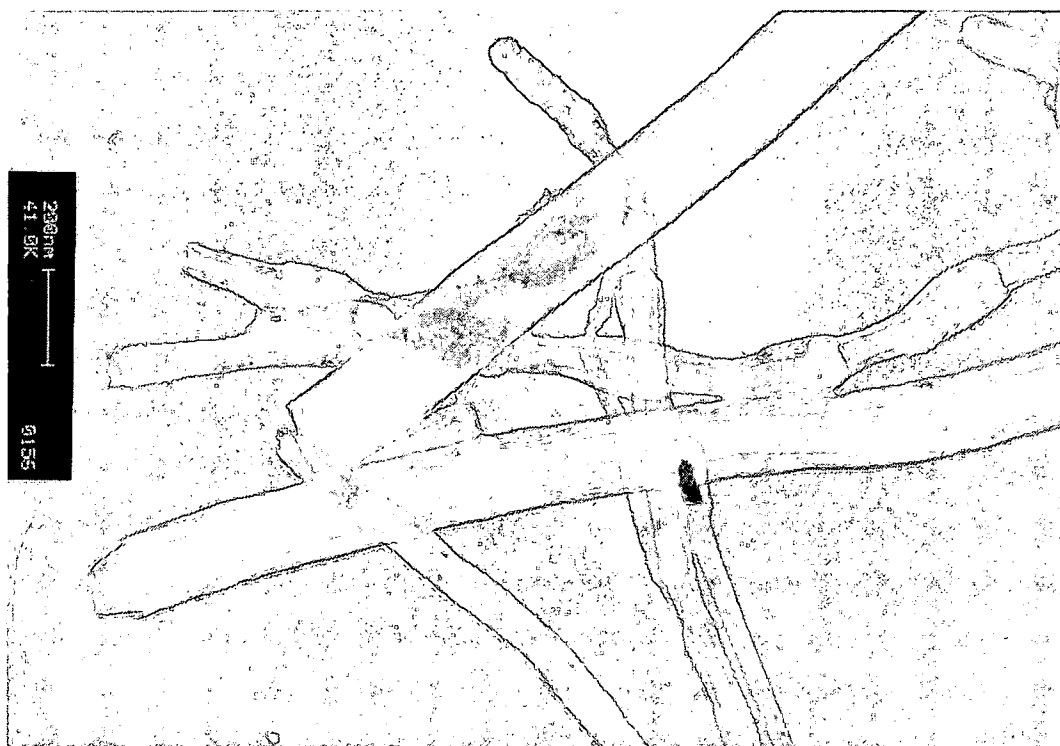


Figure 4.3 – SEM micrograph of as-received carbon nanofibers indicating thick, dark edges

Initial attempts at manufacturing nanocomposites using as-received nanofibers lead to a complete failure due to a lack of adhesion between the nanofiber and the host matrix (Figure 4.4). This is a further indication of the difficulty in having the various nanofiber structures as a result of manufacturing. If the nanofiber structure was comprised entirely of nested cone stacked layers, the resulting large surface area and surface energy should be sufficient to allow for adhesion to the resin matrix. Since this was not observed, and it is known that the nanofibers likely consist of a variety of structures, surface functionalization should be required to improve adhesion with the matrix.

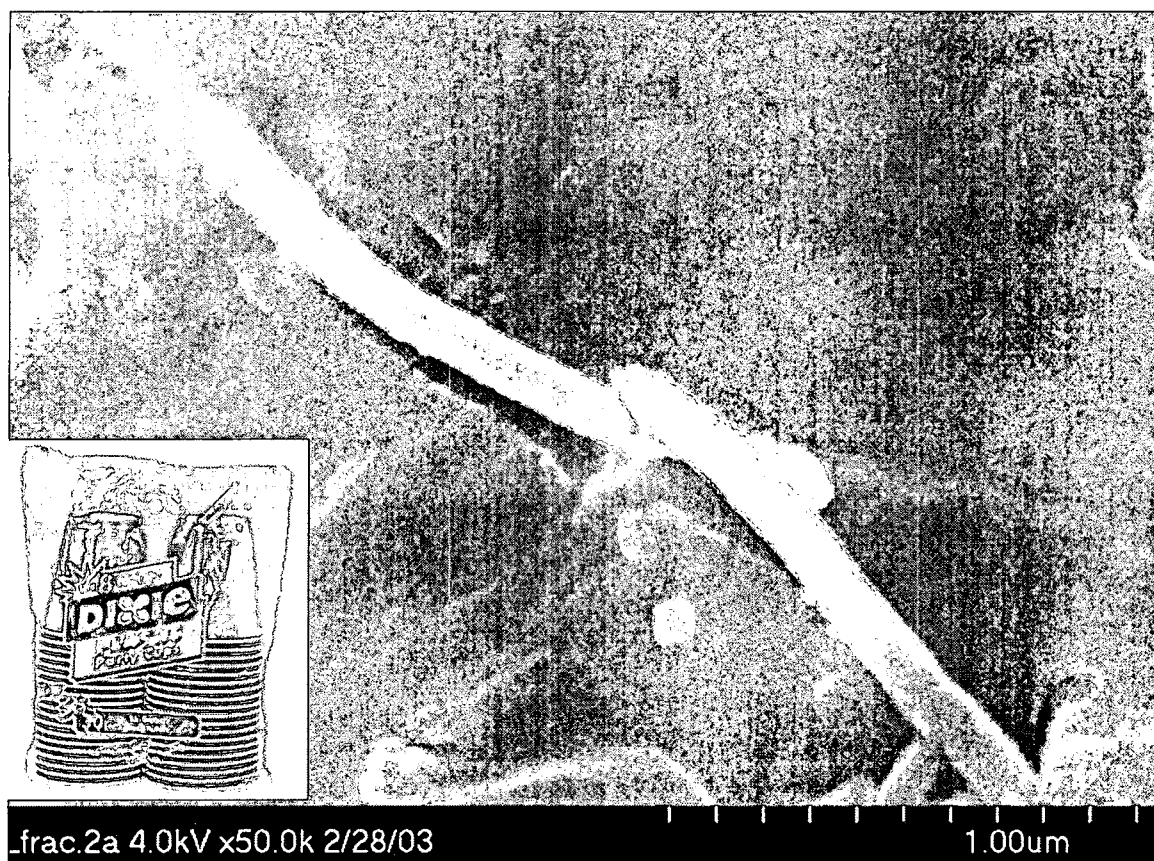


Figure 4.4 – SEM micrograph indicating no adhesion between the nanofiber and the resin matrix

The structure of carbon can be altered by heat treatment. Carbon at low temperatures exhibits local molecular ordering. As a carbon sample is heat treated, the increase in temperature results in the aromatic molecules stacking into a columnar structure. Further heat treatment causes these columns to join together forming a distorted, wavy structure [39]. Heat treatment temperatures of 2500°C or higher compress the distorted graphene layers forming an aligned structure. Heat treatment of carbon nanofibers to 3000°C results in a straightening of the graphene layers and the attainment of minimum interlayer spacing (Figure 4.5).

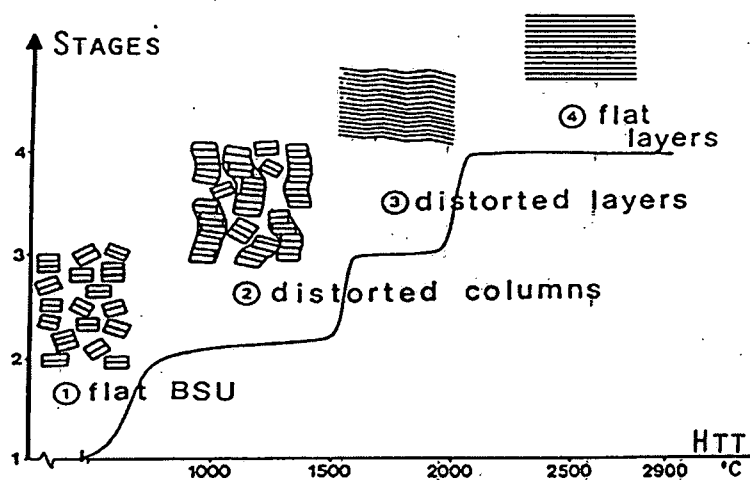


Figure 4.5 – Carbon plane structure as a function of heat treatment temperature

As shown by a TEM micrograph (Figure 4.6), the graphene layers within the nested cone type carbon nanofiber coalesced following heat treatment to 3000°C resulting in localized ordering of the graphene layers and continuous planes. At this magnification the inclination angle of each cup is apparent.

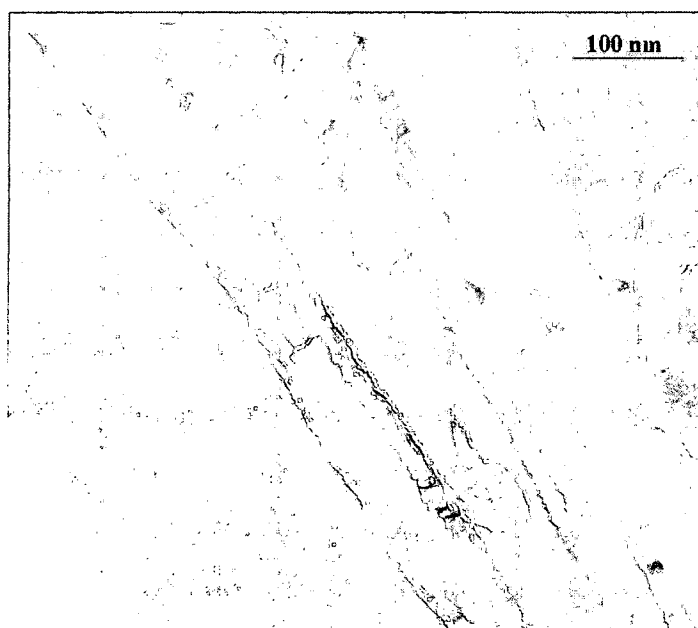


Figure 4.6 – Bright field micrograph of nested cone type carbon nanofiber structure following heat treatment to 3000°C

At high-magnification (Figure 4.7), the graphene layers appear very straight without any disclination defects. There is no change in the inclination angle to the central core axis. The edge of any pair of graphene layers have been rounded encapsulating carbon planes' exposed edge. This allows the graphene planes to attain minimal interlayer spacing and a level of maximum stability.



Figure 4.7 – High-resolution image of localized area of nested cone type carbon nanofiber structure following heat treatment to 3000°C

#### 4.2 CARBON NANOFIBER CLEANING AND PURIFICATION AND ITS EFFECT ON NANOFIBER PROPERTIES

There existed a need to establish a selective, quality control test to identify the purity of a carbon nanofiber. While microscopy may be the best test to visually see the surface of the material and determine the presence of residual



surface impurities, it is a lengthy and costly test. Conversely, volume resistivity testing represented a cheap and quick test to determine the cleanliness of a sample.

A description of each of the nanofibers used in the cleaning and purification experiments is provided in Table 4.1. Each of the as-received carbon nanofibers was tested for electrical volume resistivity measurement. The results of the volume resistivity testing on as-received carbon nanofibers are presented in Figure 4.8. There was a significant drop in the volume resistivity between the AG and PS nanofibers and between the PS and LHT nanofibers. However, the change in the heat treated between the AG, PS, and LHT is only 400°C. This indicated an anomaly in the observed decrease in resistivity. Further heat treatment of the nanofibers did not significantly reduce the volume resistivity. If the volume resistivity were only a function of heat treatment temperature, the values should result in a relatively linear decrease with a sharp decrease after 2500°C. The anomalous results indicated the likelihood of an additional factor in the determination of volume resistivity, residing either in the surface contact or the deposition of a dielectric material on the nanofiber surface as a result of manufacturing.

Table 4.1 – Description of tested carbon nanofibers

ASI Sample	Description
AG Grade	As-grown nanofiber (processing temperature 1100°C)
PS Grade	Pyrolytically stripped nanofiber (processing temperature 1100°C)
LHT Grade	Nanofiber after heat treatment temperature up to 1500°C
HHT Grade	Nanofiber after heat treatment temperature to 3000°C

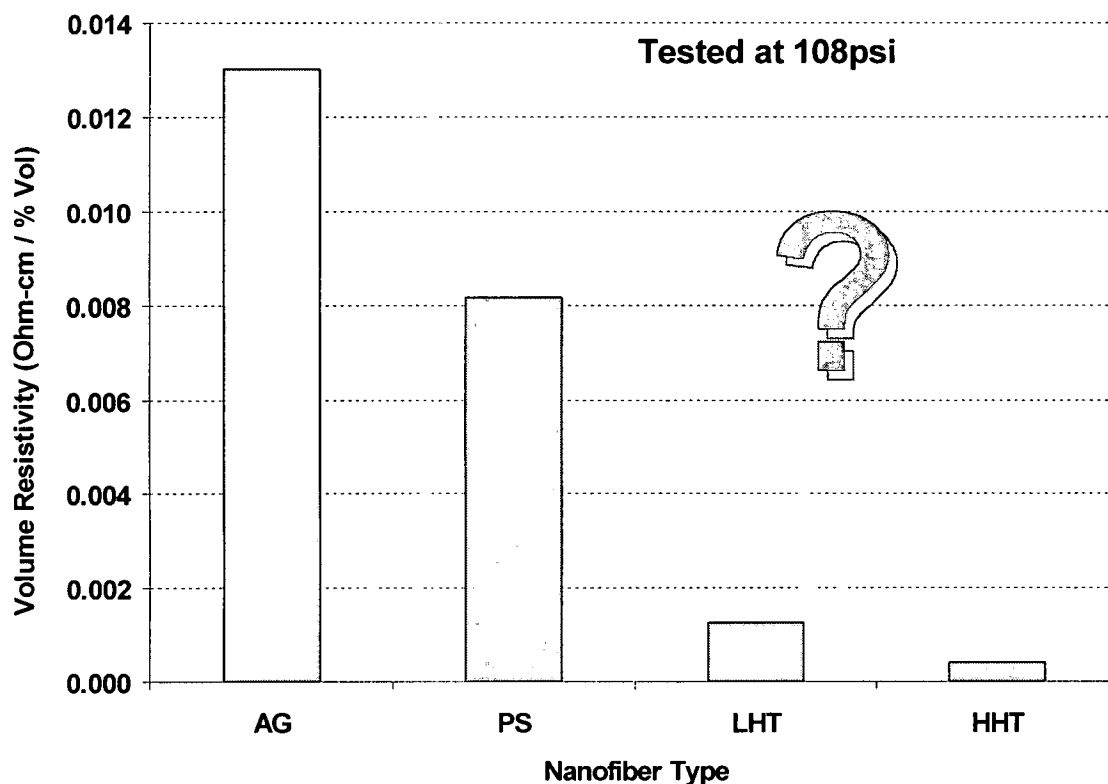


Figure 4.8 – Volume resistivity of as-received carbon nanofibers

Further evidence for the necessity of nanofiber purification lies in the extremely low surface energy and surface area test results presented in Table 4.2. If the samples were of a 100% nested cone type structure, both surface energy and surface area should be on the order of one magnitude higher in value. This indicated that the surface of the sample was passivated by adsorbed organic or inorganic molecules. Additionally, the surface energy and surface area did not change with the increase in heat treatment temperature. If the sample was clean, the surface energy and surface area should have been significantly higher with the alignment of the graphene layers. Also, upon completion of the degassing stage for the BET surface area tests for the PS and

LHT grade nanofibers, the glass sample holder was stained with a brownish residue as shown in Figure 4.9. The resulting residue represented polyaromatic hydrocarbons that adhered to the surface of the sample during manufacturing.

Table 4.2- Surface area and surface energy of carbon nanofibers

Nanofiber	BET Surface Area (m <sup>2</sup> /g)	Surface Energy (mJ/m <sup>2</sup> )
PS	32.9	40.4
LHT	33.2	42.4
HHT	36.5	36.7

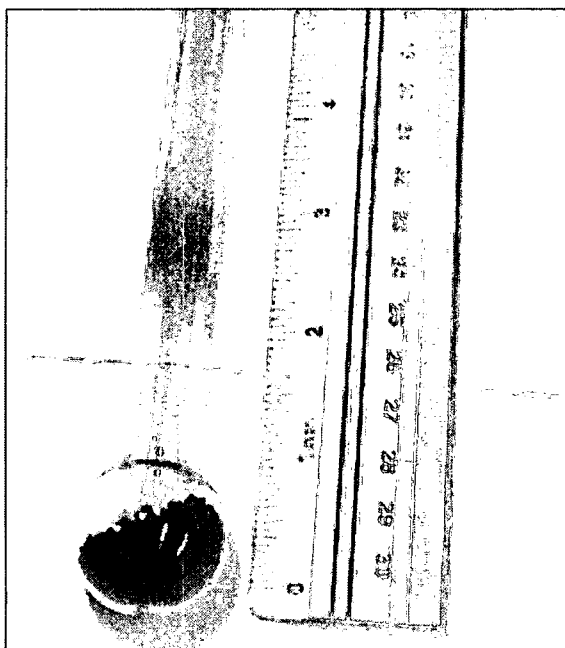


Figure 4.9 – Residue on sample tube following BET surface area testing

Support for the presence of polyaromatic hydrocarbons on the surface of the PS and AG nanofibers is shown in the TGA results (Figure 4.10). This yielded a 33% weight loss for the PS material when heated to 1000°C and a 12% weight loss for the AG material. The onset of degradation occurred prior to 600°C indicating that some organic material other than processing impurities

(metal, sulfur) was present on the surface of the material. Conversely, heat treatment of the nanofibers removed a significant amount of the organic material that had passivated the nanofiber surface as evidenced by the degradation onset temperatures for the LHT and HHT nanofibers being around 700°C and the low total weight loss for these samples when heated to 1000°C.

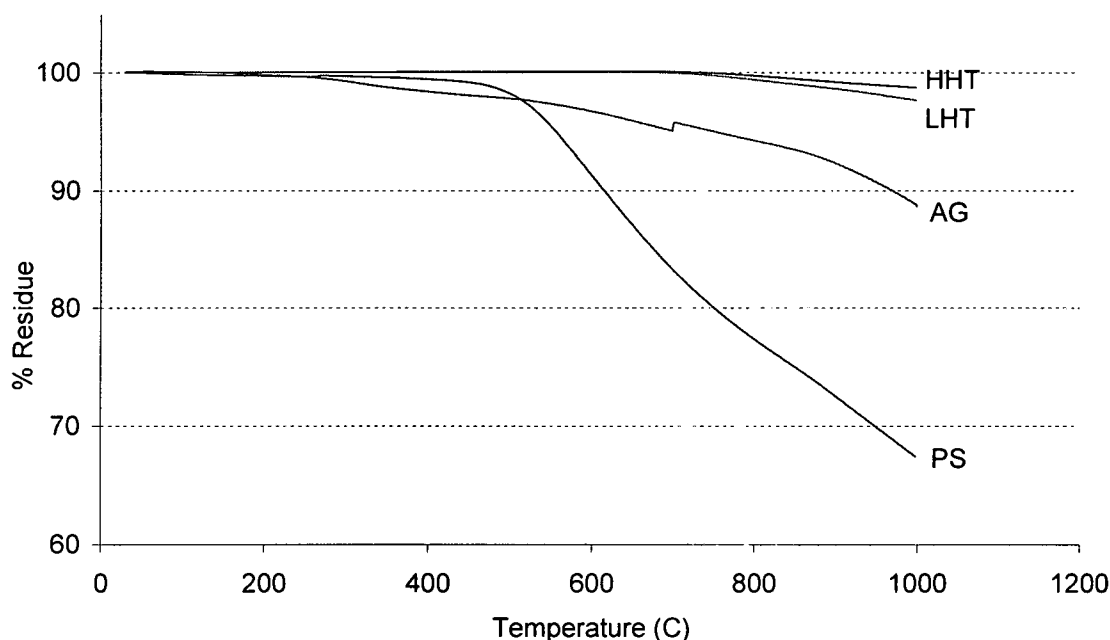


Figure 4.10 – TGA results for carbon nanofibers

Because of the weight loss that occurred in the TGA tests under 600°C, the residual material on the surface of the carbon nanofibers can be assumed to be carbonaceous and soluble in polar solvents. Therefore a Soxhlet extraction method was used to clean the nanofiber surface with solvents of increasing solubility intensity, providing progressive cleaning by fractionating the impurities. The TGA results also indicated that heat treatment of the as-received nanofibers

could also be used to remove impurities. In this case, heat treatment was completed in a carbonization furnace on nanofibers packed into a ceramic crucible. The furnace was purged of air, and the heat treatment to 1000°C took place in a nitrogen environment.

Measurement of the weight loss of the PS nanofibers following Soxhlet extractions with solvents of increasing solubility intensity is shown in Table 4.3. The weight loss for the PS sample from TGA was 33%. The weight loss following each of the extractions summed to 38%. This indicated that the solvent extraction method was more effective at cleaning the surface than heat treatment. While heat treatment improved electrical properties by minimizing spacing of the graphitic layers, extraction cleaning of the nanofiber surfaces should also result in improved electrical properties by allowing for improved contact between the nanofibers. When the PS grade nanofibers were extracted in acetone, the remaining solvent was a yellowish color (Figure 4.11). Further extraction with solvents of increasing polarity resulted in filtrates with less intense color, culminating in the extraction with pyridine resulting in a clear filtrate. This is further evidence of polyaromatic hydrocarbons that adhered to the surface of the sample following manufacturing.

Table 4.3 – TGA weight loss of PS nanofibers following sequential Soxhlet extraction

Sample	Weight Loss
TGA Testing	32.6
Acetone Extraction	17.3
THF Extraction	5.5
Toluene Extraction	9.5
Pyridine Extraction	5.7

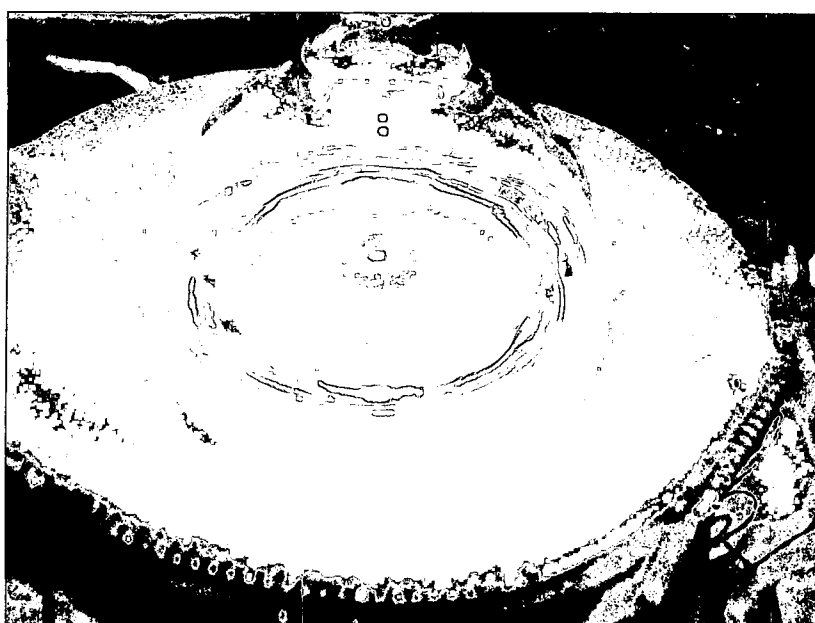


Figure 4.11 – Filtrate following PS nanofiber Soxhlet extraction in acetone

The presence of polyaromatic hydrocarbons on the surface of the AG and PS nanofibers would account for the anomaly in the volume resistivity testing. The chart shown in Figure 4.12 indicates volume resistivity results for both 16 and 108psi showing that for the higher pressures, improved contact between the nanofibers resulted in lower resistivity. While both pressures show the same trend – concentrating on the 108psi pressure to compare to the previous results – a progressive change in the resistivity was observed as a function of the

degree of cleaning using solvents with increasing solubility intensity. The polyaromatic hydrocarbons formed a dielectric layer on the surface of the nanofibers, altering the contact between the nanofibers resulting in a decreased resistance measurement. Extraction progressively removed the dielectric layer, and following pyridine extraction, the volume resistivity was on the same level as that of the heat treated nanofibers tested previously. In addition, Figure 4.12 shows the decrease in the color intensity following Soxhlet extractions with acetone, THF, toluene, and pyridine.

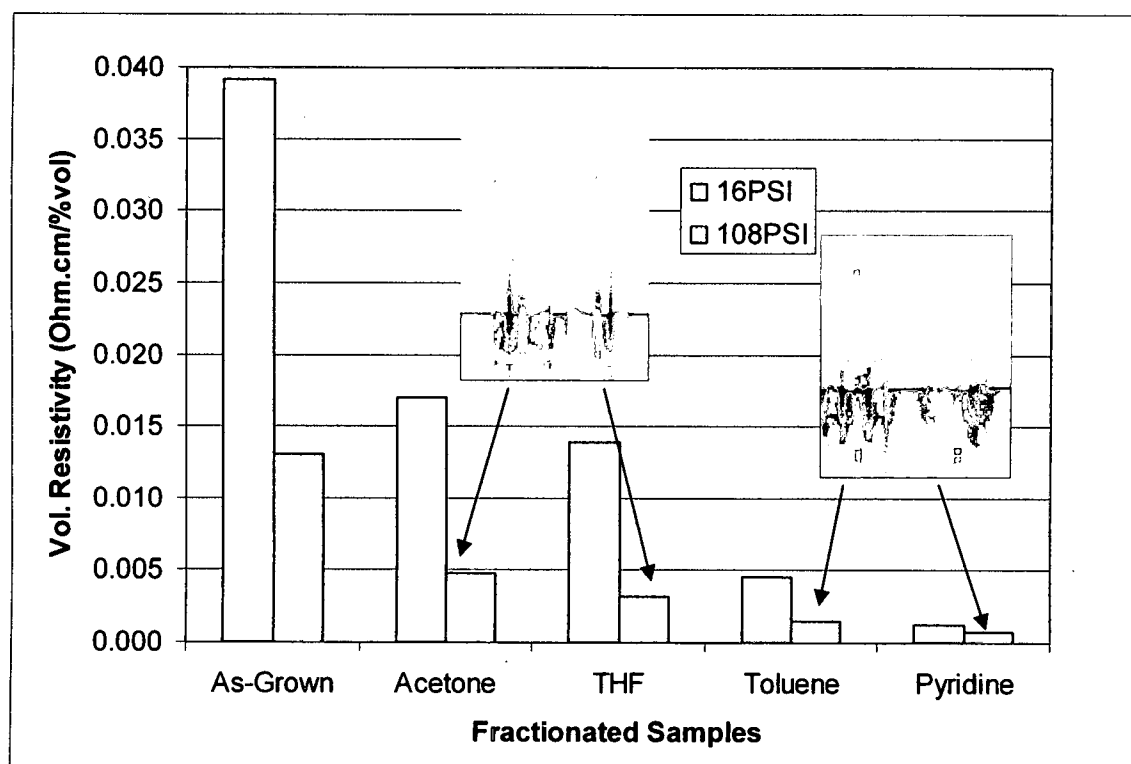


Figure 4.12 – Volume resistivity of AG nanofibers as a function of extraction solvent and coinciding filtrate colors

#### 4.3 EFFECT OF CARBON NANOFIBER CLEANING AND PURIFICATION ON POLYMERIC NANOCOMPOSITE CURING REACTION

The procedure for making a carbon nanofiber-reinforced epoxy nanocomposite involves combining a given weight percent of the nanofibers with the stoichiometric ratio of EPON862 epoxy and the EPI-CURE curing agent W (79.17 weight percent resin to 20.83 weight percent catalyst). In making a neat resin sample, the measured differential scanning calorimetry (DSC) curve is shown in Figure 4.13. The reaction is initiated at 93.4°C and has a heat of reaction of 369.6 J/g.

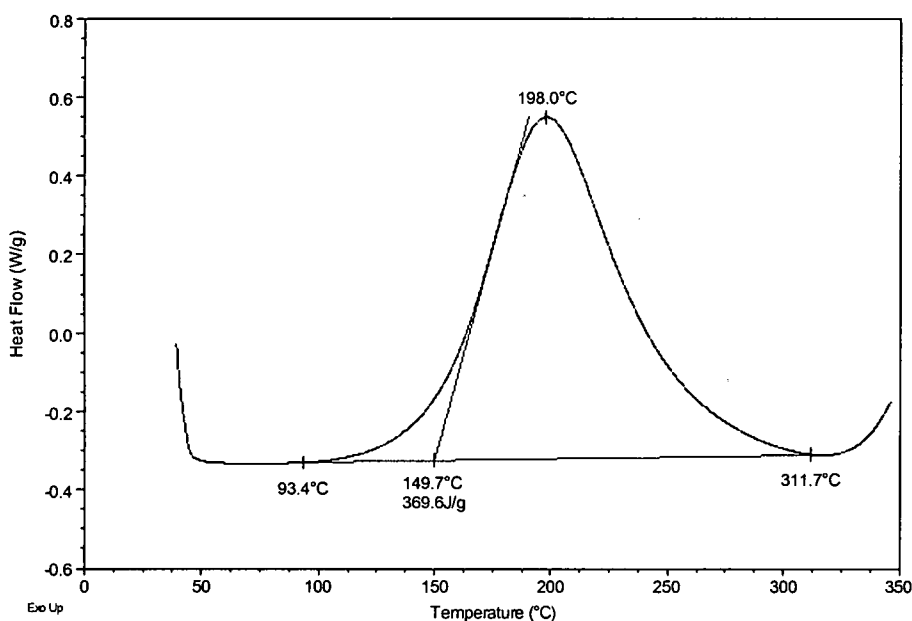


Figure 4.13 – DSC curve for neat epoxy resin

Addition of as-received PS nanofibers to the EPON 862 and curing agent resulted in two significant changes to the reaction of the neat resin (DSC curve, Figure 4.14). The first is the reduction in the total heat of reaction, indicating that the nanofibers actually aided in the curing process by reacting with the epoxy.



The second is the presence of an early reaction, likely due to the presence of polyaromatic hydrocarbons on the surface of the nanofibers.

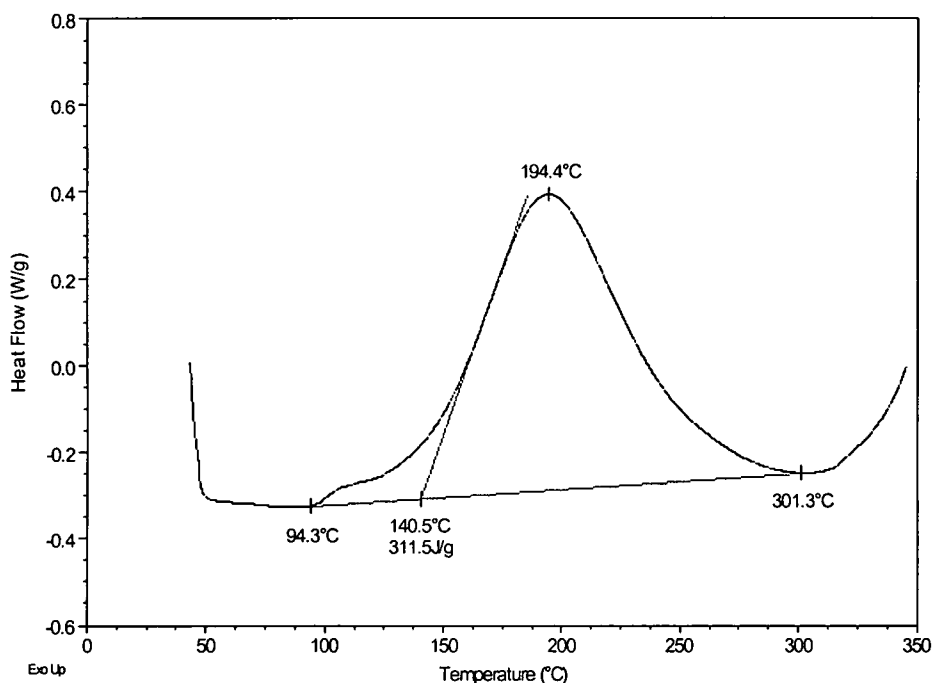


Figure 4.14 – DSC curve for 5 wt. % as-received PS nanofibers in EPON 862 / W

The early reaction is likely due to the presence of polyaromatic hydrocarbons on the surface of the nanofibers. To prove this assumption, a series of DSC tests were run mixing nanofibers and EPON 862 without the required curing agent. As shown in Figure 4.15, the presence of both as-received PS and LHT nanofibers in EPON 862 without curing agent did indeed cause a small reaction to occur. Two samples were run for each type of carbon nanofiber resulting in the four curves on the graph. With the HHT nanofibers (Figure 4.16), there was no apparent reaction, and the curve was very similar to that of the EPON 862 by itself. At the high heat treatment temperature, the

polyaromatic hydrocarbons should be completely removed from the surface of the nanofibers, indicating that the reaction apparent with the PS and LHT nanofibers mixed with EPON 862 is due to the presence of polyaromatic hydrocarbons.

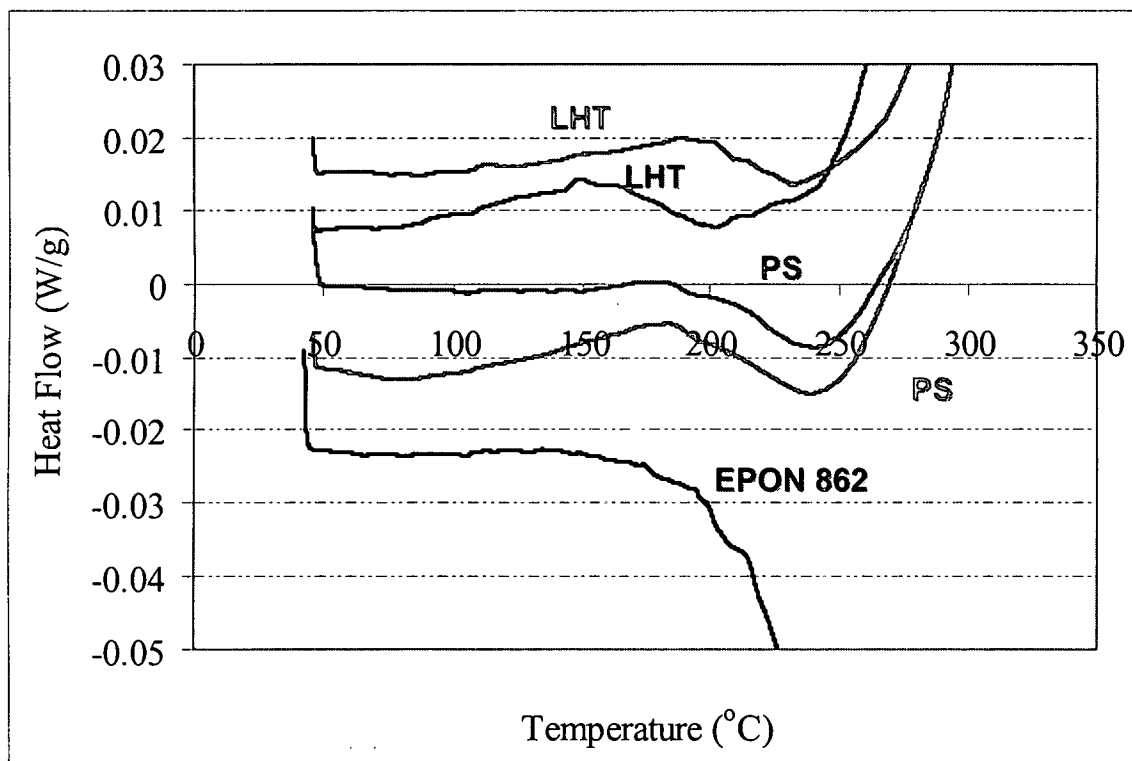


Figure 4.15 – DSC curves for as-received PS and LHT nanofibers in EPON 862 without curing agent

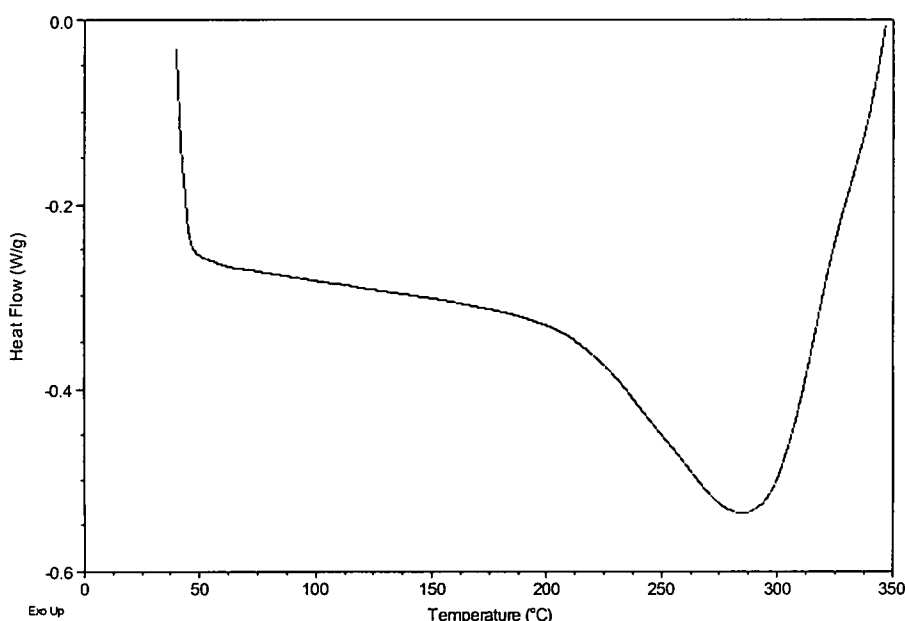
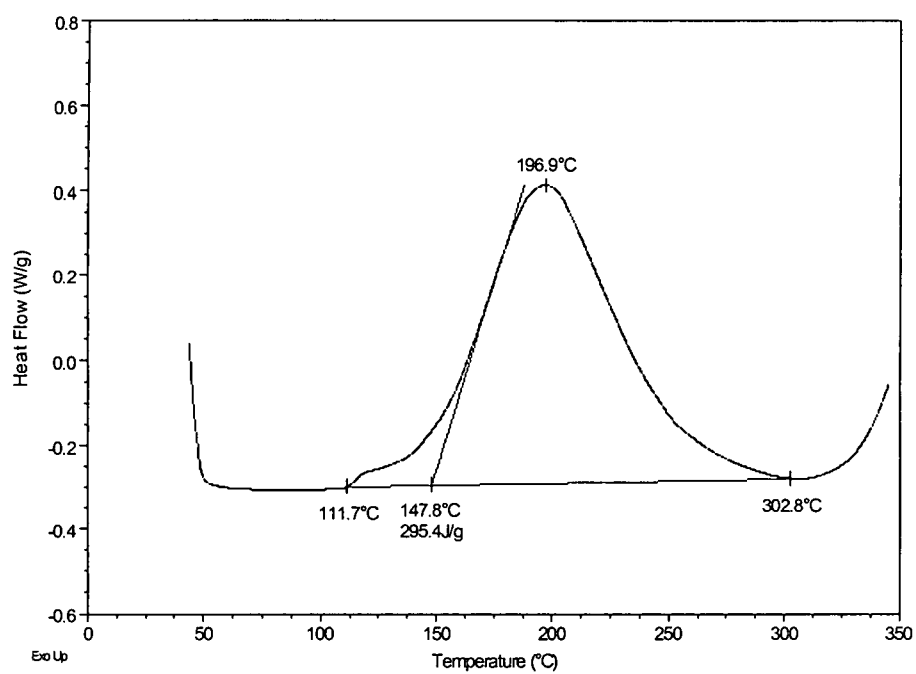
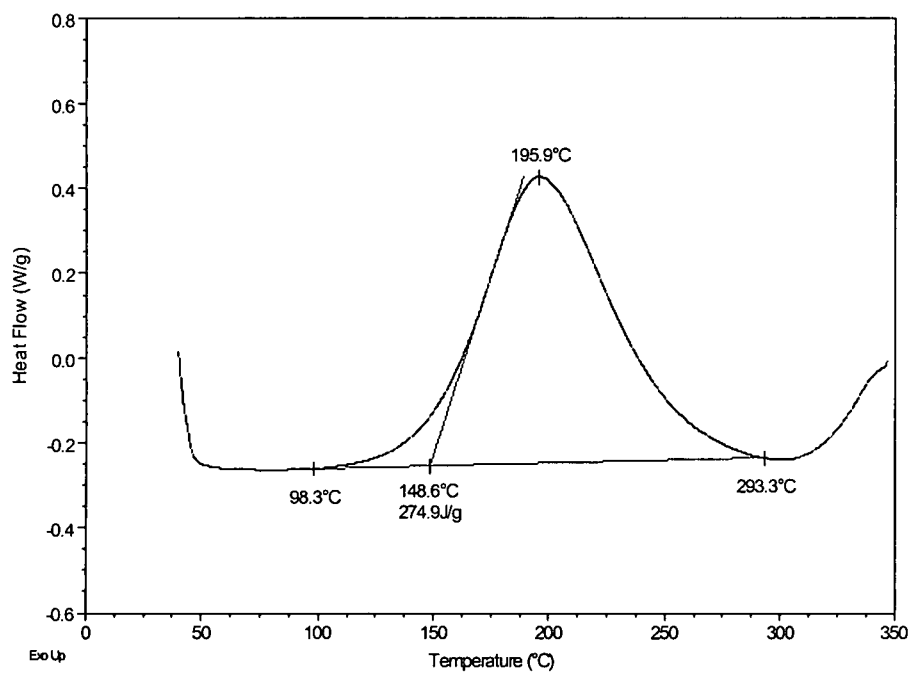


Figure 4.16 -- DSC curve for as-received HHT nanofibers in EPON 862 without curing agent

In order to determine the effect of extraction cleaning on the nanofiber-epoxy reaction, a series of DSC tests were run incorporating five percent by weight nanofibers following Soxhlet extraction with solvents of increasing solubility intensity. With increased nanofiber cleaning, the early reaction began to disappear from the DSC curve. Sequential extraction with acetone, THF, and toluene of the nanofibers still resulted in the presence of an early reaction (Figure 4.17a). It was not until the nanofibers were extracted with pyridine that the early reaction was completely eliminated (Figure 4.17b). Similarly, the DSC curve of the reaction of EPON 862 with catalyst and HHT nanofibers showed no early reaction (Figure 4.17c). Each of these results in combination further support the hypothesis that the early reaction present for the as-received nanofiber composites was in fact caused by the presence of polyaromatic hydrocarbons.



(a)



(b)

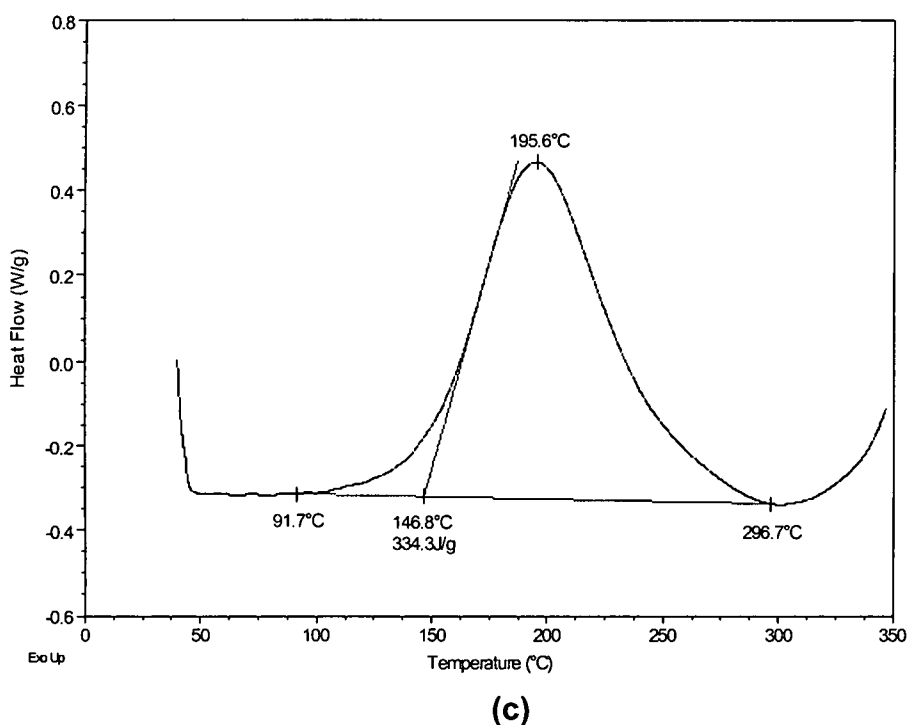


Figure 4.17 – DSC curves for (a) EPON 862 / W with 5 wt. % PS nanofibers extracted in toluene, (b) EPON 862 / W with 5 wt. % PS nanofibers extracted in pyridine, and (c) EPON 862 / W with 5 wt. % HHT nanofibers; note: for each figure, the heat of reaction was calculated for the entire reactive system, and not normalized for resin content

#### 4.4 CONCLUSIONS

The presence of impurities on the surface of PS and LHT nanofibers was shown through volume resistivity, TGA, and DSC testing of the resulting nanocomposites. As-received carbon nanofibers yielded inconsistent volume resistivity results. TGA testing indicated a 33% loss in weight for the PS nanofibers. When PS and LHT fibers were added to the epoxy, DSC testing showed the presence of an early reaction

Cleaning and purification of the nanofibers by subsequent heat treatment or Soxhlet extraction resulted in property improvements. The volume resistivity

tests were more consistent due to the removal of the dielectric layer. The cleaning procedures resulted in no weight loss prior to 600°C. Both Soxhlet extraction of the nanofibers progressively with acetone, THF, toluene, and pyridine and nanofiber heat treatment resulted in an elimination of the early reaction with epoxy.

In addition, carbon nanofibers are sensitive to temperature. High heat treatment temperature resulted in significant reductions in volume resistivity. Heat treatment to 1500°C did not eliminate an early reaction with the epoxy, while heat treatment to 3000°C completely eliminated a reaction. The structure of carbon nanofibers changes with heat treatment, and because of this the effect of heat treatment temperature on resulting nanocomposite properties must be established.

## CHAPTER V

### EFFECT OF CARBON NANOFIBER HEAT TREATMENT ON PHYSICAL PROPERTIES OF POLYMERIC NANOCOMPOSITES

#### 5.1 INTRODUCTION

In this study, carbon nanofibers were subjected to heat treatment temperatures ranging from 1500°C to 3000°C to alter the properties of the reinforcement and the physical and chemical interaction between the nanofiber and the epoxy polymer. The strength of adhesion between the fiber and an epoxy (thermoset) matrix was characterized by the flexural strength and modulus, and the electrical and thermal properties of the composites were investigated from the viewpoint of heat treatment temperature of the carbon nanofibers.

#### 5.2 EXPERIMENTAL SETUP

The carbon nanofibers used in this study were produced at Applied Sciences, Inc. and were from the Pyrograf III family of fibers. This group of nanofibers (labeled PS) has diameters between 60 and 100 nanometers and lengths ranging from 30 to 100 microns.

The nanofibers were heat treated in an atmosphere-controlled batch furnace. Approximately 300g of nanofibers were placed in a ceramic crucible for the heat treatment. The furnace was purged with nitrogen gas for one hour prior to heating. The heating rate was 100°C per hour, and the furnace was held at

the target temperature for one hour prior to cooling. The target temperatures were 1500, 1800, 2000 and 3000°C.

The carbon nanofibers were dispersed within the epoxy resin at loading rates of four, eight and twelve percent by weight. Previous work [59] indicated that loading beyond twelve percent by weight actually lead to a decrease in nanocomposite mechanical properties. In addition, processing nanocomposites with loads beyond twelve percent by weight becomes difficult in establishing a homogenous mixture. The as-received carbon nanofibers, designated as PS, and the neat resin were used as a baseline for the study.

The mechanical properties of the nanocomposites were measured using the three-point flexural strength test according to ASTM D790-00. Thermal diffusivity of each nanocomposite incorporated a xenon flash diffusivity test. The thermal diffusivity parameter was used in conjunction with the specific heat and density of the nanocomposite to calculate the thermal conductivity. The tests for specific heat and density were carried out according to ASTM E1269-89 and ASTM C693-74 respectively. The electrical resistivity of each nanocomposite was tested utilizing a four-point test according to ASTM B193-87.

### 5.3 *RESULTS AND DISCUSSION*

The improvements in mechanical properties are shown in Figures 5.1 and 5.2. The flexural modulus increased with increasing nanofiber load. The maximum modulus of 3.5GPa was achieved for the nanocomposite sample with twelve weight percent loading of nanofibers heat treated to 1800°C. With



increasing heat treatment temperature, the modulus for twelve weight percent loading of nanofibers heat treated to 2000°C and 3000°C decreased to 3.1 and 3.0 GPa respectively. This indicated that with increasing amount of graphitization, the adhesion between the carbon nanofiber and the epoxy resin decreased. The increased graphitization of the nanofibers may cause the previously truncated graphene layers to loop together, thereby eliminating free edges for bonding with the polymer matrix. However, the heat treatment of the carbon nanofibers did show an improvement over the pristine nanofibers. For the as-received PS nanofibers, the modulus at twelve weight percent loading was 2.6 GPa. This increase in modulus may be due to the removal of “dirt” – polyaromatic hydrocarbons, sulfur, and oxygen and nitrogen based functional groups – allowing for free ends of the graphene sheets to bind with the epoxy.

The ultimate strength of the nanocomposites decreased with increasing nanofiber load for the heat treated nanofiber composites. Again, the nanofibers heat treated to 1800°C exhibited the highest strength values for the heat treated samples at all nanofiber loading levels. Heat treatment had a positive effect on strength for low (four weight percent) nanofiber loading; however at higher nanofiber loadings (eight and twelve weight percent), heat treatment of nanofibers actually lead to a lower strength than the pristine PS nanofiber composites. The minimal improvements in strength compared to that of modulus may be an indication that the chemical adhesion between the nanofiber and the epoxy matrix is not optimized. This can be improved through chemical

functionalization of the nanofiber. In addition, strength of the nanocomposite could be improved in one direction by alignment of the nanofibers in the matrix.

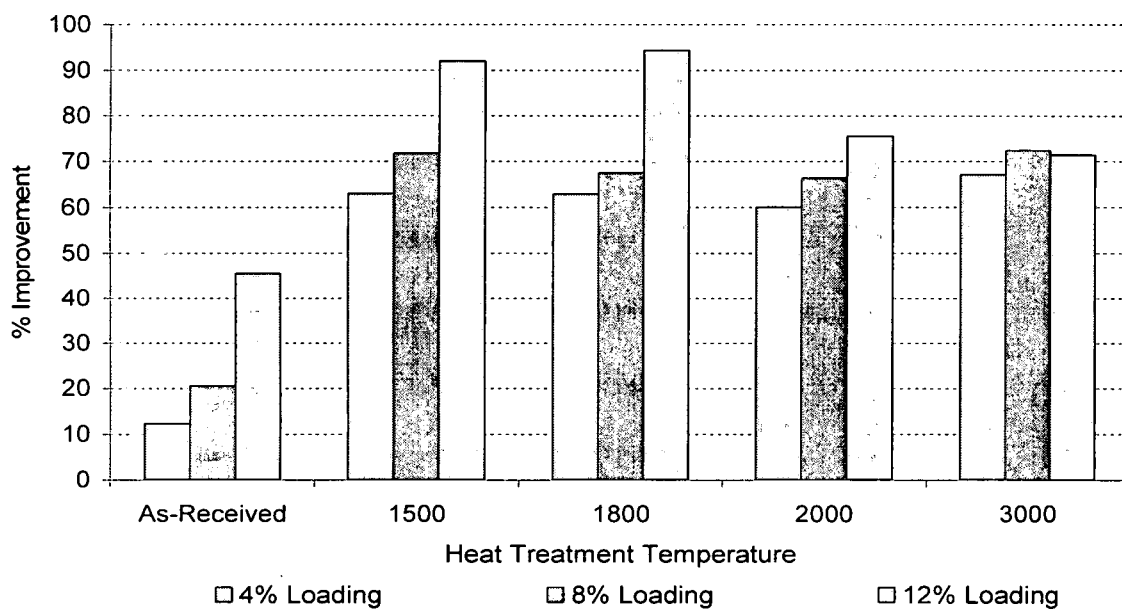


Figure 5.1 – Nanocomposite flexural modulus percent improvement over neat resin as a function of nanofiber heat treatment temperature

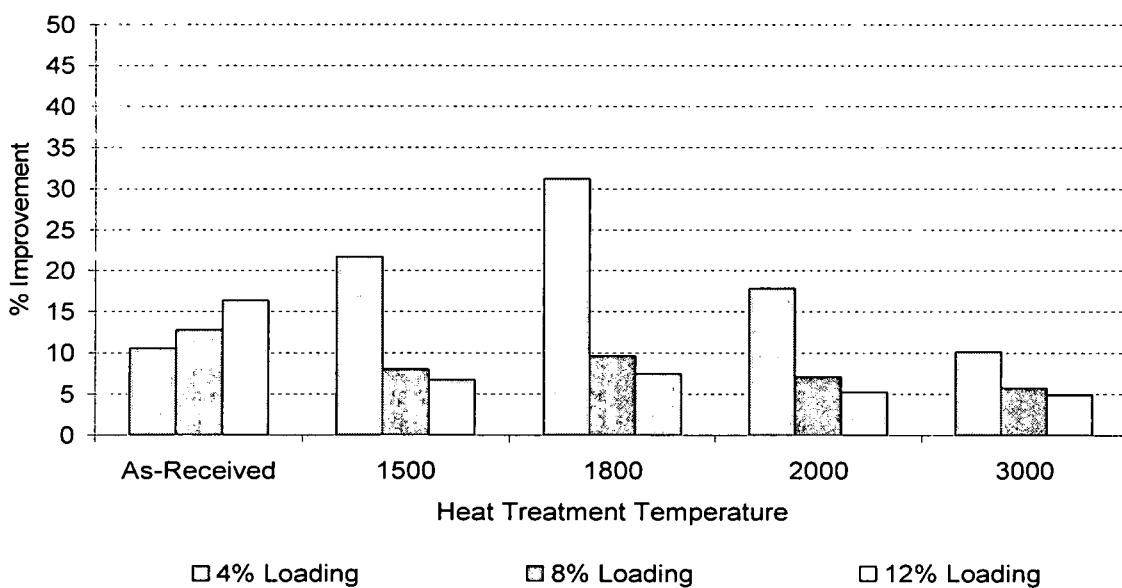


Figure 5.2 – Nanocomposite flexural strength percent improvement over neat resin as a function of nanofiber heat treatment temperature

The improvement in electrical and thermal properties of the nanocomposites comprised of heat treated nanofibers was significant. This drastic improvement of thermal and electrical properties of the high heat treated nanofiber based composite over that of the PS nanofiber based composite is due to the structural changes that occur during heat-treatment. The alignment of the graphene layers within the nanofibers allow for a more efficient transfer of phonons and electrons.

The improvement in electrical resistivity is shown in Figure 5.3. While the addition of pristine PS nanofibers at four weight percent loading decreased the resistivity of the nanocomposite by five orders of magnitude over the neat epoxy resin, heat treatment of the nanofibers to 1500°C reduced the resistivity by eight orders of magnitude and heat treatment of the nanofibers to 3000°C decreased the resistivity by nine orders of magnitude. In addition, with increasing heat treatment temperature, the electrical resistivity decreased – from 440Ω-cm at four weight percent loading of nanofibers heat treated to 1500°C to 94Ω-cm at four weight percent loading of nanofibers heat treated to 3000°C. Increasing the nanofiber loading further decreased the electrical resistivity. The electrical resistivity of the nanocomposite with twelve weight percent loading of nanofibers heat treated to 1500°C was 6.5Ω-cm, and the electrical resistivity of the nanocomposite with twelve weight percent loading of nanofibers heat treated to 3000°C was 1.2Ω-cm.

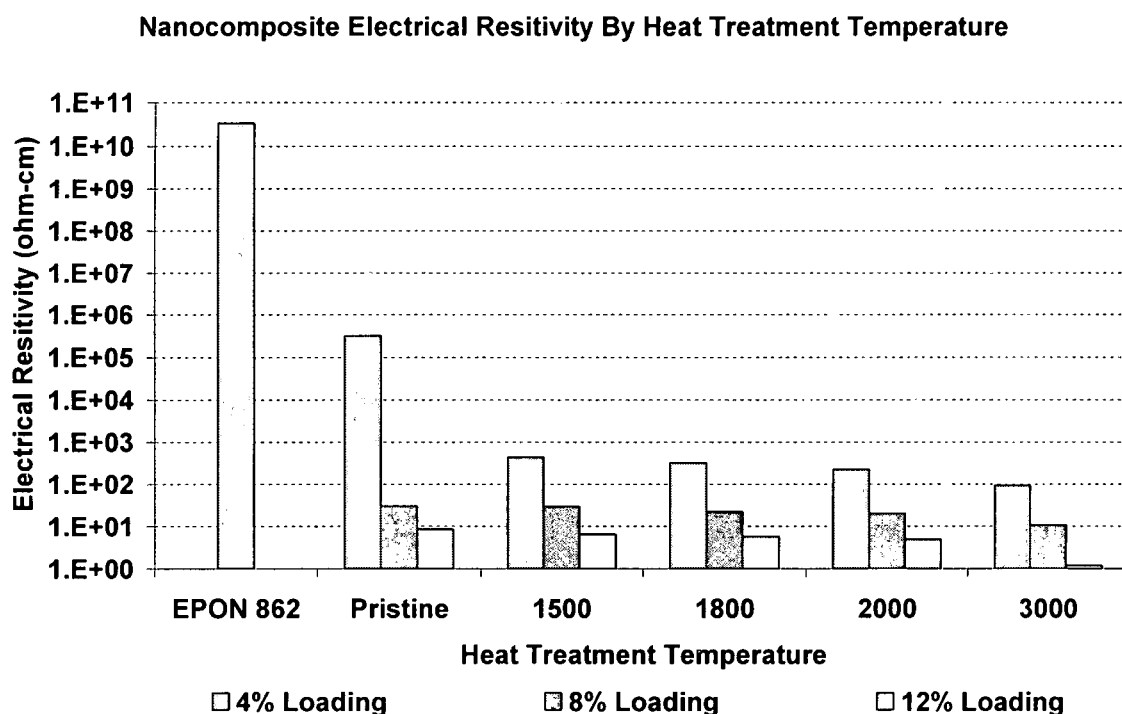


Figure 5.3 – Nanocomposite electrical resistivity as a function of nanofiber heat treatment temperature

In a similar manner, the thermal conductivity of neat epoxy resin increased significantly with the addition of nanofibers (Figure 5.4). While the addition of as-received PS nanofibers at four and twelve weight percent loading increased the thermal conductivity of the neat resin by 21% and 105% respectively, the heat treatment of the nanofibers to 1500°C increased the thermal conductivity by 64% at four weight percent loading and 194% at twelve weight percent loading. Heat treatment of the nanofibers to 3000°C increased the thermal conductivity by 133% at four weight percent loading and 6191% at twelve weight percent loading. With increasing heat treatment temperature, the thermal conductivity increased – from 64W/mK at four weight percent loading of nanofibers heat

treated to 1500°C to 133W/m-K at four weight percent loading of nanofibers heat treated to 3000°C.

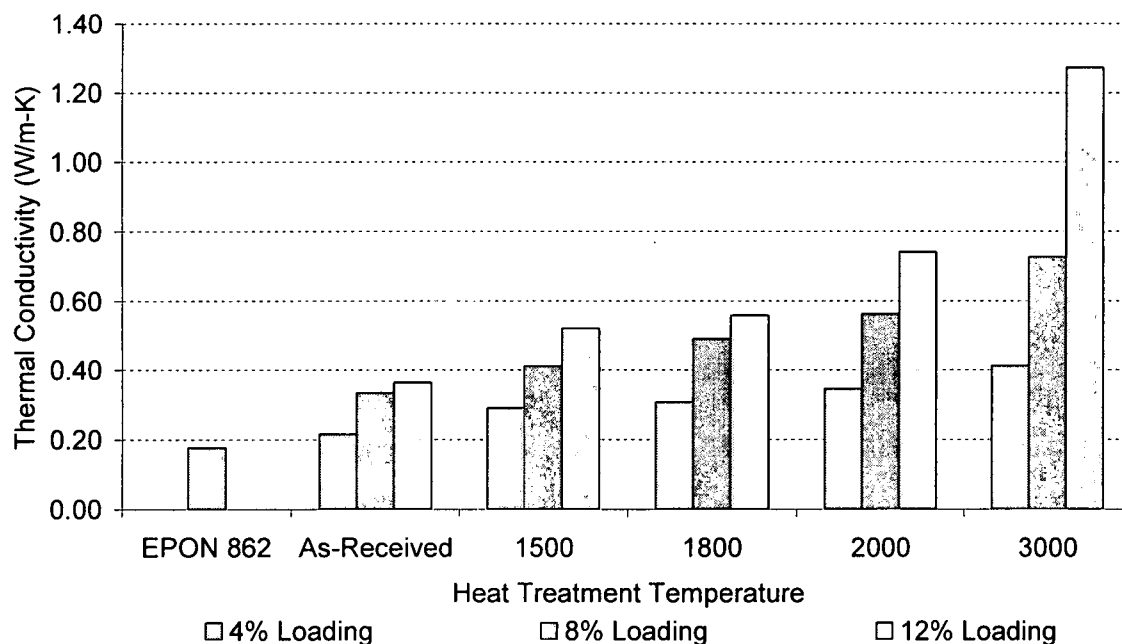


Figure 5.4 – Nanocomposite thermal conductivity as a function of nanofiber heat treatment temperature

#### 5.4 CONCLUSIONS

The heat treatment of carbon nanofibers lead to the removal of impurities from the nanofiber and resulted in altered physical properties of a nanofiber reinforced epoxy composite. During heat treatment the structure within the carbon nanofibers is changed from local molecular ordering to that of coalesced, flattened graphene layers. Heat treatment up to 1800°C resulted in improved flexural modulus and strength of the nanocomposite. Additional heat treatment to higher temperatures lead to increased conversion to graphene layers and resulted in lower mechanical properties due to poor adhesion to the epoxy matrix

caused by the elimination of the free truncated edges of the graphene layers available to bond to the polymer matrix. The alignment of graphene layers within the nanofibers allowed for a more efficient transfer of phonons and electrons resulting in significant decreases in electrical resistivity and increases in thermal conductivity of the neat epoxy resin. Heat treatment of the nanofibers allowed for the attainment of superior electrical and thermal properties at low fiber loadings that are not possible with pristine pyrolytically stripped carbon nanofibers.

The testing of heat treated nanofiber based nanocomposites demonstrated that the resulting nanocomposite properties must be compromised. If the end result of the nanocomposite is a desired high mechanical property, the nanofibers should not be heat treated above 1800°C. However, if the end result is a desired high electrical or thermal property, the nanofiber must be heat treated to 3000°C. At this higher temperature, while the graphene layers are aligned with minimal interlayer spacing to allow efficient electron and phonon transfer, the ends of the graphene planes tend to loop together and reduce the number of available sites for bonding with the resin. Therefore, a better method for improving interfacial adherence may be to chemically functionalize the nanofiber surface. This would impart groups on the surface that would bind to the resin without changing the structure of the nanofiber resulting in reduced chemical bonding sites.

## CHAPTER VI

### ELECTROCHEMICAL OXIDATION OF CARBON NANOFIBERS: SURFACE CHEMISTRY AND POLYMER ADHESION

#### 6.1 INTRODUCTION

In this study, carbon nanofibers were subjected to electrochemical oxidation in 0.1M nitric acid for varying times to modify the interface between the nanofibers and epoxide molecules in polymeric nanocomposites. X-ray photoelectron spectroscopy was employed to characterize surfaces with regard to the content of carbon, oxygen, and nitrogen. The strength of adhesion between the fiber and an epoxy (thermoset) matrix was characterized by the flexural strength and modulus, and the electrical and thermal properties of the composites were investigated from the viewpoint of surface treatment extent of the carbon nanofibers.

#### 6.2 EXPERIMENTAL SETUP

The carbon nanofibers used in this study were produced at Applied Sciences, Inc. and were from the Pyrograf III family of fibers. This group of nanofibers (labeled PS) has diameters between 60 and 100nm and lengths ranging from 30 to 100 $\mu$ m.

### 6.2.1 *ELECTROCHEMICAL TREATMENT*

Electrochemical treatment of carbon nanofibers represents an example of the inability to transfer surface functionalization techniques utilized on micrometric filler material to the nanometric scale. Electrochemical treatment of micrometric carbon fibers allows for a tow of carbon fibers to be used as the anode in the process. However, without being able to "hold" carbon nanofibers, a method for optimal subsection of the nanofibers to the electrochemical treatment was devised. The nanofibers were electrochemically surface treated using nitric acid as an electrolyte in a concentration of one weight percent as diagrammed in Figure 6.1. Approximately fifteen grams of nanofibers for each trial were packed into porous plastic beakers, covered with a Teflon cap, and submerged in the acidic solution. A graphite electrode was placed into the packed nanofibers, and a specific applied current was set at 0.1 Amps. The time of the treatments was 30 seconds, one, two, four, eight, ten, twelve, and fifteen minutes. Following treatment, the oxidized fibers were washed with distilled water until attaining a neutral pH and dried in a vacuum oven at 100°C for 48 hours.



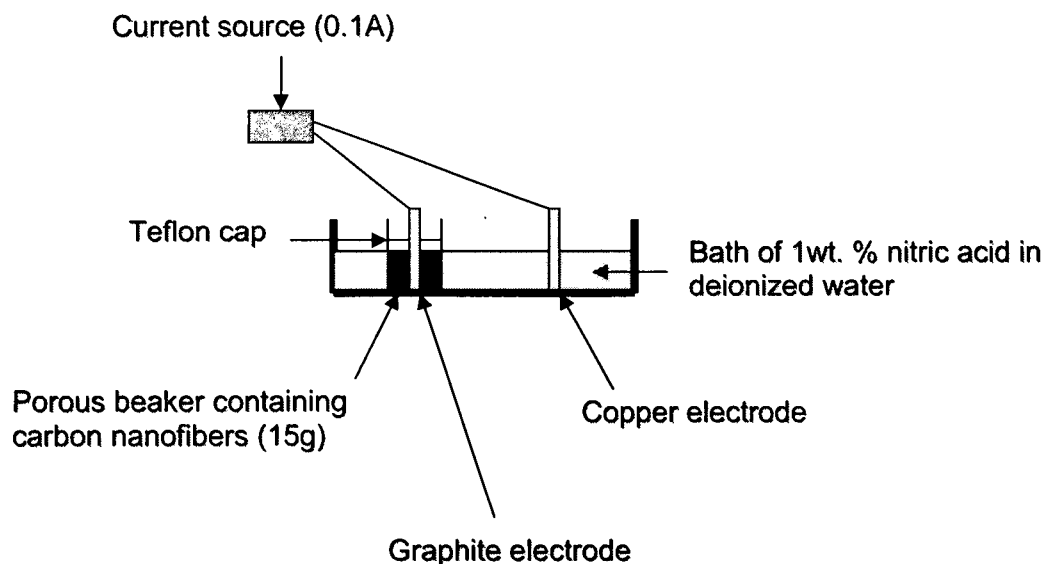


Figure 6.1 – Procedure for electrochemical treatment of carbon nanofibers

#### 6.2.2 NANOFIBER CHARACTERIZATION BY X-RAY PHOTOELECTRON SPECTROSCOPY

The functionalized carbon nanofibers were characterized using X-ray photoelectron spectroscopy (XPS). A non-linear least squares curve fitting program with a Gaussian-Lorentzian mix function and background subtraction was used to deconvolve the XPS peaks.

While investigation of surface chemistry was performed by XPS using chemical shift phenomena, in several cases, relative chemical shifts of different groups are below the energy resolution attainable by XP spectrometers due to the existence of significant intrinsic peak widths. In these cases, other sample properties, like chemical reactivity, could operate the requested discrimination. Chemical derivatization XPS (CD-XPS), based on selective reaction labeling groups of interest was used to improve the selectivity and sensitivity of the XPS analysis. The methodology has been applied mainly to organic polymers, even

though some inorganic materials have also been studied. Derivatization reactions have been established for C-OH, COOH, and C=O groups. Information obtained by the simple XPS evidence of the marker element must be complemented by careful analysis of the main signals, to which both the organic material and the derivatizing agent contribute.

Alcohol groups can be esterified by trifluoroacetic anhydride (TFAA) [60]. A procedure for the derivatization of a polymer sample calls for the sample to be introduced into a glass test tube. Two milliliters of TFAA was injected into the test tube below the sample, without contacting it. The test tube was sealed, and the reaction with the TFAA vapor was allowed to proceed for fifteen minutes at room temperature. The sample was then removed from the test tube, and transferred to the XP spectrometer for analysis.

Derivatizing the sample with TFAA vapor results in the conversion of the alcohol substituent to a trifluoroester group according to the reaction in Figure 6.2. This leads to the appearance of new peaks at 290.4 and 293.7 eV which are attributed to the ester and  $\text{CF}_3$  carbon atoms respectively. The peak area of the trifluoroacetic ester ( $\text{CF}_3\text{COO}$ ) component is used for a quantitative estimate for the C-OH groups by calculating one third of the F1s area due to the introduction of three fluorine atoms for each phenol functional group. TFAA labels virtually all of the alcohol groups within the XPS sampling depth.

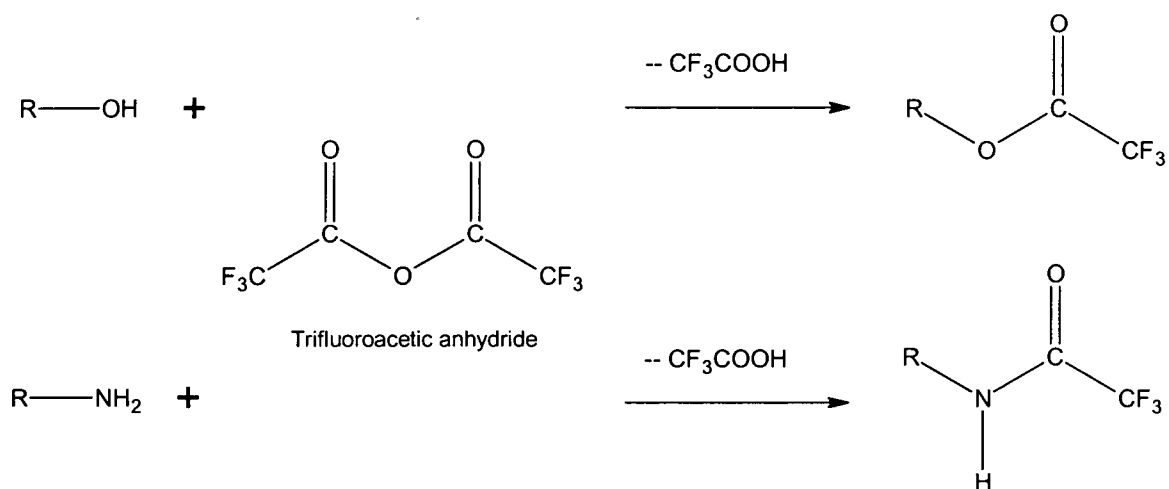


Figure 6.2 – Esterification of C-OH groups by TFAA

An example of the resulting XPS plots of a functionalized carbon nanofiber is shown Figure 6.3. The peaks for fluorine are present following the derivatization reaction. Quantification of these fluorine peaks results in three times the amount of alcohol functional groups in the sample.

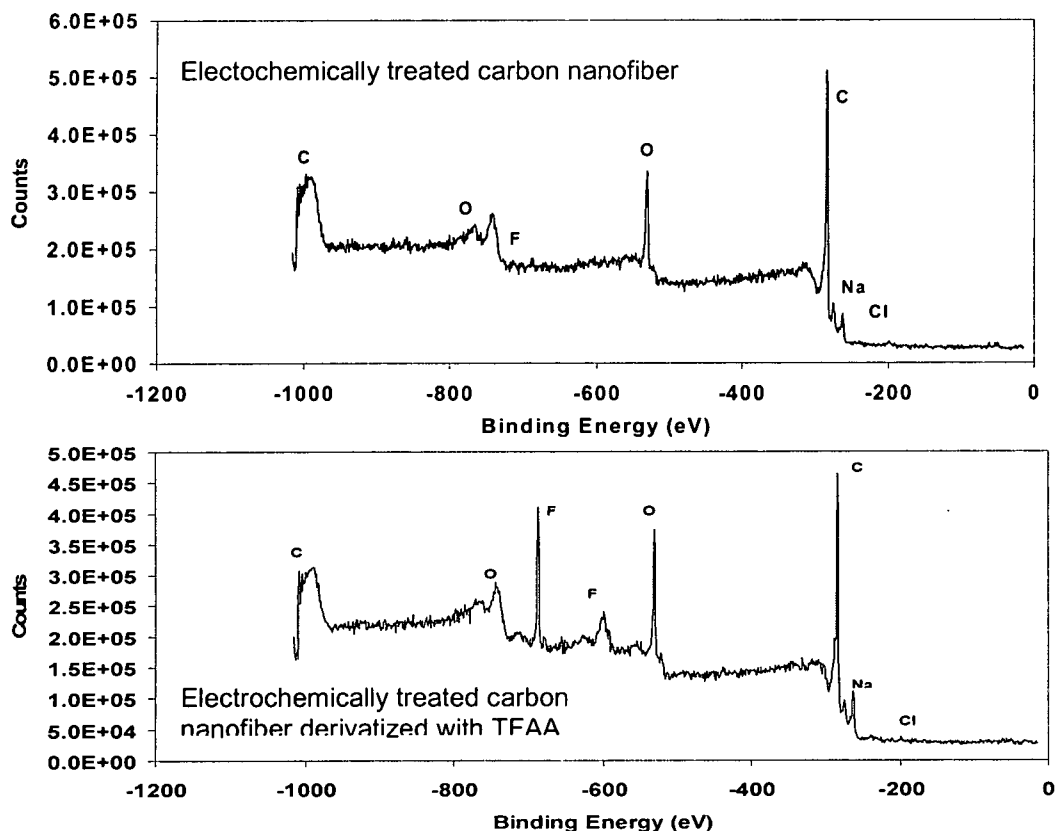


Figure 6.3 – XPS plots of chemically derivatized carbon nanofibers

Carboxylic groups can be esterified by trifluoroethanol (TFE) vapors, making use of di-*t*-butyl carbodiimide (DtC) as a dehydrating agent according to the reaction in Figure 6.4 [61]. A procedure for the derivatization of a polymer sample calls for the sample to be suspended in a glass test tube; TFE (0.9 mL), pyridine (0.4 mL), and DtC (0.3 mL) were sequentially injected below the sample, without contacting it, at fifteen minute intervals. The test tube was sealed with a cap and the reaction was allowed to proceed at room temperature for twelve hours. The samples were then transferred to the XP spectrometer and analyzed.

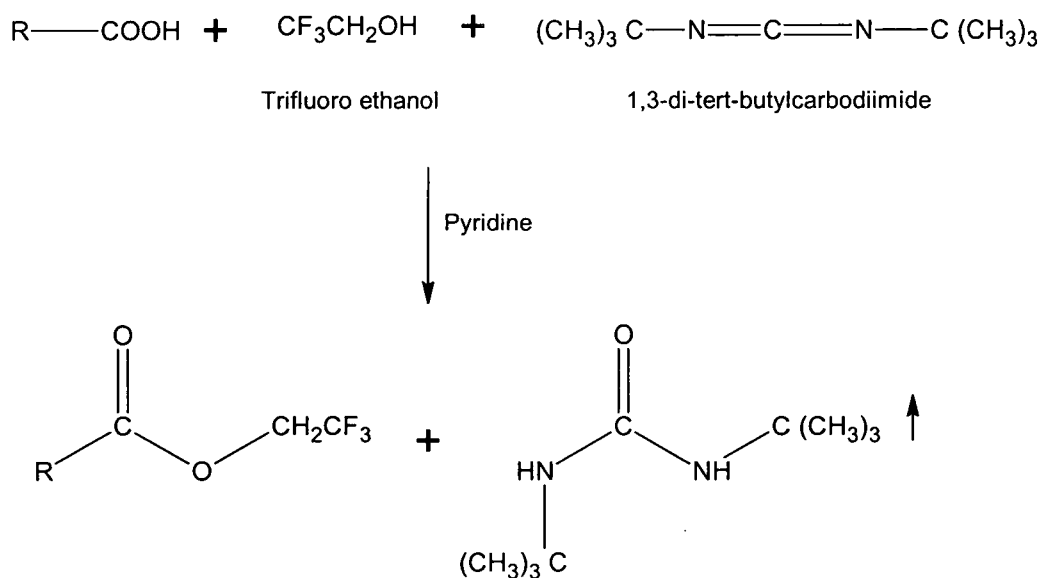


Figure 6.4 – Esterification of C-OOH groups by TFE

An assumption of the reaction is that the reaction product of DtC (*N,N'*-di-*t*-butyl)-urea), is completely removed from the surface of the reacted organic material, though no washing stage is performed. This behavior has been confirmed in literature. The reaction has been shown to yield about 99% esterification of the C-OOH groups by TFE. Esterification by TFE causes three fluorine atoms to be introduced into the sample for each C-OOH group. An enhancement of the response factor should be obtained and the XPS detectability of this functionality then improved. One source of error could be due to the presence of ionized C-OOH groups, which are not susceptible to esterification mediated by carbodiimides.

Aldehyde or ketone groups can be reacted with pentafluorophenylhydrazine (PFPH), leading to the formation of the relevant hydrazone according to the reaction in Figure 6.5 [61].

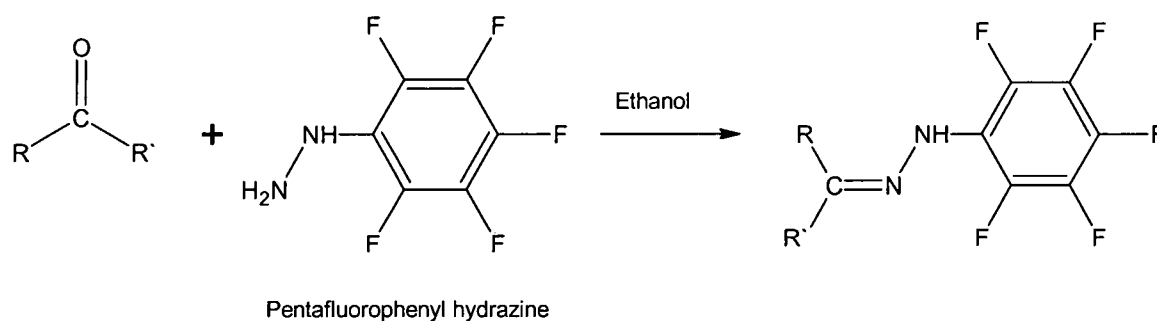


Figure 6.5 – Esterification of C=O groups by PFPH

A procedure for the derivatization of a polymer sample calls for the sample to be immersed in a solution of PFPH and anhydrous ethanol (150mg in fifteen milliliters, with the addition of a drop of concentrated hydrochloric acid). Subsequently, the samples were washed three times with anhydrous ethanol, dried under nitrogen and transferred to the XP spectrometer.

The reaction with PFPH leads to the introduction of five fluorine atoms for each derivatized C=O group, which is converted to PFP-hydrazone. Further, two nitrogen atoms are also added to the sample during the formation of a PFP-hydrazone moiety.

### 6.2.3 NANOCOMPOSITE CHARACTERIZATION

Electrochemically treated carbon nanofibers were added to an epoxy resin matrix (EPON 862) at a loading rate of twelve percent by weight and cured under pressure in a silicone mold. The mechanical properties of the nanocomposites were measured using the three-point flexural test according to ASTM D790-00. The electrical resistivity of the nanocomposites was measured using a four-point test according to ASTM B193-87. The thermal diffusivity of each nanocomposite

incorporated a xenon flash diffusivity test outlined in ASTM C714-72. The thermal diffusivity parameter was used in conjunction with the specific heat and density of the nanocomposite to calculate the thermal conductivity. The tests for specific heat and density were carried out according to ASTM E1269-89 and ASTM C693-74 respectively.

### 6.3 RESULTS AND DISCUSSION

Surface characterization of the nanofibers by XPS (Figure 6.6) showed an increase in oxygen content from 2% in the as-received fibers to 8.5% in the fibers treated for fifteen minutes. The N 1s peak was negligible in all cases.

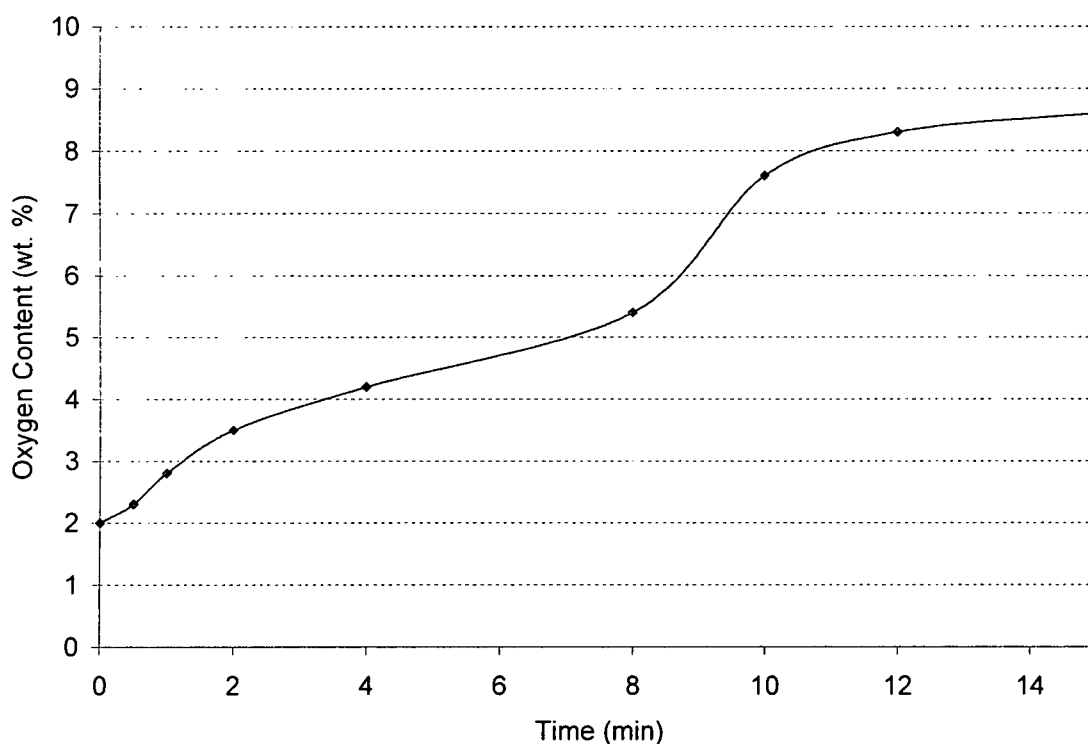


Figure 6.6 – Oxygen content weight percent as a function of nanofiber electrochemical treatment time

Deconvolution of the C 1s spectra (Table 6.1) gives the potential for five peaks: (I) graphitic carbon (284.6 eV), (II) carbon present in phenolic, alcohol, ether, or C=N groups (286.1-286.3 eV), (III) carbonyl or quinone groups (287.3-287.6 eV), (IV) carboxyl or ester groups (288.4-288.9 eV), and (V) carbonate (290.4-290.8 eV). There is a significant decrease in the relative content of graphitic carbon (peak I) and a rise in the relative content of carbon bonded to oxygen containing functions (peaks II, III, IV, and V) with increasing amount of electrochemical treatment. The increase in relative concentration of carbon oxygen complexes occurs because the outer layers of the fibers become increasingly porous. The fraction of carbon atoms in the region which exist on the pore surfaces increases. These carbon atoms are the sights of oxidation, thereby increasing the relative amount of oxygen.

Table 6.1 – Deconvolution of XPS C 1s spectra indicating weight percent of five specific carbon bonds as a function of nanofiber electrochemical treatment time

Sample	I Graphitic Carbon	II C=N	III Carbonyl/ Quinone	IV Carboxyl/ Ester	V Carbonate
30 sec Treatment	90	0	6	4	0
1 min Treatment	87	0	13	0	0
2 min Treatment	86	3	7	2	2
4 min Treatment	80	0	14	6	0
8 min Treatment	78	3	9	6	4
10 min Treatment	79	0	11	9	0
12 min Treatment	75	0	21	4	0
15 min Treatment	74	0	23	2	0

As shown in Figure 6.7, a modest degree of electrochemical treatment improved the flexural modulus of the nanocomposite by enhancing the interfacial adhesion between the fiber and resin. The treatment time of 30 seconds allowed



for a 4% increase in flexural modulus. A maximum improvement of 74% occurred with an electrochemical treatment time of twelve minutes. Prolonged subjection to the electrochemical treatment beyond twelve minutes showed a drop in flexural modulus. This may be due to the additional treatment time possibly causing damage to the fiber surface or generation of different functional groups. To clarify which of the assumptions is valid, various chemical derivatizations were applied to quantify the amount of functional groups and understand the mechanism involved in the high mechanical performance of nanocomposites.

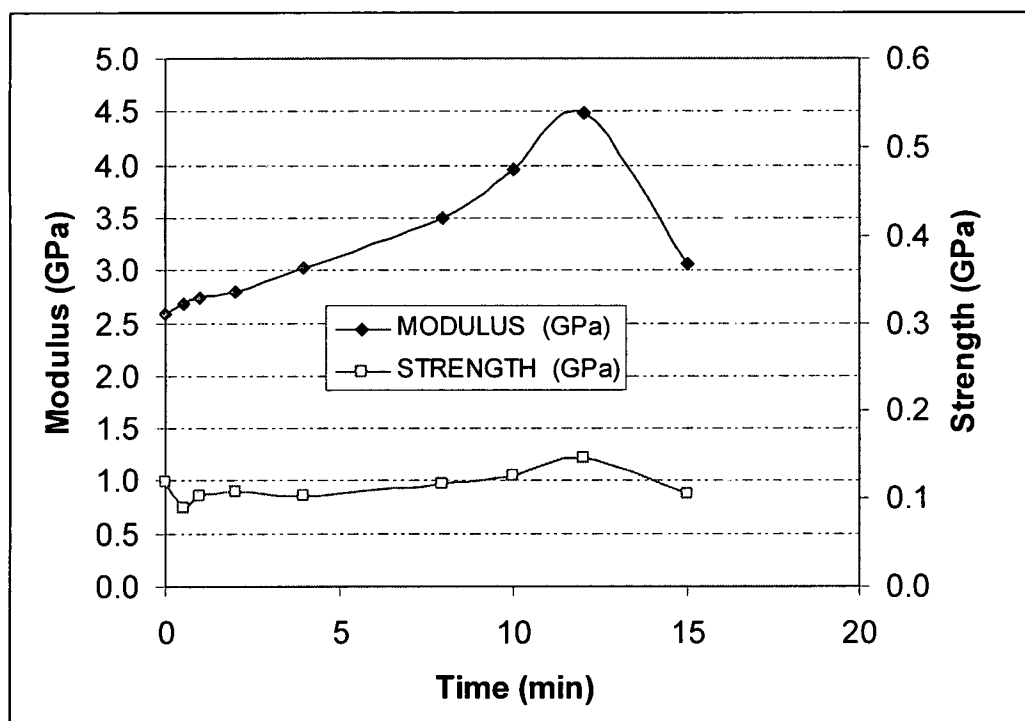


Figure 6.7 – Nanocomposite flexural modulus and strength as a function of nanofiber electrochemical treatment time

Results of the chemical derivatization XPS (Figure 6.8) showed that there is a strong correlation between the increase in the alcohol group concentration and the mechanical properties. The amount of alcohol groups increased with electrochemical treatment time and reached a peak value at twelve minutes coinciding with the observed peak in mechanical properties. Further electrochemical treatment time caused both the alcohol group concentration and the mechanical properties to decrease. This result indicated that mechanical properties of chemically functionalized nanofibers is not solely dependent on the amount of oxygen in the sample, but also on the type of functional groups present on the nanofiber. The alcohol group seems to be the most reactive among all oxygen functional groups, and therefore should provide enhanced adhesion to the polymer matrix.

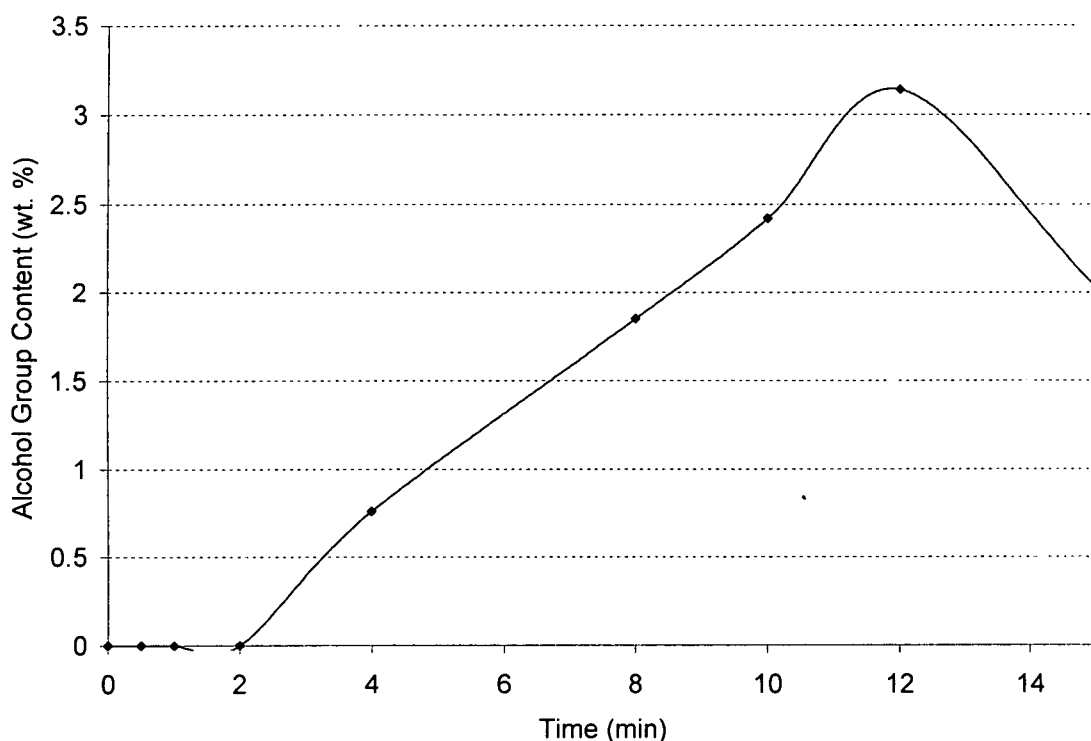


Figure 6.8 – Alcohol group content weight percent as a function of nanofiber electrochemical treatment time

The electrochemical treatment had a significant effect on the electrical resistivity of the manufactured nanocomposites (Figure 6.9). The electrical resistivity of the nanocomposites increased with increasing electrochemical treatment time. This may be due to the increase in oxygen content causing the formation of a narrow insulating layer along the surface of the fibers or the breaking of conjugation along the graphene layers altered the electron transfer along the graphene path. The C-C bond is the shortest possible bond length. Any additional elements that bond to carbon will change this bond length resulting in a longer time to transfer electrons.

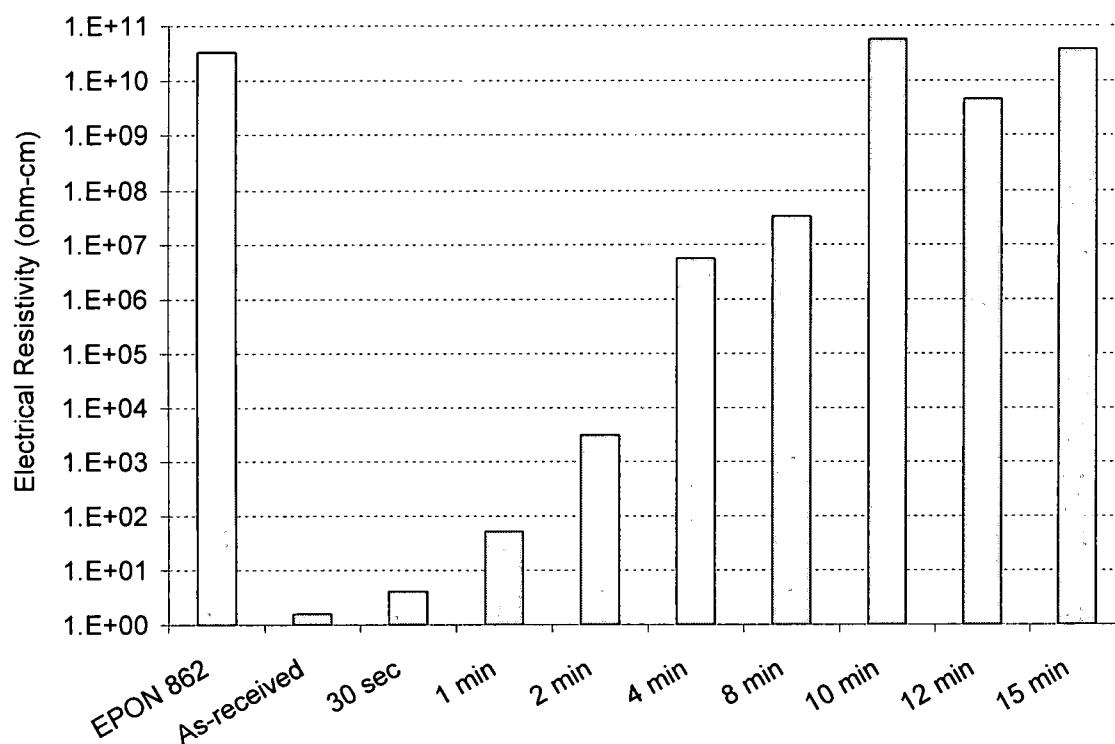


Figure 6.9 – Nanocomposite electrical resistivity as a function of nanofiber electrochemical treatment time

The thermal conductivity of the manufacture nanocomposites was not significantly altered with electrochemical treatment (Figure 6.10). Regardless of the treatment time, the thermal conductivity was only slightly decreased over that of the as-received PS nanofiber reinforced polymeric composite with the same nanofiber loading.

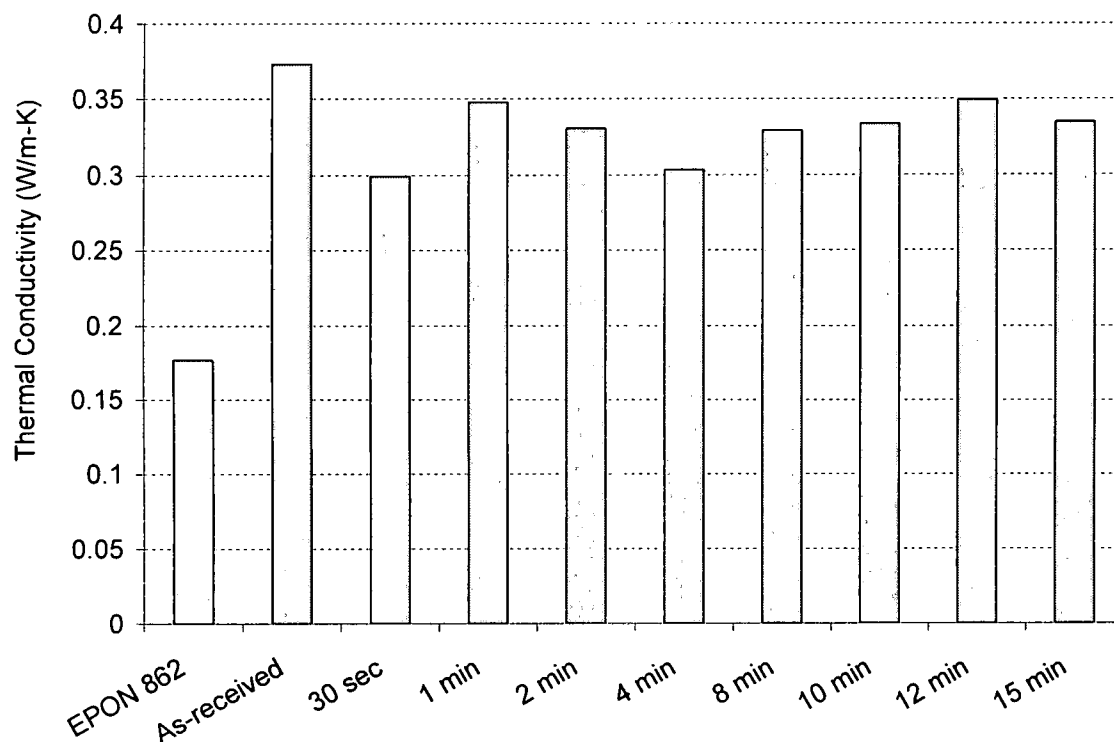


Figure 6.10 – Nanocomposite thermal conductivity as a function of nanofiber electrochemical treatment time

#### 6.4 CONCLUSIONS

There was a significant decrease in the relative content of graphitic carbon and an increase in the relative content of carbon bonded to oxygen with increasing amount of electrochemical treatment. The increase in relative concentration of carbon oxygen complexes occurred because the outer layers of the fibers become increasingly porous allowing for additional sights of oxidation. A modest degree of electrochemical treatment improved the flexural modulus of the nanocomposite by enhancing the interfacial adhesion between the fiber and resin. However, electrochemical treatment time over twelve minutes caused a decrease in mechanical properties. This trend correlated to the amount of

alcohol groups determined by chemical derivatization XPS indicating that the type of functional groups present following functionalization is an indicator of nanofiber-matrix adhesion. The electrochemically treated carbon nanofibers did not significantly affect the thermal conductivity of the resulting manufactured polymeric nanocomposite. The electrical resistivity of the nanocomposites increased with increasing electrochemical treatment time due in part to the breaking of the conjugation along the graphene layers hindering the electron transfer along the graphene path.

Due to the significance of the specific type of functional groups imparted onto the carbon nanofiber surface by electrochemical treatment on the physical properties of the resulting manufactured polymeric nanocomposites, a wet chemical functionalization technique should be determined to attach beneficial oxygen based functional groups to the carbon nanofiber surface.

## CHAPTER VII

### ATTACHMENT OF CARBOXYLIC ACID AND ALCOHOL FUNCTIONAL GROUPS TO CARBON NANOFIBERS: THE CHEMISTRY, ANALYSIS, AND EFFECT ON POLYMER ADHESION

#### 7.1 INTRODUCTION

In this study, carbon nanofibers were subjected to wet chemical treatments to attach specific oxygen based functional groups to the surface of the nanofibers, thereby modifying the interface between the nanofibers and epoxy molecules in polymeric nanocomposites. Carboxylic acid and alcohol groups were added to carbon nanofibers. X-ray photoelectron spectroscopy was employed to characterize surfaces with regard to the content of oxygen. BET surface area and IGC surface energy testing determined the alteration in nanofiber surface characteristics caused by the functionalization reactions. Stoichiometric calculations were made to determine the amount of functionalized fibers and curing agent to add to the epoxy such that the curing reaction would be favorable, and DSC and rheology tests were made to determine the properties of the nanocomposite during curing.

## 7.2 EXPERIMENTAL SETUP

### 7.2.1 CHEMICAL MODIFICATIONS OF CARBON NANOFIBERS

Two series of chemical modifications were applied to the carbon via the diazonium formation reaction mechanism in order to covalently attach carboxylic acid and alcohol functional groups. The first attempt at functionalization was performed on as-received PS carbon nanofibers. For secondary attempts at functionalization, the as-received carbon nanofibers were purified by heat treatment and Soxhlet extraction in order to remove surface impurities.

The diazonium formation reaction is a well known covalent modification method for preparing chemically modified carbon products that include an organic group attached to the surface. The diazonium formation reaction mechanism includes four main steps: formation of nitrous acid by the reaction of sodium nitrite ( $\text{NaNO}_2$ ) and a strong acid such as hydrochloric acid ( $\text{HCl}$ ), the formation of a nitrosonium ion, the formation of diazonium salt by the reaction of the nitrosonium ion and an amino group, and finally the reaction of the diazonium salt with the carbon product.

In all reactions, the carbon nanofibers were added to the reaction mixture without isolation of the diazonium salt. At the end of the reaction, the modified carbon product was isolated and dried. In order to remove impurities, the resultant functionalized carbon nanofibers were treated with a sodium bicarbonate ( $\text{NaHCO}_3$ ) solution and acetone for C-OOH and C-OH modifications respectively. In carboxylic acid group modification, the unreacted diazonium salt



of 4-aminobenzoic acid was converted to 4-hydroxybenzoic acid at room temperature and all impurities including carboxylic acid groups were removed from carbon samples by washing them with 0.1N  $\text{NaHCO}_3$  solution and 0.1N HCl solution respectively. In alcohol group modification, all washing and purification steps with deionized water and acetone were made at  $2^\circ\text{C}$  because the diazonium salt of 4-aminophenol can react with alcohol groups attached to the carbon sample and create nitrogen double bonds because of the coupling reaction at the end of the reaction at room temperature.

*Preparation of carboxylic acid modified carbon nanofibers via diazonium formation reaction (Figures 7.1 and 7.2)*

8.98g (0.065mol) 4-amino benzoic acid, 13.7mL 37% HCl, 10mL acetone and 90mL deionized water were charged into a jacketed glass reactor equipped with a constant temperature circulator, a mechanical stirrer, a thermometer and a dropping funnel. A solution of 4.61g (0.066mol)  $\text{NaNO}_2$  in 50mL deionized water was added to the reaction mixture in a drop wise manner while keeping the reaction temperature at  $2^\circ\text{C}$ . Since the reaction is exothermic, the reaction temperature was kept constant at  $2^\circ\text{C}$  because of the instability above  $5^\circ$ .

Five grams of carbon nanofibers were added after the reaction mixture was completely dissolved and stirring was continued at  $2^\circ\text{C}$  until no further nitrogen gas evolution was observed. After two days the reaction mixture was vacuum filtered and washed with deionized water. The wet cake was washed with 0.1N  $\text{NaHCO}_3$  solution. The slurry was vacuum-filtered, washed with deionized water and then acidified with 0.1N HCl solution. Finally the wet cake

was washed with deionized water until the water phase was neutral. The sample was dried in an oven at 105°C under vacuum.

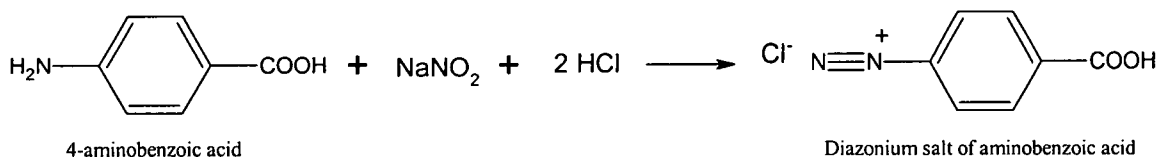


Figure 7.1 –Diazonium salt of aminobenzoic acid formation reaction

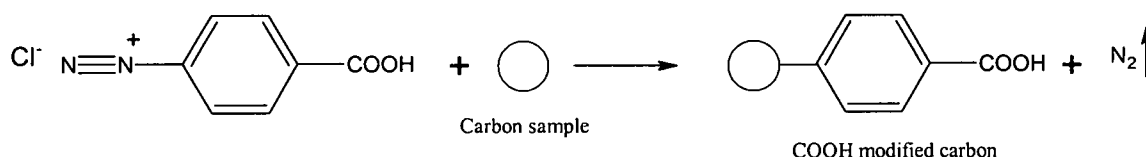


Figure 7.2 – Reaction resulting in covalent attachment of aminobenzoic acid diazonium salt to the carbon surface

*Preparation of alcohol group modified carbon nanofibers via diazonium formation reaction (Figures 7.3 and 7.4)*

7.2g (0.065mol) 4-amino phenol, 14mL 37% HCl, 10mL acetone and 90mL deionized water were charged into a jacketed glass reactor equipped with a constant temperature circulator, a mechanical stirrer, a thermometer and a dropping funnel. A solution of 4.7g (0.068mol) NaNO<sub>2</sub> in 50mL deionized water was added to the reaction mixture in a drop wise manner while keeping the reaction temperature at 2°C. Since the reaction is exothermic, the reaction temperature was kept constant at 2°C because of the instability above 5°C.

Five grams of carbon nanofibers were added after the reaction mixture was completely dissolved and stirring was continued at 2°C until no further nitrogen gas evolution was observed. After two days the reaction mixture was

vacuum filtered and washed with deionized water at 2°C. The wet cake was washed with acetone. The slurry was vacuum filtered and washed with deionized water. Finally the wet cake was washed with deionized water until the water phase was neutral. The sample was dried in an oven at 105°C under vacuum.

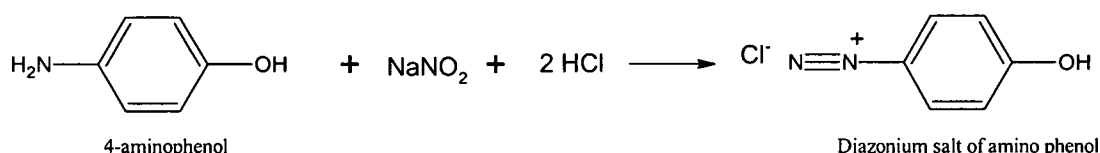


Figure 7.3 – Diazonium salt of amino phenol formation reaction

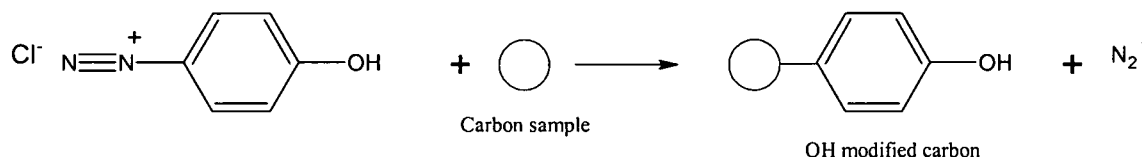


Figure 7.4 – Reaction resulting in covalent attachment of amino phenol diazonium salt to the carbon surface

The percentage of functional groups attached to the surface of the carbon nanofiber can be controlled by monitoring the evolution of nitrogen gas in the second stage of both reaction mechanisms. If the nitrogen gas is allowed to evolve to completion, the percentage of functional groups attached to the nanofiber surface will be maximized. Conversely, stopping the reaction short of completion of nitrogen gas evolution will result in fewer functional groups being attached to the surface. The amount of functional groups attached to the surface

can also be controlled by varying the amount of carbon nanofibers subjected to the treatment.

For both functionalization methods, the resulting modified carbon nanofiber has the ability to aid in epoxy curing and form covalent bonds with the epoxy resin. The mechanism for these reactions is presented in figure 7.5a-b. In both cases, a lone pair of electrons present on the alcohol group will attack the carbon atom next to the epoxide oxygen, thereby opening the epoxy ring. The epoxy oxygen's extra pair of electrons will swipe the positively charged hydrogen making an alcohol group and forming an ether linkage between the epoxy and the carbon nanofiber.

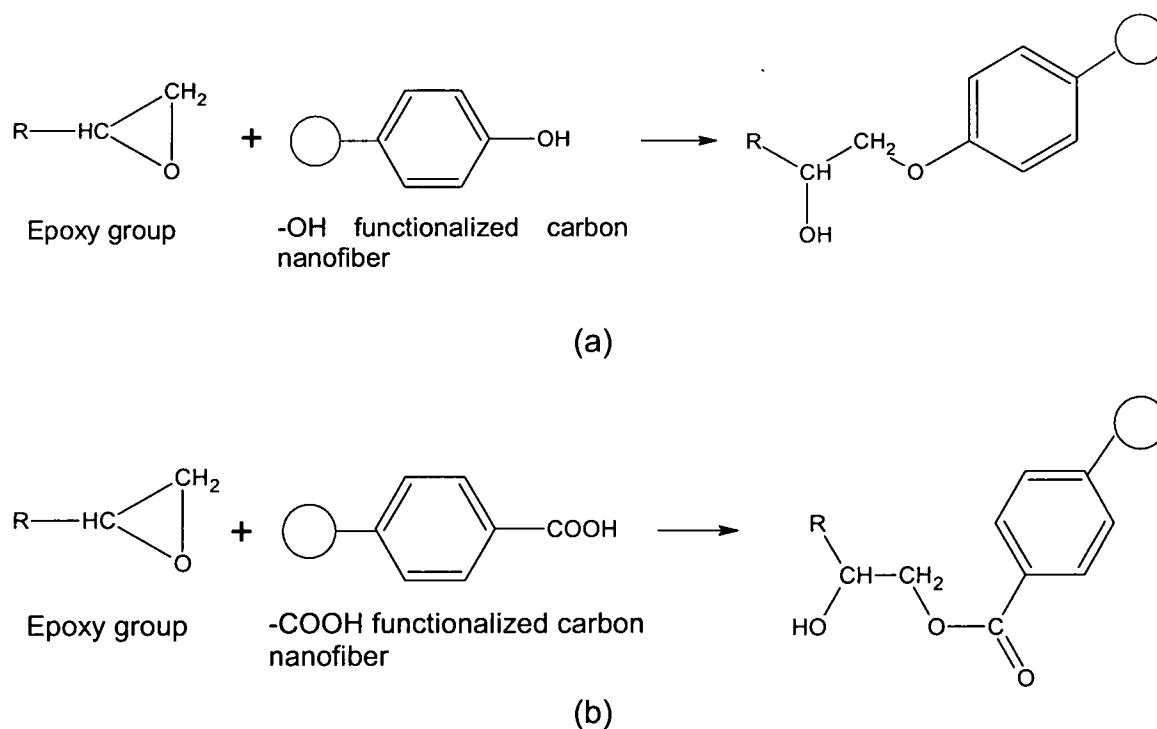


Figure 7.5 – Mechanisms for the covalent attachment to an epoxy polymer of  
 (a) alcohol group functionalized carbon nanofibers and  
 (b) carboxylic acid functionalized carbon nanofibers

### 7.2.2 NANOFIBER CHARACTERIZATION

The percent oxygen present on the nanofibers after functionalization was measured by X-ray photoelectron spectroscopy (XPS). The carbon nanofibers were tested for surface energy prior to and after functionalization reactions using inverse gas chromatography (IGC). The surface area of the nanofibers was analyzed using the BET method. Thermogravimetric analysis (TGA) was completed to determine the onset degradation temperature of the nanofibers as well as the percent weight loss after heating the nanofibers to 1000°C.

### 7.2.3 NANOCOMPOSITE SAMPLE PROCEDURE

For the EPON 862 epoxy resin system, diethyltoluene diamine (DETDA) and nanofiber including C-OOH and C-OH groups were used as curing agent and co-curing agent, respectively. The amount of C-OOH and C-OH groups on the surface of carbon nanofibers was calculated using XPS results.

For the composite sample preparation, the stoichiometric calculations were made based on the amount of amine hydrogen present in DETDA. The chemically modified carbon nanofibers were added in stoichiometric proportions (1-10 w/w %) relative to the total amount of amine hydrogen in DETDA and all formulations were based on 100 parts of epoxy resin.

A mixture of the epoxy resin and DETDA was mixed homogeneously and the chemically modified carbon nanofiber sample was added with stirring to the mixture.

#### 7.2.4 NANOCOMPOSITE CHARACTERIZATION

Nanocomposite heat of reaction was tested using a TA Instruments DSC Q1000 according to ASTM E2160. Nanocomposite glass transition temperature was tested using a TA Instruments DSC Q1000 according to ASTM D3417. The rheology of the nanocomposite mixture was analyzed using a TA Instruments AR 2000 Advanced Rheometer. The sample was tested at 150°C for thirty minutes at a constant angular frequency (6.283 rad/s) of oscillation to determine the gelation time.

#### 7.3 RESULTS AND DISCUSSION

Initial functionalization reactions were performed on as-received PS nanofibers. Figure 7.6 shows a DSC curve for 5% by weight as-received carboxylic acid functionalized nanofibers reacted with EPON 862 without any catalyst. The presence of an early, small reaction suggests that the functional group may play a role in the curing reaction. However, as noted in Chapter 4, the likely cause of the early reaction is the presence of polyaromatic hydrocarbons on the nanofiber surface. Figure 7.7 shows a DSC curve for a 5% by weight extraction cleaned carboxylic acid functionalized nanofibers with EPON 862 without any catalyst. The DSC curve shows no apparent reaction. This indicates that the polyaromatic hydrocarbons apparent on the uncleaned nanofibers were in fact responsible for the reaction shown in Figure 7.6. It is therefore imperative that the nanofibers be purified prior to functionalization in order to realize the true benefit of the addition of specific functional groups.

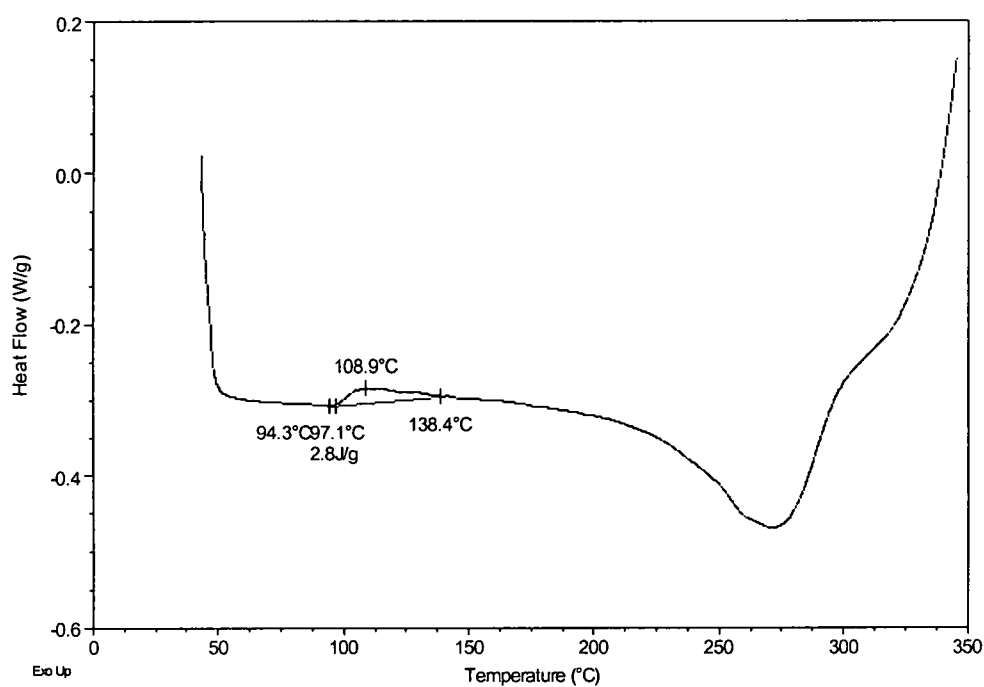


Figure 7.6 – DSC curve for as-received C-OOH functionalized nanofibers in EPON 862 without curing agent

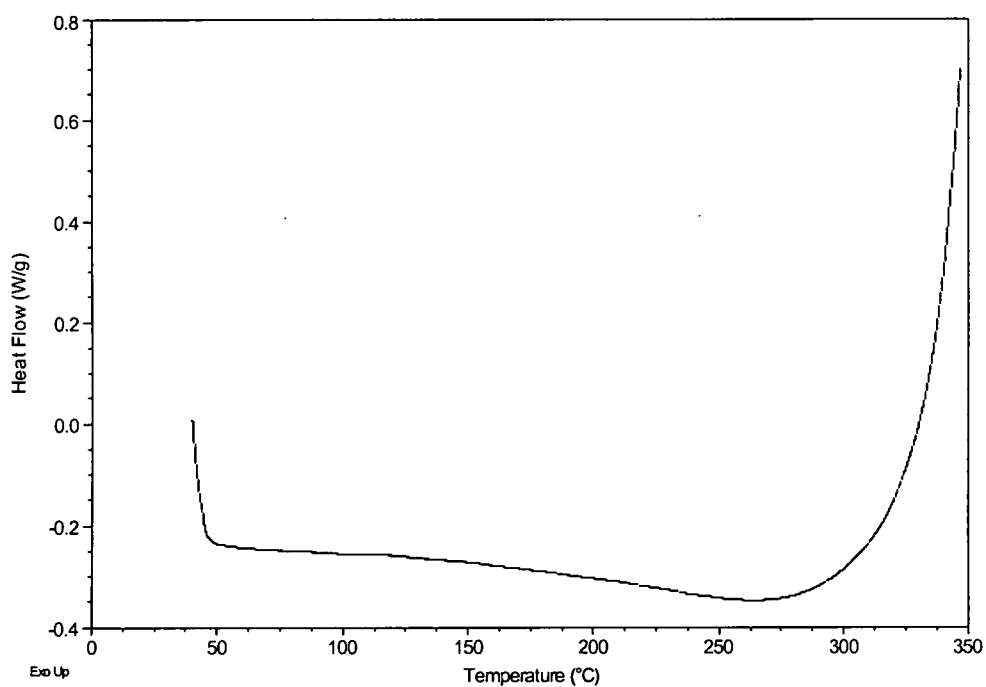


Figure 7.7 – DSC curve for Soxhlet extracted C-OOH functionalized nanofibers in EPON 862 without curing agent

A second example of the detrimental effect of nanofiber manufacturing impurities not being removed prior to subjection to functionalization is demonstrated in the reduction in epoxy degradation temperature. Figure 7.8 shows a series of DSC curves for the carboxylic acid functionalized nanofibers in increasing weight percentage mixed with EPON 862 and curing agent. The DSC curves indicate the presence of a second reaction initializing at approximately 275°C. With increasing weight percent of the carboxylic acid functionalized nanofibers, the heat of reaction of the second reaction increases. The presence of this second reaction is likely due to the degradation of the epoxy.

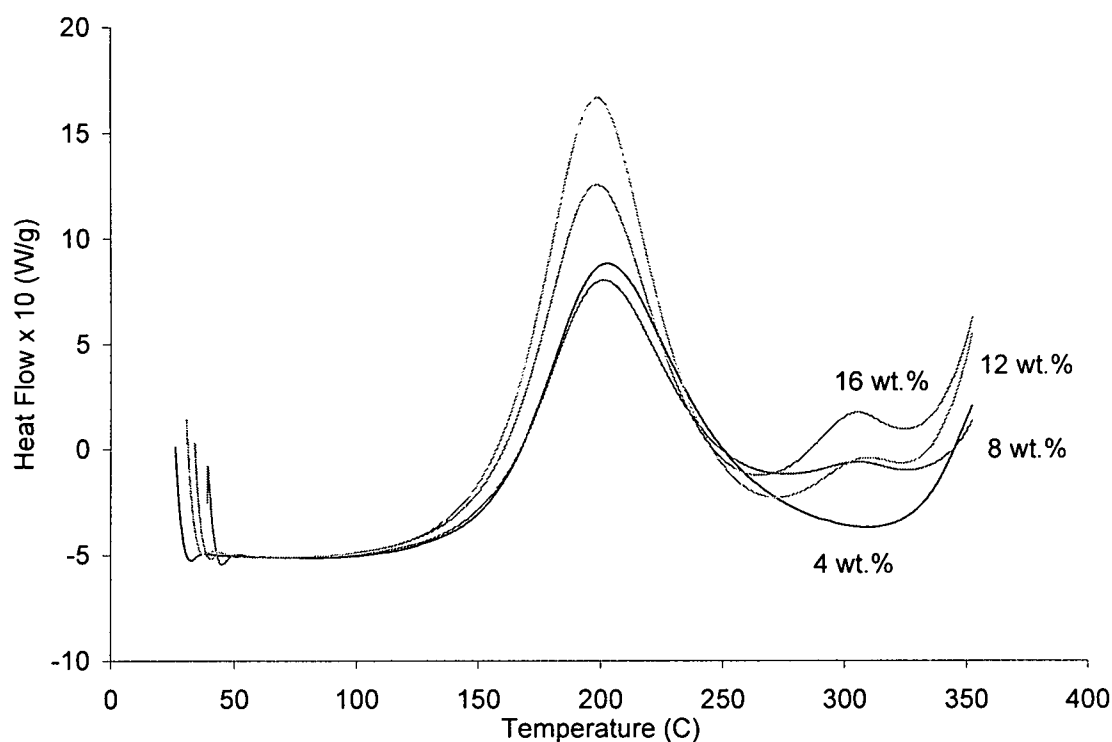


Figure 7.8 – DSC Curves for as-received C-OOH functionalized nanofibers in EPON 862 / W

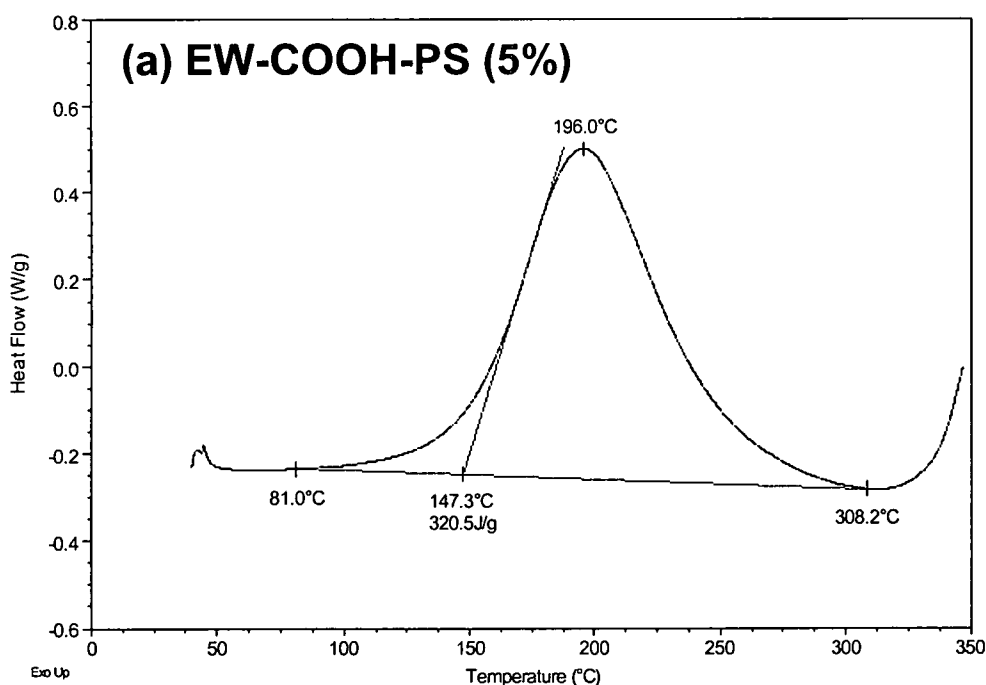


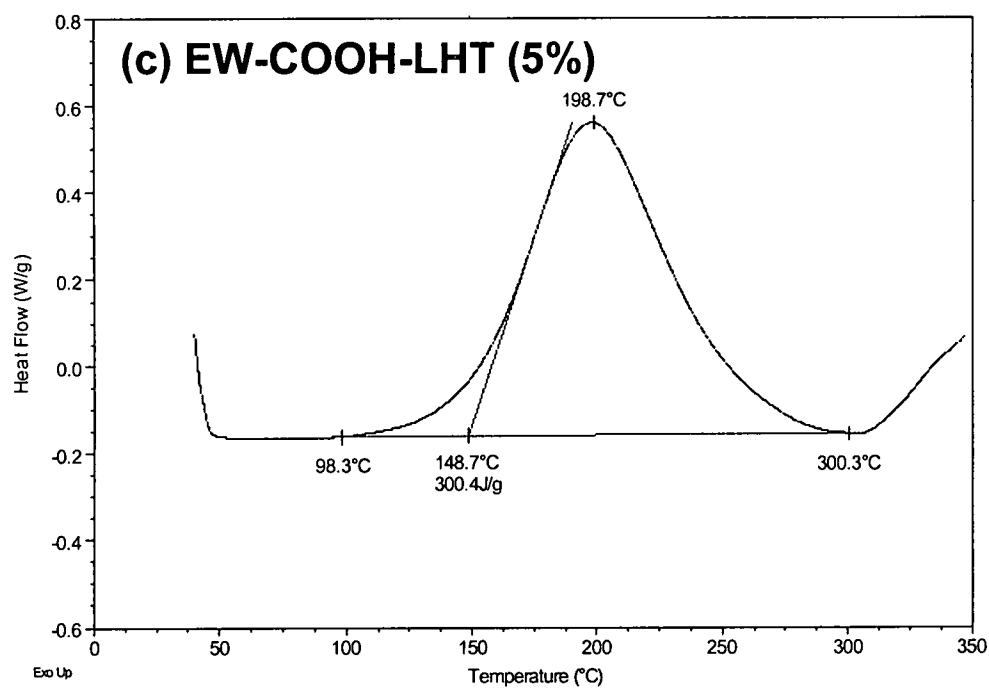
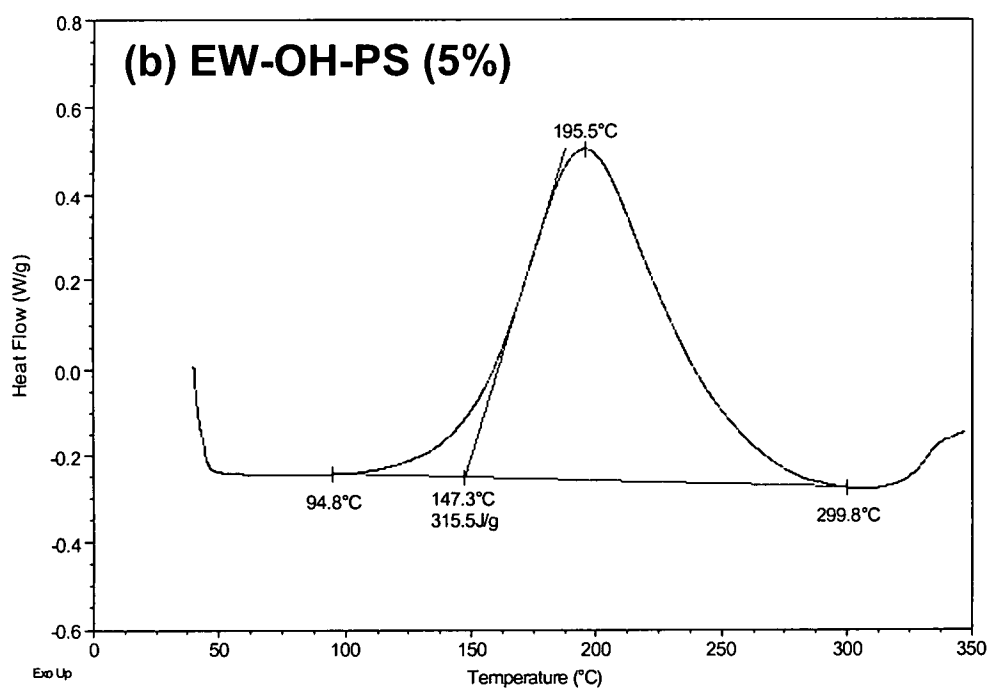
To verify the assumption that the functionalization of as-received carbon nanofibers with residual manufacturing-imposed surface impurities actually decreased the degradation temperature of the neat resin, a series of TGA tests were run on the neat resin and nanocomposite samples to identify the degradation temperatures (Table 7.1). The onset of degradation for the neat resin occurred at 370°C, and the onset of degradation for a nanocomposite incorporating 8% loading of as-received PS nanofibers was only slightly decreased. Conversely when 8% loading of the as-received carboxylic acid functionalized nanofibers were added to the resin, the onset of degradation occurred at 294°C and when 16% loading of the as-received carboxylic acid functionalized nanofibers were added to the resin, the onset of degradation occurred at 304°C. This significant decrease in the degradation onset temperature coincides with the peak temperatures of the second reaction noted in the DSC tests, indicating that the functionalization of as-received carbon nanofibers with carboxylic acid actually lead to deterioration of the nanocomposite at lower temperatures than that of the neat resin.

Table 7.1 – Degradation onset temperatures for neat resin and nanocomposites

<b>Sample</b>	<b>Onset of Degradation Temperature (°C)</b>
Neat Resin	370
8% As-received PS Nanofibers	363
8% As-received Carboxylic Acid Functionalized PS Nanofibers	294
16% As-received Carboxylic Acid Functionalized PS Nanofibers	304

In order to show the importance of cleaning the nanofibers prior to functionalization, a series of Soxhlet extractions were performed on the as-received nanofibers. Following extraction of both PS and LHT grade nanofibers by acetone, THF, toluene, and pyridine, the nanofibers were functionalized with carboxylic acid and alcohol groups. The resulting DSC curves are shown in Figures 7.9a-d. In each of the nanocomposite curing mechanisms, there was no presence of an early reaction. Regardless of the level of heat treatment temperature of the nanofibers, the cleaning procedures lead to the same result of no prompt reaction due to organic or inorganic impurities. This indicated that the removal of the polyaromatic hydrocarbons by extraction allowed for an improvement in the ability of the functionalized nanofibers to adhere to the epoxy matrix.





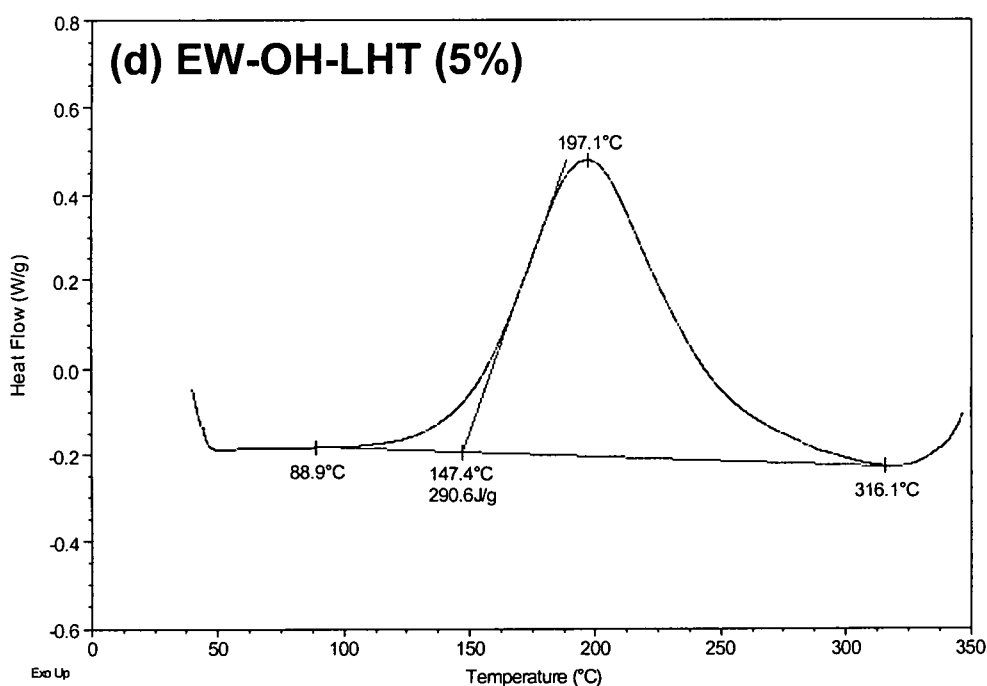


Figure 7.9 – DSC curves for (a) cleaned PS grade nanofibers functionalized with carboxylic acid groups reacted with EPON 862 / W, (b) cleaned PS grade nanofibers functionalized with alcohol groups reacted with EPON862 / W, (c) cleaned LHT grade nanofibers functionalized with carboxylic acid groups reacted with EPON 862 / W, (d) cleaned LHT grade nanofibers functionalized with alcohol groups reacted with EPON 862 / W; note: for each figure, the heat of reaction was calculated for the entire reactive system, and not normalized for resin content

Heat treatment of the as-received nanofibers will also remove impurities present on the nanofiber surface. TGA testing of heat treated, functionalized PS grade nanofibers indicated the type of bond between the functional groups and the carbon nanofiber surface. The TGA results of weight loss percent before and after 600°C are shown in Table 7.2 for as-received PS grade nanofibers, heat treated PS grade nanofibers, and heat treated and functionalized PS grade nanofibers. For the functionalized nanofibers, there was no weight loss prior to 600°C, indicating that the functional groups are covalently bonded to the carbon

nanofiber surface. Since the degradation temperature is above 600°C, there is no chance of the functional groups degrading during the curing cycle of the nanocomposite. Therefore, the functional groups will be able to aid in the curing of the epoxy polymer and improve the adhesion between the nanofiber and the matrix.

Table 7.2 – TGA results for PS, heat treated PS, and heat treated and functionalized PS nanofibers

Sample	Degradation Onset Temp (°C)	% Wt. Loss @ 600° C	% Wt. Loss @ 1000°C
PS	500	8.7	33
PS-HT	645	0	5.1
PS-HT C-OOH	623	0	3.2
PS-HT C-OH	624	0	2.8

In order to examine the percentage of organic functional groups imparted onto the carbon nanofiber surface, XPS analysis was performed for both the chemically modified and as-received carbon nanofibers. The resultant XPS C1s spectra for C-OOH group modified carbon nanofibers and C-OH group modified carbon nanofibers exhibited a large peak around 285 eV, which can be attributed to the sp<sup>2</sup> carbon atoms of the carbon skeleton. The XPS results indicating the amount of oxygen present in the chemically modified carbon nanofibers and as-received carbon nanofibers samples are shown in Table 7.3.

There was a significant increase in surface energy observed for the functionalized nanofibers compared to the as-received nanofibers (Table 7.3). The presence of oxygen allows for the surface to be more chemically active and should result in improved adhesion between the nanofibers and an epoxy matrix.

The alcohol group modified carbon nanofibers exhibited a larger surface energy indicating that the alcohol group is likely to be more efficient in reactions with epoxy molecules than the carboxylic acid group.

BET surface areas for the chemically modified carbon nanofibers are shown in Table 7.3. The surface area of the as-received carbon nanofibers was  $33\text{m}^2/\text{g}$  using BET determinations. The surface areas decreased very slightly with functionalization. The major conclusion is that BET surface area tests could observe very little change in surface area during these oxidations. This is an unexpected result considering the strongly oxidizing conditions these fibers were exposed to and the much larger surface area increases that occur when PAN-based carbon fibers are oxidized.

Table 7.3 – Nanofiber properties following functionalization

Sample Code	O %	Disp. Surface Energy ( $\text{mJ}/\text{m}^2$ )	Surface Area ( $\text{m}^2/\text{g}$ )
PS Pristine	2	40.4	32.9
PS C-OOH Functionalized	10	145	27.2
PS C-OH Functionalized	6	173	30.2

Results of differential scanning calorimetry (DSC) and rheology tests performed on the series of nanocomposites functionalized with carboxylic acid groups with decreasing curing agent weight percentage are presented in Table 7.4. The heat of reaction for the nanocomposites when normalized by resin content reached a minimum with a seven percent reduction in curing agent weight. At this point the heat of reaction was 24% less than that of the neat resin. The glass transition temperature for the nanocomposites reached a peak

of 136°C for the nanocomposite with five percent reduction in curing agent weight. Additional weight percent nanofibers did not exhibit further increase in glass transition temperature. The addition of nanofibers to the resin served to increase the gelation time at 150°C over the neat resin. However, increasing the weight percent of nanofibers from 1.48 to 13.35 showed a decrease in gel time from 1563s to 1437s.

Table 7.4 – DSC and rheology results for carboxylic acid modified carbon nanofiber polymeric nanocomposites

Wt. % Reduction in Curing Agent	Wt. % Nanofiber	Total Heat of Reaction (J/g)	Normalized Heat of Reaction by Epoxy Content (J/g)	T <sub>g</sub> (°C)	Gel Time at 150°C (s)
0 (Neat Resin)	0	370		105	1290
1	1.48	367	373	103	1563
3	4.35	353	365	125	1550
5	7.08	281	304	136	1434
7	9.69	254	281	118	1444
10	13.35	271	311	123	1437

Results of DSC and rheology tests performed on the series of nanocomposites functionalized with alcohol groups with decreasing curing agent weight percentage are presented in Table 7.5. The heat of reaction for the nanocomposites when normalized by resin content reached a minimum with a five percent reduction in curing agent weight. At this point the heat of reaction was 34% less than that of the neat resin. The glass transition temperature for the nanocomposites reached a peak of 121°C for the nanocomposite with seven percent reduction in curing agent weight. Additional weight percent nanofibers did not exhibit further increase in glass transition temperature. The addition of

nanofibers to the resin served to increase the gel time at 150°C over the neat resin. However, increasing the weight percentage of nanofibers from 1.24 to 11.33 showed a decrease in gel time from 1559s to 1432s.

Table 7.3 – DSC and rheometry results for alcohol modified carbon nanofiber polymeric composites

<b>Wt. % Reduction in Curing Agent</b>	<b>Wt. % Nanofiber</b>	<b>Total Heat of Reaction (J/g)</b>	<b>Normalized Heat of Reaction by Epoxy Content (J/g)</b>	<b>T<sub>g</sub> (°C)</b>	<b>Gel Time at 150°C (s)</b>
0 (Neat Resin)	0	370		105	1290
1	1.24	350	352	111	1559
3	3.64	245	255	114	1552
5	5.94	234	243	120	1511
7	8.16	246	268	121	1496
10	11.33	237	266	112	1432

#### 7.4 CONCLUSIONS

Functionalization of as-received carbon nanofibers with carboxylic acid groups resulted in the presence of a reaction when mixed with epoxy without curing agent likely due to the polyaromatic hydrocarbons that adhered to the surface of the nanofiber following manufacturing. In addition, the introduction of these nanofibers to the epoxy and curing agent caused the presence of a second reaction when the curing reaction was examined with DSC indicating that the functionalization of the manufacturing-induced residual impurities caused the epoxy to degrade at a lower temperature than the neat resin. Therefore the nanofibers should be cleaned by either Soxhlet extraction or heat treatment in order to remove impurities that may negatively impact the functionalization of the material.



Functionalization of carbon nanofibers with specific addition of carboxylic acid groups and alcohol groups allowed for curing of an epoxy resin reinforced nanocomposite with decreased amounts of curing agent by utilizing the functional groups to aid in the curing process. The addition of the functionalized carbon nanofibers to the epoxy matrix resulted in decreased heats of reaction. Functionalization alters the curing process, and the adhesion between the nanofiber and the epoxy is a chemical reaction that alters the glass transition temperature of the resulting nanocomposite. This increase in glass transition temperature is significant in that the potential application operating conditions is also increased. To fully optimize the functionalization techniques, the glass transition temperature must be maximized with a high nanocomposite heat capacity.

The surface energy of the carbon nanofibers is significantly increased with addition of the oxygen-based functional groups. Alcohol groups on the surface of carbon nanofibers resulted in a 115% increase in surface energy, and carboxylic acid groups on the surface of carbon nanofibers resulted in an 81% increase in surface energy. These results are reflected in the heats of reaction and gel times at 150°C for the two nanocomposites. The heat of reaction for the alcohol functionalized nanocomposites was less than that of the carboxylic acid functionalized nanocomposites. Similarly, the gel times for the alcohol group functionalized nanocomposites were less than that of the carboxylic acid functionalized nanocomposites. This indicated a greater degree of reactivity for

the alcohol group over the carboxylic acid group which can be explained by the chemical form of the two functional groups – the alcohol groups do not have the same degree of steric hindrances present in the carboxylic acid groups caused by the presence of a carbonyl group, thereby allowing reaction with the epoxy molecules to take place at a faster rate.

Functionalization of the nanofiber by wet chemistry methods offers the ability to improve nanocomposite mechanical properties without altering the structure of the nanofiber. This offers an improvement over heat treatment of the carbon nanofiber in that the properties of the nanocomposite do not need to be compromised due to the changes in nanofiber structure. In addition, the method of attaching specific functional groups to the surface of the carbon nanofiber allows for the attachment of specific beneficial molecules to the carbon nanofiber surface that aid in adhesion between the nanofiber and the matrix.

## CHAPTER VIII

### SUMMARY OF CARBON NANOFIBER PURIFICATION AND SURFACE TREATMENT METHODS

Nanocomposites consist of incorporating a nanofiller into a host matrix. In order to optimize the properties of a nanocomposite, the nanofiller must be thoroughly dispersed and capable of interacting with the host matrix. If the nanofiller is not dispersed properly, it has a tendency to agglomerate and form inclusions, thereby reducing its benefit. Poor adhesion to the matrix will cause the nanofiller to act as a defect in the continuous phase. To promote the benefit of using nanocomposites, (i) The nanofiller must be free of all organic volatiles (polyhydrocarbons) and inorganic impurities (catalyst residues, sulfur, and other ash impurities), (ii) Nanofiller surface functionalization and activation will enhance both dispersion and adhesion to the matrix, (iii) In using carbon as a nanofiller material, the inherent properties can be tailored by a further heat treatment temperature. This will allow for a variation in structure to improve nanocomposite properties.

In this study, carbon nanofibers were adapted to further nanocomposite characteristics. Two methods were used (heat treatment and Soxhlet extraction) for purification of the as-received carbon nanofibers. Heat treatment of the carbon nanofibers at various temperatures were tested for resulting

nanocomposite properties. In addition, the nanofibers were surface functionalized by electrochemical treatment and wet chemistry using specific oxygen functional groups to determine the result on nanofiber and nanocomposite characteristics.

The presence of impurities on the surface of PS and LHT nanofibers was shown through volume resistivity, TGA, and DSC testing of the resulting nanocomposites. Testing on pristine PS and LHT nanofibers resulted in inconsistent volume resistivity readings. TGA testing resulted in an approximately 35% loss in weight for the PS nanofibers. In addition when the PS and LHT fibers were added to the epoxy, DSC testing resulted in an early reaction.

Cleaning and purification of the nanofibers by subsequent heat treatment and Soxhlet extraction resulted in property improvements. The volume resistivity tests were more consistent with high heat treatment nanofiber results due to the removal of the dielectric layer. The cleaning procedures resulted in no weight loss prior to 600°C. Soxhlet extraction of the nanofibers progressively with acetone, THF, toluene, and pyridine resulted in an elimination of the early reaction with epoxy.

The heat treatment of carbon nanofibers lead to the removal of impurities from the nanofiber resulting in altered physical properties of a nanofiber reinforced epoxy composite. In addition, during heat treatment the structure within the carbon nanofibers is changed from local molecular ordering to that of

coalesced, flattened graphene layers. Heat treatment up to 1800°C resulted in improved flexural modulus of the nanocomposite. Additional heat treatment to higher temperatures lead to increased conversion to graphene layers and resulted in lower mechanical properties due to poor adhesion to the epoxy matrix caused by encapsulation of the graphene planes. The alignment of graphene layers within the nanofibers allowed for a more efficient transfer of phonons and electrons resulting in significant decreases in electrical resistivity and increases in thermal conductivity of the neat epoxy resin. Heat treatment of the nanofibers allowed for attainment of superior electrical and thermal properties at low fiber loadings that were not possible with as-received pyrolytically stripped carbon nanofibers.

Electrochemical treatment of PS nanofibers showed that increasing amounts of oxygen with treatment time corresponded to an increase in the flexural modulus of nanocomposites up to twelve minutes of treatment time. Additional treatment caused a decrease in mechanical properties. This trend correlated to the amount of alcohol groups determined by chemical derivatization XPS indicating that the type of functional groups present following functionalization is an indicator of nanofiber-matrix adhesion. The treated nanofibers did not affect the thermal conductivity of the nanocomposites. The electrical resistivity of the nanocomposites increased with increasing electrochemical treatment time due in part to the breaking of the conjugation

along the graphene layers hindering the electron transfer along the graphene path.

Wet chemistry functionalization of carbon nanofibers with specific addition of carboxylic acid groups and alcohol groups allowed for curing of an epoxy resin reinforced nanocomposite with decreased amounts of curing agent. The functional groups aid in curing of the epoxy, thereby decreasing the necessary amount of curing agent material. Alcohol groups on the surface of carbon nanofibers increased the surface energy of the nanofiber to a greater extent than that of carboxylic acid groups. These results are reflected in the heats of reaction and gel times at 150°C for the two nanocomposites. The heat of reaction for the alcohol group functionalized nanocomposites was less than that of the carboxylic acid functionalized nanocomposites. Similarly, the gel times for the alcohol group functionalized nanocomposites were less than that of the carboxylic acid functionalized nanocomposites. This indicated a greater degree of reactivity for the alcohol group over the carboxylic acid group.

Based on the results of the testing of heat treated and surface functionalized nanofiber based polymer composites, the possibility exists for tailoring of nanocomposite physical properties. High heat treatment temperature of the nanofibers resulted in the lowest electrical resistivity and highest thermal conductivity of the resulting nanocomposites, but heat treatment temperature above 1800C resulted in decreased mechanical properties. Surface functionalization of carbon nanofibers yielded nanocomposites with enhanced

mechanical properties, increased electrical resistivity, and minimal effect on thermal conductivity. Therefore, the properties of a nanocomposite could be tailored by blending the functionalization techniques of the nanofibers. For example, surface functionalization of high heat treatment nanofibers to introduce alcohol groups on its surface should allow for improved mechanical properties of the nanocomposite with only a slight effect on the electrical and thermal properties.

The manipulation of nanofiber properties allows nanofibers to be used as a nucleating, degrading, or cleaning agent. For example, using the enhanced strength and degradation rate apparent in carbon nanofibers allows for potential use in a bone regeneration material application. In a bone regeneration application, the ability of the material to degrade with the growth of tissue over time is an essential property. As-received nanofibers are a viable option to be added to a porous structure for use in a bone regeneration application due to their ability to strengthen materials and aid in the degradation rate.

## CHAPTER IX

### BIOLOGICAL APPLICATION OF CARBON FOAM

#### 9.1 INTRODUCTION

There are a number of techniques used to regenerate bone including the use of polymers, ceramics, transplanted cells, and bioactive molecules. Polymeric implants design flexibility because the polymer composition and structure can be tailored to the specific need. In addition, polymers are biodegradable. Polymers can include chemical bonds that undergo hydrolysis upon exposure to the body's aqueous environment and they can also degrade by cellular or enzymatic pathways. The products of this degradation must be carefully examined prior to implantation as the liberated chemical species may adversely affect the regeneration of bone cells by altering the localized pH or even prove toxic [62]. The degradation rate is tailorable through manipulation of the polymer's hydrophobicity and crystallinity [62]. The most frequently investigated polymers include poly( $\alpha$ -hydroxy esters), polydioxanone, poly(propylene fumarate), poly(ethylene glycol) poly(orthoesters) polyanhydrides, and polyurethanes. Polymeric composites can be used to create a structural scaffold and a delivery system for bone morphogenetic proteins (BMPs) and mesenchymal stem cells to accelerate cell regeneration. The mechanical



properties of the polymeric implants are inferior to that of healthy bone and therefore fail upon physical loading due to regular usage. Polymers may be used to create a porous structure or in the case of small defects a polymeric membrane can be used in guided tissue regeneration to prevent the interference and contamination of foreign tissues during healing [63]. This technique is only successful for defects of limited size. Regrowth covering larger spans require the implantation of a porous scaffold allowing osteoconduction.

Injectable polymeric materials have become the focus of bone tissue engineering research because of their minimally invasive implantation. The material is poured in place of the removed, defective bone and then cured. To complete the cure of the polymer the injected material must be photopolymerized to localize the material. Gogolewski et al. [64] used this process to cover a 1cm defect in rabbits to regenerate cortical bone to span the defect in 18-24 months with a poly-L-lactide (PLLA) membrane. The choice of the PLLA polymer was due to its pore size of 5-15 $\mu$ m to best facilitating bone ingrowth [64]. The membrane facilitated the rapid formation of new bone growth without grossly adverse reactions. Photocrosslinkable polyanhydrides are new materials that present certain advantages in orthopedic applications. They absorb via surface erosion and therefore are not susceptible to sudden losses in mass in delivery applications. The photopolymerizable element allows for mass fabrication of porous scaffolds or for specific applications. Polymer composites with ceramic fillers have also been investigated. Poly(lactide-co-glycolide) constructs were

formed with hydroxyapatite (HA) to improve the polymer's mechanical strength. The polymerization of the material itself can be modulated to cause foaming through the release of carbon dioxide, thereby producing a porous scaffold necessary for bone ingrowth. The injectable nature of the material allows it to fill irregular osseous defects and the release of carbon dioxide during the crosslinking allows room for bone ingrowth and creates a press-fit between prosthesis and natural bone.

When implanted into the body polymeric materials can cause inflammation and are slow to be resorbed, but may be used to introduce BMPs to specific areas to promote bone regeneration and combat inflammation [65]. Ferguson et al. demonstrated that purified bovine BMP and poly-lactide-co-glycolide (PGLA) could successfully treat experimentally created trephine defects. New bone quickly grew around the implant; however the polymer remained unabsorbed preventing its complete replacement with regenerated bone. A polymer with a faster degradation time would be better suited to deliver the BMPs while allowing for its own replacement by natural bone.

Ceramics have also been investigated for bone regenerative implantation because of their structural similarity to natural bone or biocompatibility. The inorganic materials are protein-free and only cause minimal immunological responses following implantation or systemic toxicity [65]. Hydroxyapatite (HA) and B-tricalcium phosphate (B-TCP) are the most common ceramics investigated for bone regeneration because they are osteoconductive and biodegradable. HA

closely resembles the structure of natural bone, but has very slow degradation rates compared to B-TCP. A slow degradation rate hinders the regenerative ability of the body by shielding the newly formed structure from local stresses that assist in the creation of new bone. With a faster degradation rate B-TCP shares the stress loading with the regenerated bone providing an environment more conducive to osteoblast cell creation, but has not been shown to be osteoinductive. Ceramics can also be used as a delivery vehicle for BMPs that accelerate bone growth [66-69].

Using a plasma-sprayed hydroxyapatite-coated scaffold for bone ingrowth Unwin et al. [70] reconstructed the proximal and distal femur and of the proximal tibia following local tumor removal. Fourteen months following the implantation bone formation was evident in 31 of 44 cases and bone ingrowth was seen in all proximal tibial and femoral prostheses and in 21 of the 27 distal prostheses. Suh et al. [65] combined 980°C heat-treated carbonate apatite (CAp), Type I atelocollagen (AtCol) extracted from bovine tail skins and bone inducing agent to create an osteoinductive bone substitute. In this study the composites with the bone inducing agent were completely replaced by regenerated host bone after four weeks, while the composites without bone inducing agent were only partially resorbed.

A further enhancement to artificial bone regeneration design is demonstrated by Yoshikawa et al. incorporating mesenchymal stem cells and BMPs into a HA scaffold to induce osteoblast regeneration [67]. In this study

porous hydroxyapatite was coated with bone morphogenetic proteins and perfused with mesenchymal stem cells to accelerate bone cell generation resulting in a high alkaline phosphatase (ALP) activity and significant ossification [67]. ALP activity is an indication of osteoblastic activity. The implants containing BMPs had ALP and osteocalcin levels six times of those that did not receive BMP perfusion. Osteocalcin levels are indicative of bone mass. Using only a few micrograms of BMP stimulated ossification due to the inclusion of mesenchymal stem cells. Without the addition of the stem cells large doses of BMP would have been necessary for direct stimulation of ossification adding considerable cost to the process [67]. The same combination of using BMPs, MSCs, and HA to form an osteogenic composite has also been investigated by Noshi et al. [71]. This study provides further evidence of the interaction effects that occur due to the incorporation of BMPs and MSCs as they effectively and efficiently regenerate bone cells.

Daculsi used the ceramics hydroxyapatite and tricalcium phosphate to create a composite that will maintain its structural integrity while being soluble and gradually dissolving into the body releasing calcium ions that seed bone cell generation [72]. At the interface between the prosthetic and natural bone degradation of the ceramic allows for the ingrowth of new bone into the structural scaffold. This shows that the interface between the two phases is not static, but dynamically evolving. The degradation of the tricalcium phosphate facilitated the

regeneration of new bone growth, but the residual hydroxyapatite scaffold prevented the complete replacement of the prosthesis with natural bone.

Kikuchi et al. synthesized a composite of HA and collagen creating an implant with the nanostructure and composition of natural bone [73]. Closely matching the mechanical properties of natural bone is just as important as recreating a chemically and topographically suitable environment for bone regeneration. The composites were constructed at various temperatures and pH levels. The composite made at a pH of 9 and at 40°C exhibited the largest bending strength of 39.5MPa with a modulus of 2.54 GPa roughly five times of the composites created at room temperature and similar to that of cancellous bone. This may be acceptable for short term replacement, but the inability of HA to efficiently degrade (1µm/year) prevents its usage in load bearing appendages. Following implantation newly formed bone gradually grew into the composite and completely spanned the defect after eight weeks. The composite was surrounded by elongated cells located at the new bone/soft tissue interface including osteoblasts and osteoclasts.

Ryu et. al. proposed a biodegradable glass ceramic that incorporated boron oxide into the composition [74]. The B<sub>2</sub>O<sub>3</sub> increased the rate of dissolution of the glass ceramic without changing the bioactivity. The glass ceramics containing B<sub>2</sub>O<sub>3</sub> demonstrated higher mechanical strengths and increased rates of formation of a hydroxycarbonate apatite layer at the bone-implant interface representing an improved ability of bioactive ceramics to bond directly to bone.

In addition, the glass ceramics were proven to be nocyctotoxic suggesting the glass ceramics of the  $\text{CaO-SiO}_2\text{-B}_2\text{O}_3$  system may be quality candidates for bioactive and biodegradable bone replacement materials.

Nanometric-scale components are attractive to material engineering designers for a number of reasons. In carbon nanotechnology they approach the theoretical limits of carbon with an exceptionally high modulus along with thermal and electrical conductivity matching that of graphite. The main attraction to carbon nanotechnology from a biological application standpoint is the ability to mimic the human body's own responses and manipulate its processes allowing for increased regenerative rates. By operating at this level recovery rate kinetics may be improved by increasing the surface area available for healing. Decreasing the time the body needs to recuperate following injury will lead to considerable cost savings, improved productivity, and an improvement to the patients' quality of life.

In this study, heat treated carbon foam was examined as a possible bone regenerative material. The open structures of carbon foam combined with its inherent physical properties make it an attractive material for use in this application. The large surface area of the foam should allow for enhanced opportunities for the bone tissue to adhere and grow. In addition, doping the carbon foam with carbon nanofibers should allow for the degradation rate to be tailored such that it is similar to the growth of new tissue. In order to improve the stiffness of the carbon foam, the foam must be infiltrated with either a polymeric

or ceramic biodegradable material that will not significantly decrease the surface area.

For purposes of this investigation, the carbon foam samples were infiltrated with the biodegradable polymer polycaprolactone, and compression tested. The samples were subjected to simulated body fluid (SBF) and temperature to determine the effect on the mechanical properties. In addition, the ability of osteoblast cells to adhere to the carbon foam surface was tested to insure biocompatibility.

## 9.2 *EXPERIMENTAL SETUP*

The infiltration of the carbon foam with polycaprolactone polymer was carried out under vacuum at the melting temperature of the polymer. ASTM C1424-99 was used in testing the bulk compressive strength and modulus of the carbon foam both prior to and after polymer infiltration. The infiltrated foam was placed in simulated body fluid and stored at body temperature. Every week for a period of ten weeks, a sample was removed and tested for compression.

To identify the biocompatibility of carbon foam with osteoblast cells, an osteoblast cell solution was applied to the surface of the carbon foam sample. The solution was administered in a manner that allowed for contact with the exposed face of the substrate in an effort to minimize the area available for adherence, thereby increasing the cell count per unit area. The adherence of the osteoblasts to the carbon foam surface was examined by optical microscopy under a UV filter.

### 9.3 RESULTS AND DISCUSSION

The compressive strength and modulus results for the polycaprolactone infiltrated foam can be seen in Figures 9.1 and 9.2 respectively. Over the course of ten weeks of aging in simulated body fluid and temperature, the strength decreased by 21.14% and the modulus decreased by 19.90%. If the material were to continue to decompose at this rate, the bone could possibly be completely regenerated in approximately one year. Increasing the strength of the carbon foam, and using a more suitable infusion polymeric or ceramic material may improve the physical properties of the composite.

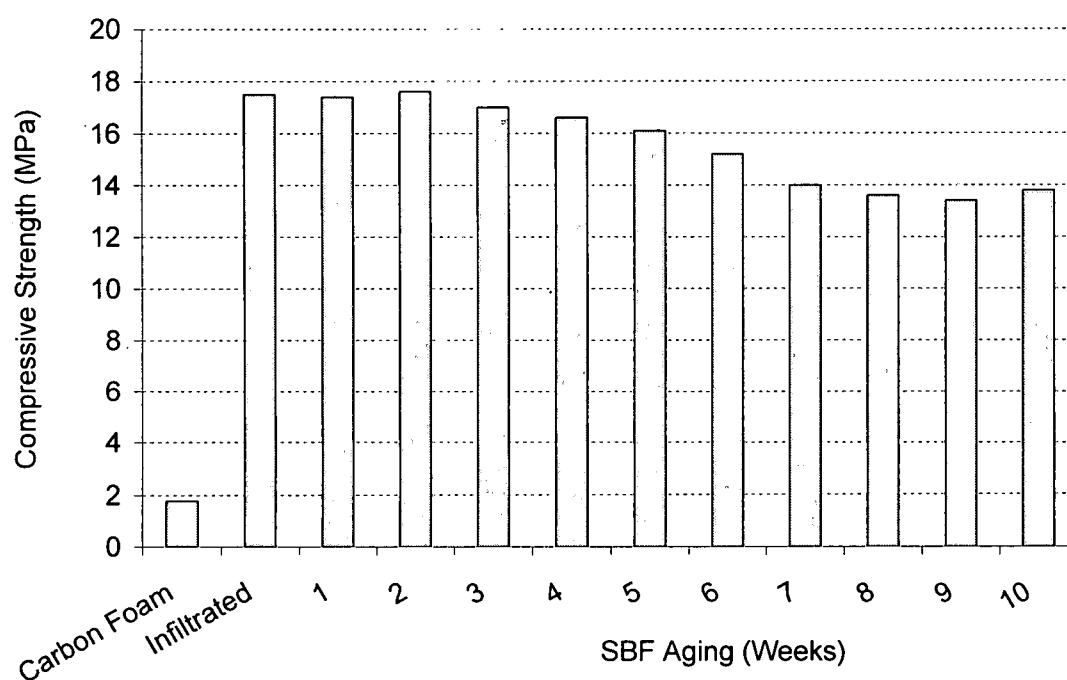


Figure 9.1 – Compressive strength of PCL-infiltrated carbon foam aged in SBF



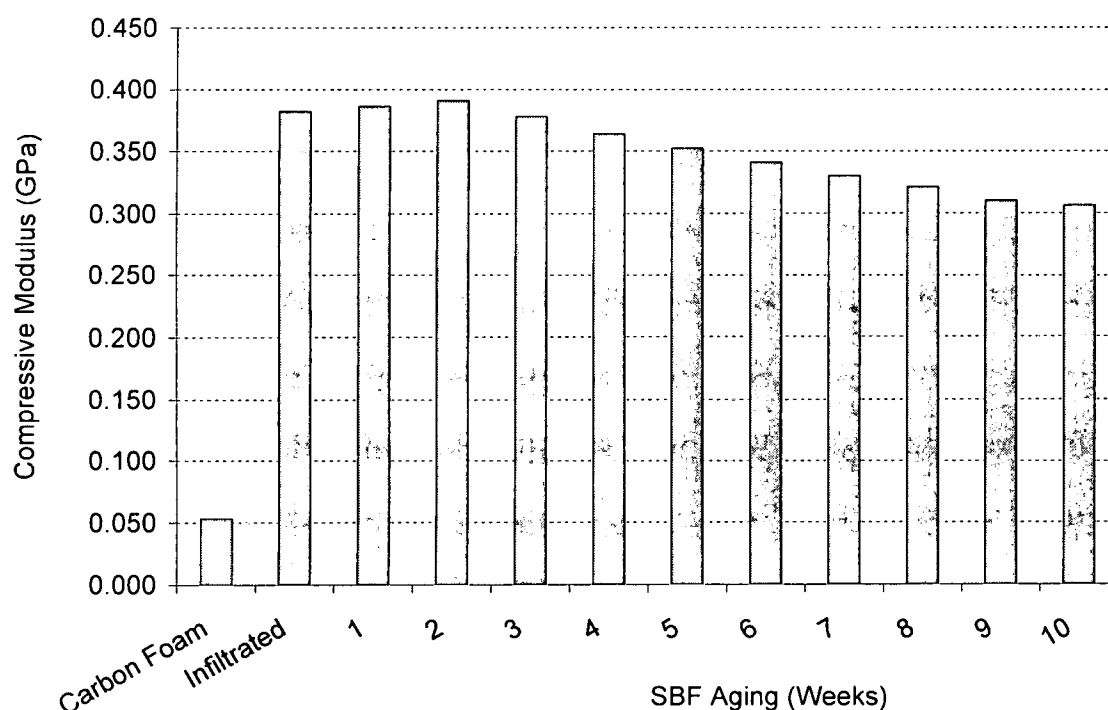


Figure 9.2 – Compressive modulus of PCL-infiltrated carbon foam aged in SBF

After application and incubation of the osteoblast solution on the carbon foam surface, optical microscopy under UV filter showed the presence of cells growing on the material (Figure 9.3). Due to the porosity of the surface, there was difficulty in obtaining an accurate count of the cells to determine a survival rate. The observation of cells adhering to the surface indicates that the carbon foam is biocompatible with bone tissue, and could serve as a regenerative material.

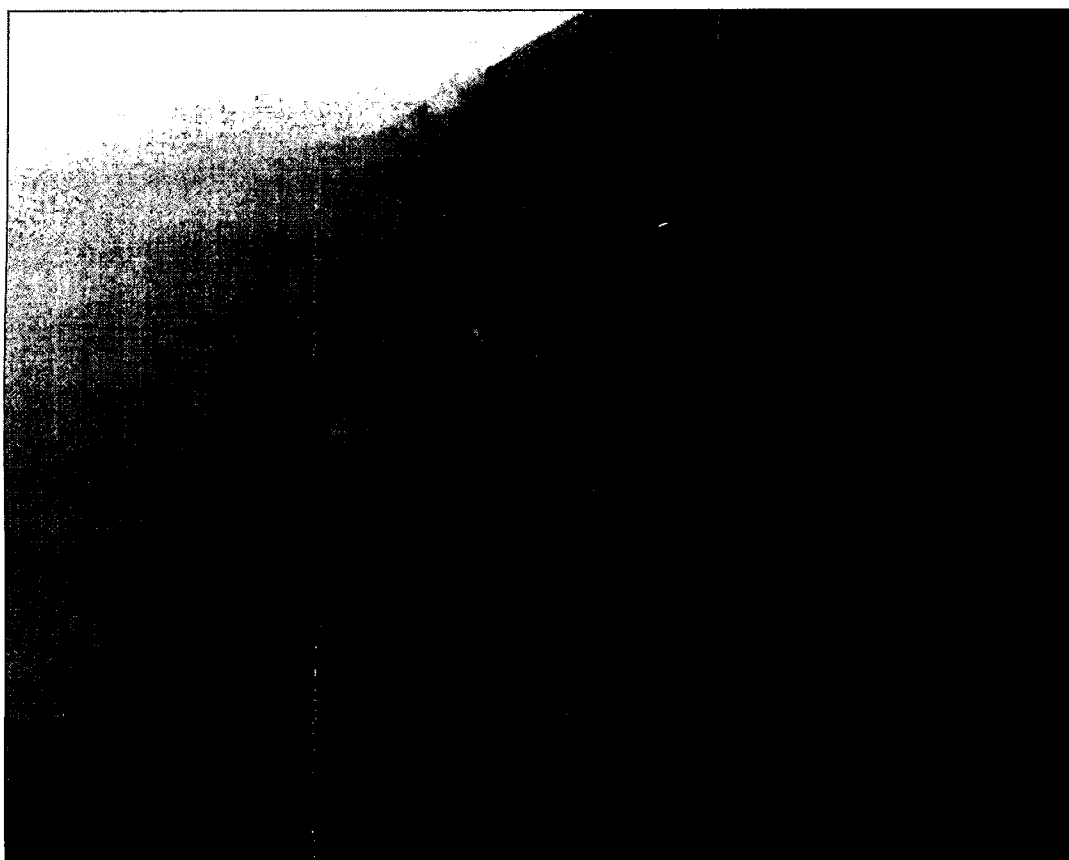


Figure 9.3 – Adherence of osteoblast cells to the carbon foam surface at 20x objective through UV filter

#### 9.4 CONCLUSIONS

The rate of degradation for the compressive bulk properties of the polycaprolactone-infiltrated carbon foam was such that after ten weeks of aging in simulated body fluid, the material had lost approximately 20% of its original strength. If this trend were to continue linearly, the material would degrade after nearly one year. A possible means to increase the rate of degradation would be to include as-received nanofibers in the material. Due to the polyaromatic hydrocarbons on the surface of the nanofibers, degradation should be increased as the impurities are relinquished from the material.

In addition, the carbon foam has been established as a suitable material for adherence of osteoblast cells. The high surface area of the foam is a significant advantage for use as a bone regenerative material. With the increased surface area and the ability of the cells to adhere to the surface, the growth of new tissue should be increased. This is an advantage over a continuous, non-porous material which would have decreased surface area, and only allow the cells to adhere to the outermost regions.

Future work on examining the adherence of osteoblast cells to the surface of the carbon foam should focus on determining an accurate cell survival rate based on count of cells following incubation period. In addition, the percentage of cells adhering to carbon foam ligaments should be compared to the percentage of cells adhering to the pore surface in order to understand the mechanism of cell growth on the carbon foam. This would allow for optimization of the carbon foam porosity structure and create a "biomodel" for the growth of osteoblast cells on the carbon foam.

## REFERENCES

1. Lozano, E. and V. Barrera, Nanofiber-reinforced thermoplastic composites. I. thermoanalytical and mechanical analyses, *Journal of Applied Polymer Science*, 2001. vol. 79, p. 125.
2. Kuriger, R.J., *et al.*, Processing and Characterization of Aligned Vapor Grown Carbon Fiber Reinforced Polypropylene" *Composites: Part A*, 2002, vol. 33, p. 53.
3. Patton, R. D., *et al.*, Vapor Grown Carbon Fiber Composites with Epoxy and Poly(Phenylene Sulfide) Matrices, *Composites: Part A*, 1999, vol. 30, p. 1081.
4. Inagaki, M., *New Carbons: Control of Structure and Functions*, Oxford: Elsevier, Sci., 2002
5. *Sciences of Carbon Materials*, Marsh, H. Ed., Alicante: Univ. di Alicante, 2000.
6. Baker, R.T.K. and Harris, P.S., The Formation of Filamentous Carbon, *Chemistry and Physics of Carbon*, Walker, P.L. and Thrower, P.A., Eds., New York: Marcel Dekker, 1978, p. 83.
7. *Carbon Nanotubes*, Endo, M., Ed., Oxford: Pergamon, 1996.
8. *Carbon Nanotubes: Preparation and Properties*, Ebbesen, T.W., Ed., New York: CRC, 1997.
9. Dresselhaus, M.S., Dresselhaus, G., and Eklund, P.C., *Science of Fullerenes and Carbon Nanotubes*, London:Academic, 1996.
10. Tibbetts, G.G. and Beetz, C.P., Mechanical Properties of Vapor-Grown Carbon Fibers, *Journal of Physics D: Applied Phys.*, 1987, vol. 20, p. 292.
11. Oberlin, A., *et al.*, Filamentous Growth of Carbon through Benzene Decomposition, *Journal of Crystal Growth*, 1976, vol. 32, p. 335.
12. Endo, M., *et al.*, Structure and Growth Mechanism of Vapor-Grown Carbon Fibers, *Japan Journal of Applied Physics, Part 1*, 1977, vol. 16, p. 1519.
13. Katsuki, H., *et al.*, Formation of Carbon Fibers from Naphthalene on Some Sulfur-Containing Substrates, *Carbon*, 1981, vol. 9, p. 148.
14. Ishioka, M., *et al.*, *Carbon*, 1992, vol. 30, p. 859.
15. Ishioka, M., *et al.*, *Carbon*, 1992, vol. 30, p. 975.
16. Tibbetts, G.G., Lengths of Carbon Fibers Grown from Iron Catalyst Particles in Natural Gas, *Journal of Crystal Growth*, 1985, vol. 73, p. 431.

17. Motojima, S., *et al.*, Vapor Phase Preparation of Micro-Coiled Carbon Fibers by Metal Powder Catalyzed Pyrolysis of Acetylene Containing a Small Amount of Phosphorus Impurity, *Carbon*, 1995, vol. 33, p. 1167.
18. PCT Patent Application No. WO92/13983
19. WO 92/13983
20. U.S. Patent 5554739
21. Vieira, R.R., *et al.*, Tailoring Activated Carbon by Surface Chemical Modification With O, S, and N Containing Molecules, *Materials Research*, 2003, vol. 6, no. 2, p. 862.
22. G.B. Patent 813486
23. Allongue, P., *et al.*, Covalent Modification of Carbon Surfaces by Aryl Radicals Generated From the Electrochemical Reduction of Diazonium Salts, *Journal of the American Chemical Society*, 1997, vol. 119, p. 201.
24. *EPON Resin 862/EPI-CURE Curing Agent W System*, Product Bulletin, Resolution Performance Products, SC:1183-01.
25. Brandl, W., *et al.*, Production and Characterisation of Vapour Grown Carbon Fiber/Polypropylene Composites, *Carbon*, 2004, vol. 42, no. 1, p. 5.
26. Lopattananon, N., *et al.*, Interface Molecular Engineering of Carbon-Fiber Composites, *Composites Part A*, 1999, vol. 30, no. 1, p. 49.
27. Park, R., *et al.*, Performance Improvement of Carbon Fiber/Polyethylene Fiber Hybrid Composites, *Journal of Materials Science*, 1999, vol. 34, no. 12, p. 2903.
28. Ma, H., *et al.*, Processing, Structure, and Properties of Fibers from Polyester/carbon Nanofiber Composites, *Composites Science and Technology*, 2003, vol. 63, p. 1617.
29. Lake, M. L., *et al.*, Carbon Nanofiber Polymer Composites: Electrical and Mechanical Properties, SAMPE, Long Beach, CA, May 1998.
30. Patton, R. D., *et al.*, Ablation, Mechanical and Thermal Conductivity Properties of Vapor Grown Carbon Fiber/Phenolic Matrix Composites, *Composites: Part A*, 2002, vol. 33, p. 243.
31. Endo, M.M., *et al.*, Microstructural changes induced in stacked cup carbon nanofibers by heat treatment, *Carbon*, 2003, vol. 41, p. 1941.
32. Katayama, T. *et al.*, Multiwalled carbon nanotubes with bamboo-like structure and effects of heat treatment, *Journal of Applied Physics*, 2002, vol. 91, no. 10, p. 6675.
33. Kiselev, N.A., *et al.*, Carbon nanotubes from polyethylene precursors: structure and structural changes caused by thermal and chemical treatment revealed by HREM, *Carbon*, 1998, vol. 36, p. 1149.
34. Xu, J., *et al.*, Preparation, electrical and mechanical properties of vapor grown carbon fiber (VGCF)/vinyl ester composites, *Composites Part A*, 2004, vol. 35, p. 693.

35. Finegan, I.C., *et al.*, Surface treatments for improving the mechanical properties of carbon nanofiber/thermoplastic composites, *Journal of Materials Science*, 2003, vol. 38, p. 3485.
36. Lim, S., *et al.*, Surface modification of carbon nanofiber with high degree of graphitization, *Journal of Physical Chemistry B*, 2004, vol. 108, p. 1533.
37. Toebes, M.L., *et al.*, The influence of oxidation on the texture and the number of oxygen-containing surface groups of carbon nanofibers, *Carbon*, 2004, vol. 42, p. 307.
38. Bubert, H., *et al.*, Basic analytical investigation of plasma-chemically modified carbon fibers, *Spectrochimica Acta Part B*, 2002, vol. 57, p. 1601.
39. Cortes, P., *et al.*, Effects of nanofiber treatments on the properties of vapor-grown carbon fiber reinforced polymer composites, *Journal of Applied Polymer Science*, 2003, vol. 89, p. 2527.
40. Harvey, J., *et al.*, X-ray photoelectron spectroscopic studies of carbon fibre surfaces, *Journal of Materials Science*, 1987, vol. 22, p. 1585.
41. Gulyas, J., *et al.*, Electrochemical oxidation of carbon fibres: surface chemistry and adhesion, *Composites Part A*, 2001, vol. 32, p. 353.
42. Yue, Z.R., *et al.*, Surface characterization of electrochemically oxidized carbon fibers, *Carbon*, 1999, vol. 37: p. 1785.
43. Chemical Modification of Carbon Black for Improved Performance in Coatings, P. Collins, *et al.*, *Cabot Corporation, Coatings Business Unit*, CRP-216-294.
44. U.S. Patent 5922118
45. Allongue, P., *et al.*, Covalent modification of carbon surfaces by aryl radicals generated from the electrochemical treatment of diazonium salts, *Journal of the American Chemical Society*, 1997, vol. 119, p. 201.
46. Delamar, M., *et al.*, Modification of carbon fiber surfaces by electrochemical reduction of aryl diazonium salts: application to carbon epoxy composites, *Carbon*, 1997, vol. 35, no. 6, p. 801.
47. Coulon, E and J. Prinson, Electrochemical attachment of organic groups to carbon felt species, *Langmuir*, 2001, vol. 17, p. 7102.
48. Delamar, M., *et al.*, Covalent modification of carbon surfaces by grafting of functionalized radical produced from the electrochemical reduction of diazonium salts, *Journal of the American Chemical Society*, 1992, vol. 114, p. 5883.
49. Lakshminarayanan, P.V., *et al.*, Nitric acid oxidation of vapor grown carbon nanofibers, *Carbon*, 2004, vol. 42, p. 2433.
50. Valde's, H., *et al.*, Effect of ozone treatment on surface properties of activated carbon, *Langmuir*, 2002, vol. 18, p. 2111.
51. Dillon, A.C., *et al.*, Storage of carbon in Single Walled Carbon Nanotubes, *Nature*, 1997, vol. 366, p. 377.

52. Ye, L., *et al.*, Hydrogen Absorption and Cohesive Energy of Single Walled Carbon Nanotubes, *Applied Physics Letters*, 1999, vol. 74, p. 2307.
53. Coen, C., *et al.*, Functionalization of graphite, glassy carbon, and polymer surfaces with highly oxidized sulfur species by plasma treatments, *Journal of Applied Physics*, 2002, vol. 92, no. 9, p. 1473.
54. "Low Temperature Plasma Functionalization of Carbon Nanotubes," Bishun Khare of SETI Institute and M. Meyyappan of Ames Research Center, NASA Tech Briefs.
55. Lei, Z., *et al.*, Sidewall Functionalization of Single-Walled Carbon Nanotubes with Hydroxyl Group-Terminated Moieties, *Chemical Materials*, 2004, vol. 16, p. 2055.
56. Sidewall Functionalization of Single-Walled Carbon Nanotubes through C-N Bond Forming Substitution Reactions of Fluoronanotubes, J. Stevens, *et al.*, *Technical Proceedings of the 2003 Nanotechnology Conference and Trade Show*, Volume 3, p. 169.
57. Mickelson, *et al.*, Fluorination of Single-wall carbon nanotubes, *Chemical Physics Letters*, 1998, vol. 296, p. 188.
58. Toebes, M. L., *et al.*, Impact of the Structure and Reactivity of Nickel Particles on the Catalytic Growth of Carbon Nanofibers, *Catalysis Today*, 2002, vol. 76, p. 33.
59. Matzek, M., Polymeric Carbon Nanocomposites: Physical Properties and Osteoblast Adhesion Studies, *M.S. Thesis*, Dayton: University of Dayton, 2004.
60. Losito, I., *et al.*, Spectroscopic investigation on polymer films obtained by oxidation of o-phenylenediamine on platinum electrodes at different pHs, *Journal of Materials Chemistry*, 2001, vol. 11, p. 1812.
61. Malitesta, C., *et al.*, Applicability of chemical derivatization – X-ray photoelectron spectroscopy (CD-XPS) to the characterization of complex matrices: case of electrosynthesized polypyrroles, *Journal of Electron Spectroscopy and Related Phenomena*, 1998, vol. 97, p. 199.
62. Yaszemski, M. J., *et al.*, Evolution of bone transplantation: molecular, cellular and tissue strategies to engineer human bone, *Biomaterials*, 1996, vol. 17, p. 175.
63. Nielsen, F., F., *et al.*, Biodegradable guide for bone regeneration: polyurethane membranes tested in rabbit radius defects, *Acta Orthopædica Scandinavica*, 1992, vol. 63, p. 63.
64. Meinig, R., P., *et al.*, Bone regeneration with resorbable polymeric membranes: treatment of diaphyseal bone defects in the rabbit radius with poly(L-lactide) membrane. A pilot study, *Journal of Orthopedic Trauma*, 1996, vol. 10, p. 178.
65. Burg, K.J.L., *et al.*, Biomaterial developments for bone tissue engineering, *Biomaterials*, 2000, vol. 21, p. 2347.

66. Suh, H., *et al.*, A bone replaceable artificial bone substitute: osteoinduction by combining with bone inducing agent, *Artificial Organs*, 2001, vol. 25, no. 6, p. 459.
67. Yoshikawa, T., *et al.*, Bone and soft tissue regeneration by bone marrow mesenchymal cells, *Materials Science and Engineering*, 2001, vol. 17, p. 19.
68. Catanese III, J., *et al.*, Characterization of the mechanical and ultrastructural properties of heat-treated cortical bone for use as a bone substitute, *Journal of Biomedical Materials Research*, 1999, vol. 45, p. 327.
69. Wang, Y.-J., *et al.*, Collagen-hydroxyapatite microspheres as carriers for bone morphogenetic protein-4, *Artificial Organs*, 2003, vol. 27, no. 2, p. 162.
70. Choong, P. F. M., and F. H. Sim, Limb-sparing surgery for bone tumors: new developments, *Seminars in Surgical Oncology*, 1997, vol. 13, p. 64.
71. Noshi, T., *et al.*, Recombinant human bone morphogenetic protein-2 potentiates the in vivo osteogenic ability of marrow/hydroxyapatite composites, *Artificial Organs*, 2001, vol. 25, no. 3, p. 201.
72. Daculsi, G., Biphasic calcium phosphate concept applied to artificial bone, implant coating and injectable bone substitute, *Biomaterials*, 1998, vol. 19, p. 1473.
73. Kikuchi, M., *et al.*, Self-organization mechanism in a bone-like hydroxyapatite/collagen nanocomposite synthesized in vitro and its biological reaction in vivo, *Biomaterials*, 2001, vol. 22, p. 1705.
74. Ryu, H-S., *et al.*, Novel bioactive and biodegradable glass ceramics with high mechanical strength in the CaO-SiO<sub>2</sub>-B<sub>2</sub>O<sub>3</sub> system, *Journal of Biomedical Materials Research*, 2004, vol. 68A, p. 79.



R002S919S6